

MUHAMMAD YOUNAS KHAN

**SYNTHESIS AND CHARACTERIZATION OF SUPERPARAMAGNETIC
NANOPARTICLES CONTAINING Fe_3O_4 CORE IN PYROLYZED TANNIN**

Thesis submitted to the Graduate Program
in Chemistry, Department of Chemistry,
Federal University of Paraná, as part of the
requirements for the degree of PhD in
Chemistry.

Supervisor: Dr. Antonio Sálvio Mangrich

Area of concentration: Inorganic Chemistry

CURITIBA
2015

K45s

Khan, Muhammad Younas

Síntese e caracterização de superparamagnético nanopartículas contendo núcleo de Fe_3O_4 em pirolisado tanino. / Muhammad Younas Khan. – Curitiba, 2015.

101f. : il. [algumas color.] ; 30 cm.

Tese (doutorado) - Universidade Federal do Paraná, Setor de Ciências Exatas, Programa de Pós-graduação em Química, 2015.

Orientador: Antonio Sálvio Mangrich

Bibliografia: p. 86-100

I. Química inorgânica. 2. Nanotecnologia. I. Universidade Federal do Paraná. II. Mangrich, Antonio Sálvio. III. Título.

CDD: 546

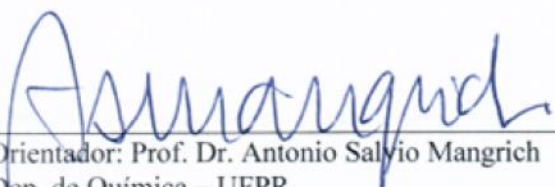
TERMO DE APROVAÇÃO

**SYNTHESIS AND CHARACTERIZATION OF SUPERPARAMAGNETIC NANOPARTICLES
CONTAINING Fe_3O_4 CORE IN PYROLIZED TANNIN**

por


MUHAMMAD YOUNAS KHAN

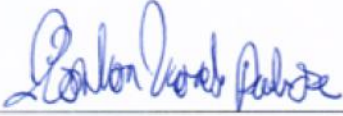
Tese aprovada como requisito parcial para obtenção do grau de Doutor no Programa de Pós-Graduação em Química, pela Comissão Examinadora composta por:


Orientador: Prof. Dr. Antonio Salyio Mangrich
Dep. de Química – UFPR


Prof. Dr. Bruno Szpoganicz
Dep. de Química – UFSC


Prof. Dr. Etelvino Henrique Novotny
Embrapa Solos – RJ


Prof. Dr. Patricio Guillermo Peralta Zamora
Dep. de Química – UFPR


Prof. Dr. Ronilson Vasconcelos Barbosa
Dep. de Química – UFPR

Curitiba, 12 de março de 2015.

DEDICATION

This thesis is dedicated to my parents, family and friends

*For their endless love, support, understanding and
encouragement.*

ACKNOWLEDMENT

First of all, I praise to Allah, the Almighty for providing me this opportunity and granting me the capability to progress successfully. This thesis appears in its current form due to the assistance and guidance of several people. I would therefore like to offer my sincere thanks to all of them.

Foremost, I would like to express my sincere gratefulness to my advisor Prof. Dr. Antonio Sálvio Mangrich for the continuous support of my Ph.D. This research would not have been possible without Prof. Mangrich's endless kindness, patience, guidance, support and persistent help. His guidance helped me in all the time of research and writing of this thesis. I could not have imagined having a better advisor and mentor for my Ph.D.

Besides my advisor, I would like to give a sincere and humble thank to the rest of my thesis committee: Prof. Dr. Bruno Szpoganicz, Dr. Etelvino Henrique Novotny, Prof. Dr. Ronilson Vasconcelos Barbosa and Prof. Dr. Patricio Guillermo Peralta-Zamora for their encouragement and insightful comments.

I wish to give a humble thanks to Dr. Prof. Dante Homero Mosca Dr. Prof. Ney Pereira Mattoso Filho for their humble suggestion and valuable advices.

I would like to give a special thanks to Prof. Dr. Ronilson Vasconcelos Barbosa whose encouragement and support also give me possible to accommodate easily in the department being a foreign student and also to the all staff of DQUI including secretary and the rest of all technicians of the DQUI and UFPR.

My sincere thanks also goes to Prof Dr. Aldo José Gorgatti Zarbin, Prof. Dr. Brás Heleno de Oliveira, and Prof Dr. Herbert Winnischofer for offering me opportunities in their groups and lectures learning some ideas.

Special thanks to Marta Doumer, Juliana Schultz and Estela Cardoso for their valuable ideas and kind suggestions.

I thank all my fellow lab mates in LABPAAM: Jaqueline Nicolini, Edi, Martha, Liliam, Aline, Pricilla, Nana, Mayara and Rafael for the stimulating discussions, and for all the work with fun we have had in the last four years.

In particular, I am grateful to the Departamento de Química Universidade Federal do Paraná for giving me a good opportunity and nice environment for my research activities.

I would also like to acknowledge the financial support I received from The World Academy of Sciences (TWAS), Conselho Nacional de Desenvolvimento Científico e Tecnológico (CNPq) and Universidade Federal do Paraná (UFPR) and TANAC Montenegro – RS – Brazil.

A special thanks to Brazilian Government and people of Brazil for their hospitality and giving me the opportunity on their land to learn and acquire something valuable.

Finally, I wish to express my love and gratitude to my beloved parents, brother Ilyas and family for their understanding, support and endless love, through the duration of my studies.

RESUMO

A nanotecnologia é uma ciência de engenharia em que o objetivo é desenvolver procedimentos e estruturas em nanoescala, com novas propriedades que podem oferecer soluções para muitos problemas atuais. Nesta pesquisa, descrevemos a síntese de nanopartículas de óxido de ferro superparamagnético (Fe_3O_4). As nanopartículas de óxido de ferro contêm um núcleo de óxido de ferro, que é cercado por um escudo de ligantes. O escopo deste trabalho foi a preparação de nanopartículas superparamagnéticas baratas e revestidas com extrato de tanino condensado pirolisado extraído de *Acacia mearnsii* formando nanopartículas estruturadas num núcleo-camada de cobertura, usando um processo de co-precipitação de passo único. Extrato seco de tanino de foi por terra e blindados (usando uma peneira de malha-80), e 200 g por litro foi adicionado a uma solução aquosa contendo cloreto férrico e cloreto ferroso relação molar de 2:1 em um meio básico de pH = 10. A mistura foi agitada vigorosamente por 30 minutos. Após a formação de precipitado, ele foi separado por centrifugação e depois de secar o precipitado foi pirolisado na temperatura desejada 400 °C ou 700 °C, respectivamente, a taxa de 5 ° C/min por 6 h. A caracterização do material preparado foi realizada utilizando espectroscopia de infravermelho com transformada de Fourier (FTIR), microscopia eletrônica de varredura (MEV), microscopia eletrônica de transmissão (TEMPLETON *et al.*), difração de raios x (XRD) e análise de Brunauer-Emmett-Teller (BET). As nanopartículas superparamagnéticas de óxido de ferro em tanino pirolisado (SPMIOBNPs) apresentaram tamanhos médios na faixa de 20-35 nm determinados com a ajuda da XRD e equação de Scherrer. As análises de BET e SEM confirmaram que a superfície das SPMIOBNPs apresentavam estrutura porosa, com multicamadas de microporos e isoterma do tipo H(III). As SPMIOBNPs preparadas mostraram atração muito forte em direção de campo magnético externo, usando espectroscopia de EPR, ou disco do ímã de neodýmium. As propriedades magnéticas revelaram que os SPMIOBNPs eram superparamagnéticas, com saturação de magnetização de 32 emu/g a 300 K utilizando magnetômetro SQUID. O desempenho das SPMIOBNPs na limpeza de águas mostraram um bom resultado na remoção de cromo hexavalente [Cr(VI)] da água contaminada. Os resultados mostraram que a adsorção de Cr(VI) pelas SPMIOBNPs era dependente pH, sendo que as maiores adsorções se deram no menor pH da solução de valor 2. O estudo por espectroscopia de fotoeletrônica de raios x (XPS) mostrou que a maior parte do Cr(VI) adsorvido foi reduzido a Cr(III). Neste estudo, podemos concluir que SPMIOBNPs têm o potencial de remoção de cromo hexavalente de águas residuais. O equilíbrio cinético do processo de sorção também foi investigado. A sorção de Cr(VI) pelas SPMIOBNPs preparadas seguiu o modelo cinético de pseudo - segunda ordem sugerindo que a taxa de reação de sorção depende de dois parâmetros, que podem ser a concentração do sorbato e dosagem do adsorvente. Segundo modelo de ordem indica que 'Quimissorção' ocorreu durante o processo de adsorção ou seja, uma nova espécie químicos foram criados na superfície do adsorvente.

Palavras-chave: Nanotecnologia, superparamagnético, biocarvão, tanino, co-precipitação, cromo hexavalente.

ABSTRACT

Nanotechnology is an engineering science in which the aim is to develop procedures and structures at the nanoscale, with novel properties that might offer solutions to many current problems. In this research, we describe the synthesis of superparamagnetic iron oxide (Fe_3O_4) nanoparticles. Iron oxide nanoparticles contain a core of iron oxide which is surrounded by a shell of ligands. The scope of this work is a preparation of cheap superparamagnetic nanoparticles and coating them with extract of condensed tannin extract of *Acacia mearnsii* to form core-shell structured biochar nanoparticles, using a single step co-precipitation process. Dry tannin extract of was ground and screened (using an 80-mesh sieve), and 200 g per liter was added to an aqueous solution containing ferric chloride and ferrous chloride 2:1 molar ratio at a basic medium of pH =10. The mixture has been vigorously stirred for 30 minutes. After the formation of precipitate it was separated by centrifugation and after drying the precipitate was pyrolysed on desired temperature 400 °C and 700 °C respectively at a rate of 5 °C/min for 6 h. Characterization of this material (acronym: SPMIOBNPs) was performed using Fourier transform infrared spectroscopy (FTIR), scanning electron microscopy (SEM), transmission electron microscopy , X-ray diffraction (XRD) and Brunauer–Emmett–Teller (BET) analysis. The SPMIOBNPs particles produced were contained iron oxide nanoparticles with average sizes in the range of 20-35 nm determined with help of XRD and Scherrer equation. The XRD diffractogram suggest the. SEM and BET analysis confirm its porous, multilayer micropores structure surface with H(III) type of isotherm. The FTIR analysis give an idea about the changes take place in the structure after pyrolysis attributing the formation SPMIOBNPs with characteristic functional groups. SPMIOBNPs prepared shows very strong attraction toward external magnetic field using a disc of neodymium magnet. The magnetic properties revealed that the SPMIOBNPs were superparamagnetic, with a saturation magnetization of 32 emu/g at 300 K using vibrating sample magnetometer SQUID. The performance of the SPMIOBNPs show a good result in the removing of hexavalent chromium Cr(VI) from contaminated water. The detection of total chromium in the solution was analyzed with the help of flame atomic absorption and hexavalent chromium was done with the help of 1,5-diphenylcarbohydrazide method. Equilibrium, kinetics, of the sorption process were also investigated which show some reduction of Cr(VI) to Cr(III). The results showed that Cr(VI) adsorption on SPMIOBNPs was dependent on lower pH of the solution i.e. 2. The X-ray photoelectron spectroscopy (XPS) study showed that during Chromium adsorption, some amount Fe(II) was transformed into Fe(III) by the redox reaction and Cr(VI) species were reduced to Cr(III) species. In this study we conclude that SPMIOBNPs have potential in removal of chromium hexavalent from waste water. The sorption kinetics of Cr(VI) onto SPMIOBNPs are followed the pseudo-second order kinetic model suggesting that the sorption reaction rate depends on two parameters, which might be the sorbate concentration and sorbent dosage. Second order kinetic model indicates that 'Chemisorption' took place during the adsorption process i.e. a new chemical species were created at the adsorbent surface.

Key-words : Nanotechnology, superparamagnetic, biochar, tannin, co-precipitation, hexavalent chromium.

LIST OF FIGURES

FIGURE 1 – THE 12 BASIC PRINCIPLES OF GREEN CHEMISTRY	7
FIGURE 2 – SCHEMATIC MODEL OF SPMIOBNP ZERO-VALENT IRON IN THE CORE MAINLY PROVIDES THE REDUCING POWER FOR REACTIONS WITH CONTAMINANTS.	9
FIGURE 3 – POURBAIX DIAGRAM FOR CHROMIUM SPECIATION	12
FIGURE 4 – SOIL POTENTIAL COMPARISON WITH AND WITHOUT BIOCHAR CONTENT SOIL	17
FIGURE 5 – SOME NATURAL PRODUCTS WHERE TANNIN CAN BE EXTRACTED.....	19
FIGURE 6 – ESTERIFICATION TO URIDINEDIPHOSPHATE GLUCOSE (UDP- GLUCOSE), WHERE G IS GALLYOL MOLECULE	20
FIGURE 7 – STRUCTURE OF 1,2,3,4,6 PENTAGALLYOL -O-D-GLUCOSE	20
FIGURE 8 – BASIC FLAVONOID RING STRUCTURE AND NUMBERING	21
FIGURE 9 – STRUCTURES OF (+)-CATECHIN, (-)-EPICATECHIN, (-)- CATECHIN AND.....	22
FIGURE 10 – LINKAGES OF C4–C8 OF FLAVONOID MONOMERS.....	23
FIGURE 11 – SCHEMATIC REPRESENTATION OF THE STAGES OCCURRING IN BINDING AND PRECIPITATION OF POLYPHENOLS BY SALIVARY PROLINE-RICH PROTEINS	23
FIGURE 12 – IMAGE OF <i>ACACIA MEARNSII</i>	24
FIGURE 13 – X-RAYS SCATTERING FROM PLANES OF ATOMS EXHIBIT INTERFERENCE EFFECTS LEADING TO SPECIFIC ANGLES WHERE REFLECTIONS ARE OBSERVED.....	26
FIGURE 14 – X-RAY POWDER DIRACTION PATTERNS FOR $Fe_3O_4^{-1}$ AND $Fe_3O_4^{-2}$	27
FIGURE 15 – A) THE PARAMAGNETIC MAGNETIZATION AND SUSCEPTIBILITY ARE POSITIVE B) THE PARAMAGNETIC SUSCEPTIBILITY IS TEMPERATURE DEPENDENT.	30
FIGURE 16 – BEHAVIOR OF MAGNETIC FIELD ON DIFFRENT TYPE OF MAGNETIC MATERIALS	31
FIGURE 17 – MAGNETIC HYSTERESIS (B-H) LOOP	32
FIGURE 18 – HYSTERESIS LOOPS OF DIFFERENT TYPES OF MATERIALS	33
FIGURE 19 – FC-ZFC CURVES PRODUCED WHEN APPLYING A MAGNETIC FIELD.	34

FIGURE 20 – BLOCK DIAGRAMS OF A TYPICAL EPR SPECTROMETER	35
FIGURE 21 – ZEEMANN EFFECT SHOWING ENERGY SPLITTING OF UNPAIRED ELECTRON SPINS IF AN EXTERNAL MAGNETIC FIELD B IS APPLIED.....	36
FIGURE 22 – COMPARISON OF ABSORPTION SPECTRUM AND EPR SPECTRUM	37
FIGURE 23 – SCHEMATIC OF THE OPTICAL, TRANSMISSION AND SCANNING ELECTRON MICROSCOPES.....	38
FIGURE 24 – TGA THERMOGRAPH FOR A HYPOTHETICAL MIXTURE.....	39
FIGURE 25 – THE SPMIOBNP AFTER PYROLIS	47
FIGURE 26 – THE PURE CLEAN SPMIOBNP AFTER WASHING AND DRYING.....	48
FIGURE 27 – EFFECT OF THE SOLUTION PH ON SIZES OF SPMIOBN	49
FIGURE 28 – EFFECT OF TEMPERATURE ON PARTICLE SIZE OF SPMIOBNS	49
FIGURE 29 – NANOPARTICLE SYNTHESIS BY THERMAL DECOMPOSITION METHOD AND SIZE SELECTION PROCESSES.....	50
FIGURE 30 – REACTION OF CR(VI) WITH 1,5-DIPHENYLCARBOHYDRAZIDE	52
FIGURE 31 – FTIR SPECTRUM OF TANNIN EXTRACT OF <i>ACACIA MEARNsii</i>	56
FIGURE 32 – COMPARATIVE FTIR SPECTRUM OF SPMIOBNP 400 AND SPMIOBNP 700.....	56
FIGURE 33 – 1.TANNIN FESO ₄ ; 2.NANO META TANFLOC ; 3. NANO META TANNIN; 4.TANNIN FECL ₂	57
FIGURE 34 – COMPARATIVE EPR SPECTRA BETWEEN THE REFERENCE I.E. SPMIOBNPS 700 AND SPMIOBNPS 400 RESPECTIVELY.	58
FIGURE 35 – SEM MICROGRAPHS OF PURE TANNIN EXTRACT FROM <i>ACACIA MEARNs</i>	59
FIGURE 36 – SEM-EDX ANALYSIS OF TANNIN EXTRACT FROM <i>ACACIA</i> <i>MEARNsII</i>	60
FIGURE 37 – SEM MICROGRAPHS OF SPMIOBNP.....	61
FIGURE 38 – SEM-EDS SPECTRA OF SPMIOBNP	61
FIGURE 39 – TEM MICROGRAPHS OF SPMIOBNP.....	63
FIGURE 40 – XRD DIFFRACTOGRAM OF THE SPMIOBNP, THE INSET SHOWS SPECIFIC 2 θ VALUES COMPARED WITH ICDD REFERENCE CARD NO. 86-1340.....	64
FIGURE 41 – TGA/ DTG ANALYSIS CURVES FOR SPMIOBNP	65
FIGURE 42 –THE ATTRACTION OF SPMIOBNP 400 AND SPMIOBNP 700 UNDER AN EXTERNAL MAGNETIC FIELD	66

FIGURE 43 – MAGNETIZATION CYCLES OF SPMIOBNP 400 MEASURED AT 10 K.....	67
FIGURE 44 – MAGNETIZATION CYCLES OF SPMIOBNP 400 MEASURED AT 300 K.....	67
FIGURE 45 – ZERO FIELD COOLING (ZFC) AND FIELD COOLING (FC) MAGNETIZATION CURVES FOR THE SPMIOBNP 400.....	68
FIGURE 46 – BET ISOTHERM OF THE SPMIOBNPS 400 NITROGEN ADSORPTION (CIRCLES) AND DESORPTION (SQUARES).....	69
FIGURE 47 – FTIR SPECTRUM OF SPMIOBNP 400 (A) , FTIR SPECTRUM OF SPMIOBNP 400 LOADED WITH HEXAVALENT CHROMIUM (B).	70
FIGURE 48 – (A), (B) SEM MICROGRAPHS OF SPMIOBNP 400 AND (C), (D) SPMIOBNP 400 LOADED WITH HEXAVALENT CHROMIUM	71
FIGURE 49 – SEM-EDS SPECTRA OF SPMIOBNP 400 WITH QUANTITATIVE TABLE INSERTED.	72
FIGURE 50 – SEM-EDS SPECTRA OF SPMIOBNP 400 LOADED WITH HEXAVALENT CHROMIUM QUANTITATIVE TABLE INSERTED	72
FIGURE 51 – XPS CORE LEVEL SPECTRA OF SPMIOBNP 400	73
FIGURE 52 – XPS CORE LEVEL SPECTRA OF SPMIOBNP 400 LOADED WITH HEXAVALENT CHROMIUM	74
FIGURE 53 – MAGNIFIED XPS CORE LEVEL SPECTRA OF SPMIOBNP 400 LOADED WITH HEXAVALENT CHROMIUM.....	74
FIGURE 54 –THE POINT OF ZERO CHARGE (PZC) OF SPMIOBNP 400	75
FIGURE 55 – PERCENTAGE REMOVAL OF HEXAVALENT CHROMIUM BY SPMIOBNP 400 AT PH 2 TO 5	75
FIGURE 56 – COMPARASON OF ALL THE CHROMIUM SPECIES REMOVED WITH TIME.....	78
FIGURE 57 – FIRST ORDER PLOT OF TOTAL CHROMIUM ADSORPTION	80
FIGURE 58 – FIRST ORDER PLOT OF HEXAVALENT CHROMIUM ADSORPTION.....	80
FIGURE 59 – FIRST ORDER PLOT OF TRIVALENT CHROMIUM ADSORPTION	81
FIGURE 60 – SECOND ORDER PLOT OF TOTAL CHROMIUM	82
FIGURE 61 – SECOND ORDER PLOT OF HEXAVALENT CHROMIUM ADSORPTION.....	82
FIGURE 62 – SECOND ORDER PLOT OF TRIVALENT CHROMIUM ADSORPTION.....	83

LIST OF TABLES

TABLE 1 – TYPES OF CHROMIUM IONS STABLE IN VARIOUS AQUEOUS CONDITIONS.....	12
TABLE 2 – QUANTITATIVE ELEMENTAL RESULTS OF TANNIN EXTRACT.....	60
TABLE 3 – QUANTITATIVE ELEMENTAL RESULTS OF SPMIOBNP.....	62
TABLE 4 – CONCENTRATIONS OF CHROMIUM (MEAN \pm SD ₆ AFTER ADSORPTION BY SPMIOBNP AT DIFFERENT PH VALUES (T = 25 \pm 0.2 °C; M = 100 MG OF ADSORBENT).....	76
TABLE 5 – PERCENTAGE REMOVAL OF CHROMIUM IN 120 HOURS.....	76
TABLE 6 – PERCENTAGE REMOVAL OF CHROMIUM.....	76
TABLE 7 – QUANTITATIVE TABLE OF INITIAL VERSAS FINAL CONCENTRATION OF CHROMIUM SPECIES AT DIFFERENT TIME INTERVAL.....	77
TABLE 8 – PERCENTAGE REMOVAL OF CHROMIUM.....	77
TABLE 9 – DETERMINATION OF Q VALUE	79
TABLE 10 – CONVERTING TIME AND CONCENTRATION DATA t/qt	81
TABLE 11 – ALL RESULTS AND KINETIC CONSTANTS	83

LIST OF ABBREVIATIONS

ATSDR – Agency for Toxic Substances and Disease Registry

BET – Brunauer–Emmett–Teller (BET) theory

BJH – Barrett, Joyner, Halenda method

CCD – Charge-Coupled Device

CPS – Counts per second

CNS – Central nervous system

CNPq – Conselho Nacional de Desenvolvimento Científico e Tecnológico (Brasil)

Cr(III) – Trivalent Chromium

Cr(VI) – Hexavalent Chromium

CS – Chemical Shift

DDT – Dichlorodiphenyltrichloroethane

DNA – Deoxyribonucleic acid

DPC – Diphenylcarbazide

DP – Diffraction pattern

DSC – Differential Scanning Colorimetry

DTG – Differential Thermal Analysis

EDS – Energy-dispersive X-Ray Spectroscopy

Fe(II) – Iron in second (2) oxidation state

Fe(III) – Iron in third (3) oxidation state

EELS – Electron Energy-Loss Spectroscopy

EG – Ethylene glycol

EN – Electronegativity

EPR – Electron Paramagnetic Resonance spectroscopy

ESCA – Electron Spectroscopy for Chemical Analysis

FC-ZFC – Field Cooling – Zero Field Cooling

FEG – Field Emission Gun

FFT – Fourier Fast Transformation

FTIR – Fourier Transformation Infrared Spectroscopy

FWHM – Full Width at Half Maximum

HPLC – High performance liquid chromatography

ICDD – International Centre for Diffraction Data

LD50 – Lethal Dosage Values

MNPs – Magnetic nanoparticles

PAHs – Polycyclic aromatic hydrocarbons

SEM – Scanning Electron Microscope

SQUID – Superconducting Quantum Interference Device

SPMIOBNPs – Superparamagnetic Iron Oxide Biochar Nanoparticles

TEM – Transmission Electron Microscope

TGA – Thermogravimetric Analysis

TMX – Thiamethoxam

TREG – Triethylene glycol

TWAS – The World Academy of Sciences

USEPA – US Environmental Protection Agency

WHO – World Health Organization

XPS – X-Ray Photoelectron Spectroscopy

XRD – X-Ray Diffraction

TABLE OF CONTENT

RESUMO	vi
ABSTRACT	vii
LIST OF FIGURES	viii
LIST OF TABLES	xi
LIST OF ABBREVIATIONS	xii
1. INTRODUCTION	1
2. LITERATURE REVIEW	4
2.1. Nanotechnology	4
2.2. Green Chemistry	5
2.2.1. 12 Principles of Green Chemistry	5
2.3. Green Chemistry and Nanotechnology	7
2.4. Properties of Iron oxides	7
2.5. Magnetic Nanoparticles	8
2.6. Superparamagnetic Iron Oxide Biochar Nanoparticles (SPMIOBNPs)	9
2.7. CHROMIUM	10
2.7.1. Chromium Speciation	10
2.7.2. Sources of Chromium	12
2.7.3. Uses of Chromium	13
2.7.4. Toxicity of Chromium in Water	14
2.7.5. Overview of Chromium Removal Technologies	15
2.8. BIOCHAR	16
2.8.1. Importance of Biochar	17
2.8.2. Some Disadvantages of Biochar	18
2.9. TANNINS	18
2.9.1. Tannin-Protein Binding	22
2.9.2. Tannins in Ruminant Nutrition	23
2.9.3. Condensed Tannin from <i>Acacia mearnsii</i>	24

2.9.4. Tanfloc.....	25
2.10. Nanoparticles Characterization Techniques.....	25
2.10.1. X-Ray Diffraction	26
2.10.2. Magnetic Properties.....	27
2.10.3. EPR Analysis.....	34
2.10.4. Scanning Electron Microscope (SEM)	37
2.10.5. Transmission Electron Microscopy (TEMPLETON <i>et al.</i>).....	37
2.10.6. Thermogravimetric Analysis (TGA)	38
2.11. Sorption Theory	39
2.11.1. Factors Affecting Adsorption	40
2.11.2. Kinetic Study of Sorption	41
3. OBJECTIVES	43
3.1. General Objectives.....	43
3.2. Specific Objectives	43
4. MATERIALS AND METHODS.....	45
4.1. Chemicals and Reagents.....	45
4.2. Experimental Equipments	45
4.2. Synthesis of SPMIOBNs	46
4.3. Co-precipitation Method of Preparation of (SPMIOBNs).....	46
4.3.1. Effect of pH on Particle Size of SPMIOBNs	48
4.3.2. Effect of Temperature on Particle Size of SPMIOBNPs.....	49
4.4. Alternative Method of Synthesis.....	50
4.5. Methods Used for Characterization of the Samples	50
4.6. Stock and Standard Solutions	52
4.7. Hexavalent Chromium.....	52
4.8. Total chromium	53
5. RESULTS AND DISCUSSION.....	55
5.1. Characterization of SPMIOBNPs	55

5.1.1.	FTIR Analysis	55
5.1.2.	EPR STUDY	57
5.1.3.	SEM-EDS of Tannin Extract and SPMIOBNPs.....	58
5.1.4.	Transmission Electron Microscopy	62
5.1.5.	XRD Diffraction Analysis.....	63
5.1.6.	Thermogravimetric Analysis (TGA).....	64
5.1.7.	Magnetic Properties of SPMIOBNPs	65
5.1.8.	BET.....	68
5.2.	Chromium Removal Results.....	69
5.2.1.	FTIR Analysis of SPMIOBNPs and SPMIOBNPs 400 Loaded with Cr(VI)	69
5.2.2.	SEM EDS and XPS analysis of SPMIOBNPs and SPMIOBNPs Loaded with Cr(VI)	70
5.2.3.	Quantitative Analysis of Hexavalent Chromium	74
5.2.4.	Kinetic Study.....	76
6.	CONCLUSIONS.....	84
6.1	Suggestions For Future Work	84
	REFERENCES	86
7.	APPENDICES.....	101

1. INTRODUCTION

The worth of life on earth is link intimately to the overall quality of the environment. In early eras, it was believed that land, water and other natural resources have unlimited abundance but today, it is not true; in greater or lesser degree the human civilization has shown the carelessness and negligence in using them. The problems linked with contaminated sites now assume increasing prominence in many countries throughout the globe. The living conditions today have certainly improved largely at the cost of environmental degradation. Global progress in industrialization, however, raises new challenges, especially in the field of environmental protection and conservation. We lost respect for the basic element to our survival. Water is the most vital compound on the earth for all the life activities. It is a powerful resource that we cannot live without it, so we must do everything possible to preserve its quality and the life inside it for today and the future. It creates, sustains and has the ability to take life. We dump sewage, chemicals and garbage into our own water and, exploit the fish and animals living in the waters almost or to the point of extinction. We pollute and destroy the water bodies (lakes, rivers, ocean and ground water etc.) without any regard for what the outcome to our ecosystem could and will be if it continues. The rapid increase in the industrialization and urbanization creates the problem of pollution including heavy metal pollution. The pollution due to heavy metals is a widespread problem and causes a major environmental degradation in each section of environment. It is truly a matter of concern to everybody as it has direct influence on human and environmental health (DHAL *et al.*, 2013). The expansion of growth is led by two major factors. Firstly, each developed or developing countries are facing problems in the environmental areas like increase of population, drinking water, global warming, ozone depletion, ground water contamination, management of wastes and other environment problems. Secondly, these problems raise awareness in parallel way to solve the above problems. The air, water and soil are getting filled up with hazardous wastes. Water is a vital natural resource, which forms the basis of all life. About 71% of the earth's surface is covered by water and about 60-70% of all the living body including plants and animals are made up of water. Water is essential for human beings for survival, sustainability and development. At the same time, water is an unusual

good, and shortage sometimes results in crises. Both facts lead to the simple conclusion that lack of water hinders development of life. This can be assessed from global trends, as well as local struggles for better access for people to safe and sufficient drinking water (ROSEMANN, 2005).

Heavy metals (Hg, Pb, Cr etc.) can be found in industrial wastewater/effluents and are considered as dangerous by many environmentalists. Prolonged exposure to heavy metal ions has been found to cause the degradation of ecosystems which harm the inhabitants. Heavy metals/ metalloids are the main group of inorganic contaminants. The discharge of Cr (VI) into aquatic ecosystems has become a matter of concern in all the tannery areas in India and Morocco over the last few decades (ILIAS *et al.*, 2011). This pollutant is introduced into the aquatic systems of leather processing units as a result because of chrome salt in tanning process of leather. A considerable huge area of land is contaminated with them due to the use of sludge or municipal compost, pesticides, fertilizers, and emissions from municipal waste, car exhausts, residues from mines, and smelting industries.

Metals are present naturally in the earth's crust at various levels but many metals are essential and beneficial in nutrition indispensable components of body cells (e.g. copper, iron, manganese, zinc). All metals are toxic at higher concentrations. Specifically, any metal or species may be considered as "contaminant" if it occurs where it is unwanted, or in a form or concentration that causes an adverse effect on humans also other living organism. (Natural waters are contaminated with a number of pesticides or their transformation products. Herbicides and nematicides are potential contaminants of natural waters, because they are directly applied to the soil, and are transported into ground water or percolated to the surface water. Insecticides are transported into ground water in dust or rainwater, which are washed out by precipitation and fall on the soil. During the last decade, the use of many chemical substances in agriculture without any control and studies about their behavior has become a focus of research.

According to the United States Census Bureau the world population is reaches 7.22 billion marks and it is estimates that, by 2050 this number reaches to 9.5 billion (USCENSUSBUREAU, 2015). The developing countries like Brazil are already under water shortage because had no policy and technology to attack the purification problems. Internationally, 780 million people lack access to safe drinking water, according to the United Nations. By 2030, 47 per cent of the world's

population will be living in areas of high water stress, according to the Organization for Economic Co-operation and Development's Environmental (OECD) Outlook to 2030 report (OECD, 2008). Some analysts and experts fears that wars of the future will be fought over blue gold, as thirsty people, opportunistic politicians and powerful corporations battle for declining resources. Because of these concerns, a number of steps being taken to control water pollution of the available water content which seems to be insufficient. More research inputs are required to avoid conflicts in future.

Rural populations depend on surface water from the rivers, lakes ,and ground water for potable uses such as washing of clothes and drinking including animals. The contamination of heavy metals in natural and ground water resource possesses a great threat to millions of people in many regions of the world such as China, India, Brazil, Pakistan, Bangladesh, Nepal, Myanmar, Cambodia and Thailand. In recent years, the development of efficient green chemistry methods for synthesis of metal nanoparticles has become a major focus of researchers. Green chemistry can be defined as the practice of chemical science and manufacturing in a manner that is sustainable, safe, and non-polluting and that consumes minimum amounts of materials and energy while producing little or no waste material. Nanotechnology refers to research on materials that are nanometer in size. Researchers agree that the safest possible future for advancing nanotechnology in a sustainable world can be reached by using green chemistry . Therefore, In this work, we offer a rapid, non-toxic, facile and green synthesis route to prepare magnetite nanoparticles in only one step reaction, characterized , and used tannin iron oxide magnetic nanoparticle to study the removing capacity of Cr(IV) from water and also tried these matrixes for adsorption and sorption of the pesticides.

2. LITERATURE REVIEW

2.1. Nanotechnology

Nanoscience and nanotechnology refer to the synthesis, characterization, and utilization of nanostructured materials which are characterized by at least one dimension in the nanometer ($1\text{nm} = 10^{-9}\text{ m}$) range. Such nanostructured systems constitute a link between single molecules and a bulk systems. Individual nanostructures involve clusters, nanoparticles, nanocrystals, quantum dots, nanowires and nanotubes (MODY *et al.*, 2010).

The chemical and physical properties of nanomaterials can significantly differ from those of bulk materials of same chemical composition. The uniqueness of the structural characteristics, energetics, response, dynamics and chemistry of nanostructures constitutes the experimental and conceptual background for the field of nanoscience. Suitable control of properties and response of nanostructures can lead to new devices and technologies. Nanotechnology development and production presents a unique opportunity to offer a more sustainable approach to protect public health and the environment. Many regions of the world face multiple challenges in sustainably supplying potable water for human use and clean water for agriculture, food processing, energy generation, mineral extraction, chemical processing, and industrial manufacturing. Demand for water is increasing due to population growth at the same time as water supplies are being stressed by the increasing contamination and salinization of fresh waters, due to anthropogenic and climate changes. Nanotechnology has the potential to provide efficient, cost-effective, and environmentally sustainable solutions for supplying potable water for human use and clean water for agricultural and industrial uses by making and introducing nanosorbents, nanocatalysts, nanobiocides and nanoparticle-based filtration systems and devices. Nanotechnology is providing materials scientists and chemists with a wide range of ingenious applications, however these new materials raises various issues and concerns (GWINN & VALLYATHAN, 2006, KARLSSON *et al.*, 2008). Some important concerns are as follow:

- Nanoparticles are small enough to be absorbed by the skin so could cause irritation.
- Nanoparticles has large surface area and are already being used in various products and the exposure (inhalation, ingestion) can make serious problem.

2.2. Green Chemistry

Green chemistry can be defined as the practice of chemical science and manufacturing in a manner that is sustainable, safe, and non-polluting and that consumes minimum amounts of materials and energy while producing little or no waste material. Green chemistry is based on the use of principles that reduce or eliminate the use of hazardous reagents and solvents in the design, preparation and application of materials. In this framework, using the strategies very promising for greener production of any synthetic materials, due to shorter reaction times, reduced energy consumption, and better yields. Green chemistry principles are, for example, used to manufacture nanomaterials from less toxic chemicals, using less energy and less of certain scarce raw resources.

2.2.1. 12 Principles of Green Chemistry

The 12 principles of green chemistry originally defined by Anastas and Warner (ANASTAS & WARNER, 2000) are summarized in Figure 1 (BACCILE *et al.*, 2009) have now been applied to the design of a wide range of chemical products and processes with the aims of minimizing chemical hazards to health and the environment, reducing waste, and preventing pollution. These 12 Principles are as follows:

1. Prevention

It is better to prevent waste than to treat or clean up waste after it has been created.

2. Atom Economy

Synthetic methods should be designed to maximize the incorporation of all materials used in the process into the final product.

3. Less Hazardous Chemical Syntheses

Wherever practicable, synthetic methods should be designed to use and generate substances that possess little or no toxicity to human health and the environment.

4. Designing Safer Chemicals

Chemical products should be designed to affect their desired function while minimizing their toxicity.

5. Safer Solvents and Auxiliaries

The use of auxiliary substances (e.g., solvents, separation agents, etc.) should be made unnecessary wherever possible and innocuous when used.

6. Design for Energy Efficiency

Energy requirements of chemical processes should be recognized for their environmental and economic impacts and should be minimized. If possible, synthetic methods should be conducted at ambient temperature and pressure.

7. Use of Renewable Feedstocks

A raw material or feedstock should be renewable rather than depleting whenever technically and economically practicable.

8. Reduce Derivatives

Unnecessary derivatization (use of blocking groups, protection and deprotection, and temporary modification of physical/chemical processes) should be minimized or avoided if possible, because such steps require additional reagents and can generate waste.

9. Catalysis

Catalytic reagents (as selective as possible) are superior to stoichiometric reagents.

10. Design for Degradation

Chemical products should be designed so that at the end of their function they break down into innocuous degradation products and do not persist in the environment.

11. Real-time analysis for Pollution Prevention

Analytical methodologies need to be further developed to allow for real-time, in-process monitoring and control prior to the formation of hazardous substances.

12. Inherently Safer Chemistry for Accident Prevention

Substances and the form of a substance used in a chemical process should be chosen to minimize the potential for chemical accidents, including releases, explosions, and fires.

WASTE - RECYCLE	HEALTH	PROCESSING - ENERGY
P.1 – Prevent waste	P.2 – Designing safer chemicals	P.5 – Catalysis
P.4 – Renewable feedstock	P.3 – Less hazardous chemical synthesis	P.7 – Atom economy
P.5 – Catalysis	P.8 – Safer solvents/ reaction medium	P.9 – Design for energy efficiency
P.6 – Reduce derivatives	P.12 – Inherently safer chemistry	P.11 – Real-time monitoring and process control
P.7 – Atom economy		
P.10 – Design for degradation/design for end of life		

FIGURE 1 – THE 12 BASIC PRINCIPLES OF GREEN CHEMISTRY
SOURCE: BACCILE et al., 2009

2.3. Green Chemistry and Nanotechnology

In recent years, the development of efficient green chemistry methods for synthesis of metal nanoparticles has become a major focus of researchers. Researchers agree that the safest possible future for advancing nanotechnology in a sustainable world can be reached by using green chemistry (KARN, 2008). Green chemistry means designing chemical products and processes in a way that reduces or eliminates hazardous substances from the beginning to end. Green nanomaterial is now a major objective of research in nanotechnology. Besides the available chemical methods, the biosynthesis of nano-materials using plants biomass is now looking promising as a source for producing nanoparticles. Magnetic nanoparticles are important due to their easy recovery from the reaction mixture. The synthesis of magnetite nanoparticles has been intensively developed not only for its fundamental scientific interest but also for many technological applications: such as magnetic resonance imaging, ferrofluids for audio speakers, magnetic targeted drug delivery, and magnetic recording media. In particular, the use of magnetite nanoparticles as adsorb-Therefore, the utilization of biomass has emerged as a novel method for the synthesis of nanoparticles (DORNIANI *et al.*, 2012).

2.4. Properties of Iron oxides

Iron is a very good element for decontamination of the environment (Benjamin, 1983) since it is both a reducing and oxidizing agent, non-toxic and cheap. It occurs as Fe(II) and Fe(III) in a diversity of minerals including many types of iron oxides. The iron oxides are in fact oxides, hydroxides or oxihydroxides. Most

of the compounds are thermodynamically stable in natural systems (e.g. goethite, hematite, and magnetite) while others can be designated as intermediates only (ferrihydrite, maghemite) (FAUCONNIER *et al.*, 1997). Iron oxides exist in many forms in nature. Hematite (α -Fe₂O₃), Magnetite (Fe₃O₄) and maghemite (γ -Fe₂O₃) are the most common forms. The different iron oxides have their own characteristics and qualities, governed by the mineral structure (SANTOYO SALAZAR *et al.*, 2011).

Research on the synthesis of iron oxide nanomaterials has increased abruptly in the recent decade. Recently, functionalized iron oxide nanoparticles have also been used in many advanced nano-technological applications. The most important advantage of nano-sized iron oxides among other nanomaterials are due to its relatively low toxicity and biodegradability. It is observed that generally, amorphous metal oxides show great industrial potential in many advanced applications such as solar energy transformation, electronics, electrochemistry, manufacture of magnetic storage media, sorption and purification processes and catalysis (PERKAS *et al.*, 2001). Applications of iron oxide nanoparticles range from technical and engineering fields to medical and neuro-biological fields which includes MRI contrast enhancement (WEINSTEIN *et al.*, 2010), Targeted drug delivery (CHERTOK *et al.*, 2008), Magnetic field-induced hyperthermia (MAIER-HAUFF *et al.*, 2007), Cell labeling / cell tracking (CROMER BERMAN *et al.*, 2011), Magnetic transfection (PICKARD & CHARI, 2010).

In above all, the applications, amorphous Fe (III) oxide plays a vital role, especially because of its superior catalytic activity, super paramagnetic behavior, and the large specific surface area of the nanoparticle (MACHALA *et al.*, 2007).

2.5. Magnetic Nanoparticles

Magnetic properties of nanomaterials are powerful manipulation and detection tools which are studied for a long time. Magnetic fields are not harmful to a human so it is believed that magnetic nanoparticles can be used for biomedical in vivo and, of course, in vitro applications. The latest researches tell about high potential of magnetic nanoparticles in environmental remediation applications, such as removal of heavy metals from waste waters. Magnetic properties depend on a size, shape, structure, crystallinity, synthesis method and chemistry of materials. The most widely investigated magnetic nanomaterials are iron, cobalt and nickel compounds and alloys.

2.6. Superparamagnetic Iron Oxide Biochar Nanoparticles (SPMIOBNPs)

Development of novel and cost-effective nanomaterials for environmental remediation, pollution detection and other applications has attracted considerable attention. For example, iron nanoparticles can remove contaminants from soil and nanosized sensors hold promise for improved detection and tracking of contaminants. The magnetic nanoparticles of rust can also be used to removed arsenic As from water (YAVUZ *et al.*, 2006). Recent advances suggest that many of the issues involving water quality could be resolved by using nanoparticles, nanofiltration or other products resulting from the development of nanotechnology. In recent years, the synthesis and utilization of iron oxide magnetic nanoparticles (MNPs) with novel properties and functions have been widely studied, due to their size in nano-range, high surface area to volume ratios and superparamagnetism. These MNPs not only have a large removal capacity, fast kinetics and high reactivity for contaminant removal due to their extremely small particle size and high surface area to volume ratio, but also one more important property, magnetism. This is a useful property for water and wastewater treatment systems. The high reactivity of the magnetic nanoparticles (Fig. 2) for pollutant removal, a compact and efficient water or wastewater treatment system can take advantage of this (TANG & LO, 2013, KHARISOV *et al.*, 2014).

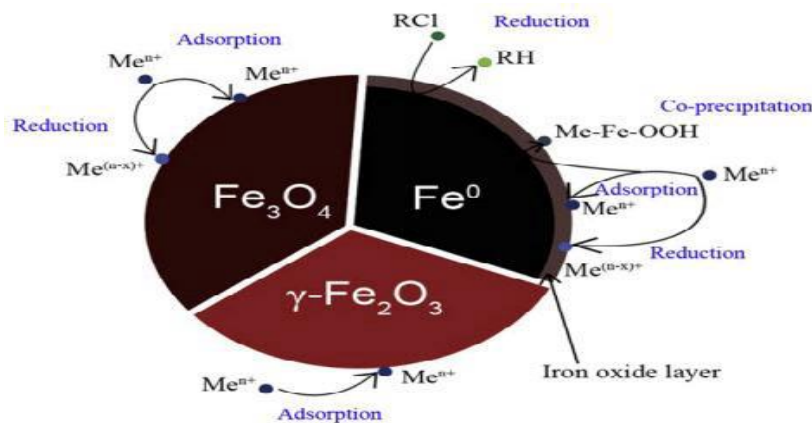


FIGURE 2 – SCHEMATIC MODEL OF SPMIOBNP ZERO-VALENT IRON IN THE CORE MAINLY PROVIDES THE REDUCING POWER FOR REACTIONS WITH CONTAMINANTS. SOURCE : KHARISOV *et al.*, 2014

The core of magnetic nanoparticles consists of mainly zero-valent iron and provides the reducing power for reactions with environmental pollutants. The shell is basically consist of Fe⁰, iron oxides and hydroxides formed from the oxidation of zero-valent iron. The shell provides sites for chemical complex formation (LI *et al.*, 2006).

In this work, we offer a rapid, non-toxic, facile and green synthesis route to prepare a superparamagnetic iron oxide biochar nanoparticles (SPMIOBNPs) from tannin and tanfloc extracted from *acacia mearnsii* in only one step reaction, characterized (BAKER *et al.*, 2013, M. AWWAD & M. SALEM, 2013), and used tannin iron oxide magnetic nanoparticle to study the removing capacity of Cr(IV) from water (PANG *et al.*, 2011) . SPMIOBNPs are subject to air oxidation and are easily aggregated in aqueous systems. Thus, for the application of these SPMIOBNPs in various fields the stabilization of the iron oxide particles by surface modification is desirable. The magnetic structure of the surface layer, which is usually greatly different from that in the core of the nanoparticles, can have a notable effect on the magnetic properties of nanoparticles.

2.7. CHROMIUM

Chromium (Cr) is a lustrous steel-gray metal present in the group 6th of periodic table having atomic number 24 and Atomic weight 51.996, density of 7.19 g cm⁻³, electronegativity (EN) value of 1.66 (Pauling scale), melting point is 2180 K or 1907 °C and the crystal structure of Cr is body-centered cubic. The ground-state electron configuration of Cr is [Ar] 3d⁵ 4s¹ (BARBALACE, 2014). Chromium was first discovered in the Siberian red lead ore (crocoite) in 1798 by the French chemist Louis Vauquelin. The word chromium was derived from Greek khr ma, meaning color, due to its ability to produce vivid, colorful compounds, such as chrome oxide. Chromium is hard, brittle and very corrosion resistant (JEFFERSON, 2014) . Chromium exist in the oxidation states of -2 to +6 as -1 and -2 are the least important states while the +2, +3 and +6 are the most common species.

2.7.1. Chromium Speciation

Chromium in natural environments occurs mainly in the oxidation states of Cr(III) and Cr(VI). In soil, the chromium mobility is dependent on the pH condition in

water and soil moisture and type of specie. Cr(VI) compounds are generally more soluble, mobile and bioavailable compared to Cr(III) species. To understand behavior of chromium and its role in the environment, it is essential to know forms (speciation) of Cr species, their stability, and inter-conversion processes between various forms of chromium. Cr(VI) compounds are found to be more toxic than Cr(III) compounds because of the high solubility and mobility of Cr(VI) in water (KABAY *et al.*, 2003). Cr(III) is less mobile, less toxic and is mainly found in organic matter of soil and aquatic environments (BECQUER *et al.*, 2003). Under reducing conditions, chromium occurs mostly as Cr(III) species. In aqueous systems, Cr(III) can be present as Cr^{3+} , $\text{Cr}(\text{OH})^{2+}$, $\text{Cr}(\text{OH})_2^+$ and $\text{Cr}(\text{OH})_4^-$. Between pH 6 – 12, Cr(III) is sparingly soluble and the precipitation of $\text{Cr}(\text{OH})_3$ predominates. Cr(VI) occurs as oxyanions HCrO_4^- or CrO_4^{2-} when $\text{pH} > 6.5$ as shown in Figure 3, Cr(VI) is primarily present in the form of CrO_4^{2-} , while when $\text{pH} < 6.5$, HCrO_4^- will be the predominant Cr(VI) species (JIANG *et al.*, 2013). In addition to pH and redox potential, the nature and concentration of reducers, oxidation mediators, and complexing agents also play an important role, and these factors appear to account for the substantial amounts of Cr(III) in many oxidizing environments. Cr(VI) occurs in the environment as oxyanions HCrO_4^- and CrO_4^{2-} depending on soil pH. Because they are negatively charged, they are the most mobile forms of chromium in soils. CrO_4^{2-} can be adsorbed by Fe and Al oxides by inner-sphere surface complexation. This adsorption is pH dependent and only favored at low pH values, where reduction to Cr(III) is favored as well (MOHAN *et al.*, 2005, REEDER *et al.*, 2006). AAA (DAI *et al.*, 2012). Cr(VI) compounds are found to be more toxic than Cr(III) compounds because of the high solubility and mobility of Cr(VI) in water and soil and oxidation power (SHARMA *et al.*, 2008).

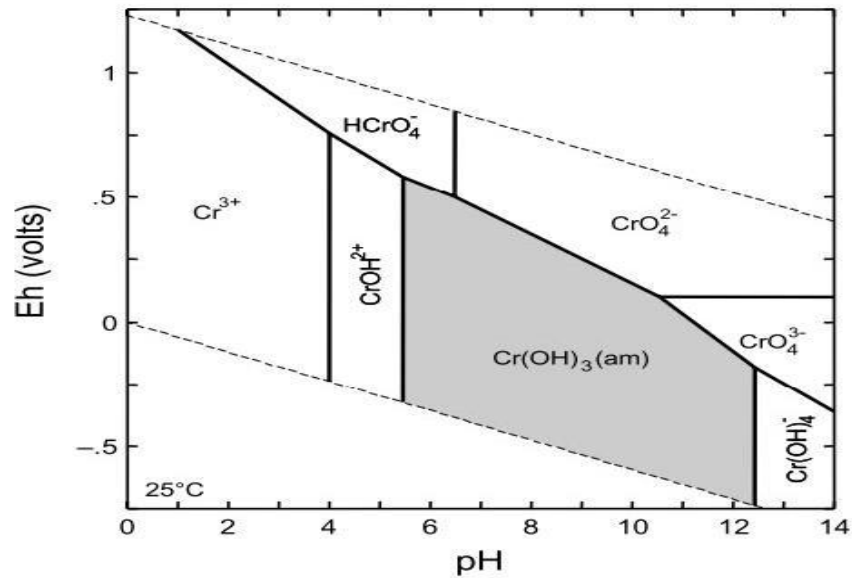


FIGURE 3 – POURBAIX DIAGRAM FOR CHROMIUM SPECIATION
SOURCE : REEDER *et al.*, 2006.

TABLE 1 – TYPES OF CHROMIUM IONS STABLE IN VARIOUS AQUEOUS CONDITIONS

Chromium Species	Aqueous pH Conditions	Dominant Cr Aqueous Species
Cr (III)	pH < 3.5	Cr ³⁺
	pH > 3.5	CrOH ²⁺
	increased pH	Cr(OH) ₂ ⁺
	increased pH	Cr(OH) ₃ ⁰ (Aq)
	increased pH	Cr(OH) ₄ ⁻
	Higher Cr concentrations	Cr ₂ (OH) ₂ ⁴⁺
	Higher Cr concentrations	Cr ₃ (OH) ₄ ⁵⁺
Cr (VI)	pH < 6.5 & Conc < 30 mM	HCrO ₄ ⁻
	pH < 6.5 & Conc > 30 mM	Cr ₂ O ₇ ²⁻
	pH > 6.5	CrO ₄ ²⁻

2.7.2. Sources of Chromium

Chromium is released in the environment due to natural sources as well as anthropogenic sources. Natural sources refer to the formation of chromium compounds naturally i.e. interaction, reaction, and degradation of naturally occurring chromium minerals, ores and rocks. Chromite (FeO.Cr₂O₃ / FeCr₂O₄) is the main source of mining chromium and some other famous natural sources of chromium

are crocoite (PbCrO_4), and chrome ochre (Cr_2O_3) respectively (MOHAN *et al.*, 2011). The largest deposits are located in Kazakhstan, South Africa and India. Chromium ores are also mined today in large quantity from Turkey, Brazil, Zimbabwe, China, Finland, Pakistan and the Philippines (KABATA-PENDIAS, 2010).

Anthropogenic activities refers the manufactured activities that are taken into consideration in the formation of chromium compounds. The level of chromium concentration in environment due to human activities is much higher compared to natural sources. Mostly Cr(VI) besides with some quantity of Cr(III) found in the industrial effluents such as metallurgical refractory, chemical and pigment industry whereas tannery, textile, and electroplating industry (DANIEL *et al.*, 2009). Some other prominent sources of chromium include the chromite-ore processing industry, automobile, paper and pulp, fertilizer, textile, steel, metal finishing, magnetic tapes, leather tanning, wood protection, petroleum refining, brass, electrical and electronic equipment (KABATA-PENDIAS & MUKHERJEE, 2007). These industries produce huge quantities of chromium containing effluents that contaminate surface and ground water resources. Thus chromium contamination in the environment is mainly due to anthropogenic sources (MOHAN & PITTMAN, 2006).

2.7.3. Uses of Chromium

According to Merchant Research & Consulting, Ltd UK (MRC, 2014), the world chromium mine production reached 30.4 million tons in 2011, up by 400,000 tones year on year. On a global basis, about 80 % of the chromium mined goes into metallurgical applications as to harden steel, manufacture stainless steel, and to form many useful alloys. About 15 % is used in chromium chemicals manufacture and the remainder is used in refractory applications, pulp production, ore refining, and wood preservation industries (MURRAY *et al.*, 2005, DHAL *et al.*, 2013).

The major uses of chromium are:

- Compounds of chromium (VI) are used in wood preservation.
- Compounds of chromium are used to make different colored pigments and dyes.
- Stainless steel an important alloy of iron with chromium, used in many applications.

- Alloys of iron, nickel and chromium are very strong and handle very high temperatures which are used in jet engines and gas turbines.
- Chromium is hard and brilliant, also resistant to corrosion. Therefore, many things are electroplated with chromium. The chromium plating is usually applied over bright nickel plating. Typical base materials include steel, aluminum, plastic, copper alloys, and zinc alloys.

2.7.4. Toxicity of Chromium in Water

International environmental standards recommend that chromium concentration in waste water should not exceed 5 mg/L for Cr(III) and 0.05 mg/L for Cr(VI) (EPA, 2000, PUGH *et al.*, 2008). The mean concentration of chromium in soil is 37.0 mg/kg, limit of chromium concentration in drinking water for humans is 5 µg/L and in air the concentration of chromium should be less than 0.5–500 µg/m³ as a result of smoking, indoor air contaminated with chromium can be 10-400 times greater than outdoor air concentrations (WHO, 2004, ATSDR, 2012).

Water soluble hexavalent chromium is easily absorbed by human tissues, and crosses body's cell membranes rapidly. Consequently, the adverse health effects of hexavalent chromium include carcinogenic, dermatological, gastrointestinal, stomachs dysfunction, ulcers, respiratory difficulties, immune systems weakness, kidney and liver damage, alteration of genetic material, lung cancer, anemia, muscle breakdown, blood clotting abnormalities (BARCELOUX, 1999, AL-JABARI *et al.*, 2012). It also leads to respiratory symptoms such as coughing and wheezing, shortness of breath, nasal itch. Occupational exposure to chromium has adverse impact mainly to the people who are working in the plating, automobile, steel, tanning industries and textile industries (ROWBOTHAM *et al.*, 2000, JAIN *et al.*, 2009, DAS & SINGH, 2011). According to the World Health Organization industrial exposure is severe, and the affected people generally died before the age of 50 (MAURICE, 2001, WHO, 2004).

Excessive chromium concentration are extremely toxic to plants also and are harmful to their growth in the form of reduced yield, effects on leaf, root growth, inhibition of enzymatic activities and mutagenesis. Although some crops are not affected by low Cr concentration but Cr is toxic to higher plants at 100 mg kg⁻¹ dry weight. The impact of Cr contamination in the physiology of plants depends on the

metal speciation which is responsible for its mobilization (MEI *et al.*, 2002, SHANKER *et al.*, 2005).

Chromium is released into the environment through natural and anthropogenic activities however; the major quantity of chromium is released into the environment from industrial sources, tannery, electroplating, paints, and chromium ore processing industrial effluents (KABATA-PENDIAS & MUKHERJEE, 2007, DANIEL *et al.*, 2009). Both the trivalent and hexavalent oxidation states chromium have been detected in industrial effluents. Chromium appears to be present worldwide in elevated concentrations in many groundwater sources that are used for public water supply has become a major concern. Health hazards due to hexavalent chromium have been widely reported around the globe.

2.7.5. Overview of Chromium Removal Technologies

There are several common procedures for removing Cr(VI) from industrial wastewater include reduction, followed by chemical precipitation (OZER *et al.*, 1997, KURNIAWAN *et al.*, 2006), solvent extraction (MAURI *et al.*, 2001), freeze separation, reverse osmosis (PADILLA & TAVANI, 1999, AKBAL & CAMCI, 2011), ion exchange (RENGARAJ *et al.*, 2003, MARTINEZ & RODRIGUEZ, 2007), electrochemical reduction (KIM *et al.*, 2002) electrolytic methods (NAMASIVAYAM & RANGANATHAN, 1993, CHAUDHARY *et al.*, 2003) and electro-deionization (FENG *et al.*, 2007, AKBAL & CAMCI, 2011).

Most of conventional methods suffer from some disadvantages, such as high capital and operational cost, high cost of reagent, limited tolerance to pH change, incomplete metal removal, require technically skilled manpower for operation, requires a large area of land, provides a low treatment efficiency and energy requirements. Yet, hexavalent chromium toxicity has no known effective treatment. Therefore, the most vital measure needed is to prevent further environmental pollution of chromium, and develop treatment processes for contaminated water and soils. In this work we use tannin content material for this purpose for removal and adsorption of chromium Cr(VI) harmful radical and also try on it some of pesticides.

2.8. BIOCHAR

Biochar is a relatively new term, as a material is defined as, a charcoal (biomass that has been pyrolysed in a zero or low oxygen environment) used as a soil amendment, has been credited with multiple benefits, including the ability to improve soil fertility, protect water quality, and generate carbon neutral energy. In other words biochar is the carbon-rich product obtained by heating biomass in a closed system under limited supply of oxygen (ZHENG *et al.*, 2010). Pyrolysis involves the heating of organic materials in the absence of oxygen to yield a series of bioproducts: biochar, bio-oil, and syngas. Pyrolysis is a simple and inexpensive process which has been used to produce charcoal for thousands of years. In fact, areas high in naturally occurring biochar, such as the North American Prairie (west of the Mississippi River and east of the Rocky Mountains), are some of the most fertile soils in the world. Historical use of biochar dates back at least 2000 years. In the Amazon Basin, evidence of extensive use of biochar can be found in the unusually fertile soils known as **terra preta** and **terra mulata** as shown in Figure 4 both means black soil, which were created by ancient, indigenous cultures (O'NEILL *et al.*, 2009, MANGRICH *et al.*, 2013). Due to the large amounts of biochar incorporated into its soils, this region still remains highly fertile despite centuries of leaching from heavy tropical rains. In parts of Asia, notably Japan and Korea, the use of biochar in agriculture also has a long history. Recently, heightened interest in more sustainable farming systems, such as Korean Natural Farming, has revived the use of biochar in Western agriculture.

Biochar is an organic material produced via the pyrolysis of C-based feedstocks (biomass) and is best described as a 'soil conditioner'. Despite many different materials having been proposed as biomass feedstock for biochar (including wood, crop residues and manures), the suitability of each feedstock for such an application is dependent on a number of chemical, physical, environmental, as well as economic and logistical factors. Evidence suggests that components of the carbon in biochar are highly recalcitrant in soils, with reported residence times for wood biochar being in the range of 100s to 1,000s of years, i.e. approximately 10-1,000 times longer than residence times of most soil organic matter (SOM). Therefore, biochar addition to soil can provide a potential sink for C.



FIGURE 4 – SOIL POTENTIAL COMPARISON WITH AND WITHOUT BIOCHAR CONTENT SOIL
 SOURCE : Photos Courtesy Of Julie Major **Error! Hyperlink reference not valid..**

It is important to note, however, that there is a paucity of data concerning biochar produced from feedstocks other than wood. Owing to the current interest in climate change mitigation, and the irreversibility of biochar application to soil, an effective evaluation of biochar stability in the environment and its effects on soil processes and functioning is paramount. The current state of knowledge concerning these factors is discussed throughout this report.

2.8.1. Importance of Biochar

Biochar can be used directly as a replacement for pulverized coal as a fuel. But one of major distinctions between biochar and charcoal (or char) is that the former is produced with the intent to be added to a soil as a means of sequestering carbon and enhancing soil quality (LEHMANN *et al.*, 2006). When used as a soil amendment, biochar has been reported to boost soil fertility and improve soil quality by raising soil pH, increasing moisture holding capacity, attracting more beneficial fungi and microbes, improving cation exchange capacity (CEC), and retaining nutrients in soil (LEHMANN, 2007). Biochar incorporation into soil is expected to enhance overall sorption capacity of soils towards anthropogenic organic contaminants e.g. polycyclic aromatic hydrocarbons - PAHs, pesticides and herbicides (NICOLINI *et al.*, 2015), in a mechanistically different (and stronger) way

than amorphous organic matter. Whereas this behavior may greatly mitigate toxicity and transport of common pollutants in soils through reducing their bioavailability, it might also result in their localized accumulation, although the extent and implications of this have not been fully assessed experimentally. The potential of biochar to be a source of soil contamination needs to be evaluated on a case-by-case basis, not only with concern to the biochar product itself, but also to soil type and environmental conditions. Biochar can improve almost any soil. Areas with low rainfall or nutrient-poor soils will most likely see the largest impact from addition of biochar. (SOHI *et al.*, 2010, AHMAD *et al.*, 2014, JEFFERY *et al.*, 2015). Primary greenhouse gases associated with the agriculture sector are nitrous oxide (N₂O) and methane (CH₄). Livestock manure management and enteric fermentation are leading agricultural sources of methane emissions. When applied to the soil, biochar can lower greenhouse gas emissions by substantially reducing the release of nitrous oxide (BRACMORT, 2010, SRINIVASARAO *et al.*, 2013).

2.8.2. Some Disadvantages of Biochar

The biochar technology is in its early stages of development, there are many concerns about the applicability of the technology in the United States. There is concern about the ideal time to apply biochar and how to ensure that it remains in place once applied and does not cause a risk to human health or degrade air quality. The availability of a plentiful feed supply for biochar production is an area of concern as it is costly.

2.9. TANNINS

Tannins comprise a large group of natural products widely distributed in the plant kingdom. Tannins are a diverse group of natural occurring poly-phenols found in plants, seeds, bark, wood, leaves fruit skins, red wine, tea and coffee (BEECHER, 2003). Tannins possess a high affinity for proteins, and create serious negative effects when consumed by seed consumers (AHARONI *et al.*, 1998, HERVAS *et al.*, 2000). Tannins are astringent, having bitter taste, protect plants from herbivores, increase resistance against pathogens, or protect tissues such as wood against decay. The term tannin refers to the use of tannin in tanning animal hides into leather, yet the word is extensively used to any large polyphenol compound having sufficient hydroxyls and carboxyls to form strong complexes with hard acid metal ions like Fe(III) and Cr(III) (PEARSON, 1963) and thereby exert their roles in the

tanning with proteins and other macromolecule (ASHOK & UPADHYAYA, 2012). Smith and Swain defined tannins as water-soluble having a molecular weight ranging from 500 to 3,000 (SMITH & SWAIN, 1962), but now there are tannins molecules reported which are lower in molecular weight and also bigger reaching up to 20,000 (HASLAM, 1989). The antimicrobial activity of tannins has been also the focus of research in many fields: food science, wood science, soil science, plant pathology, pharmacology, and human and animal nutrition (WATERMAN & MOLE, 1994, DOANE & MBUGUA, 2001).



FIGURE 5 – SOME NATURAL PRODUCTS WHERE TANNIN CAN BE EXTRACTED
SOURCE : <http://winefolly.com/review/what-are-tannins-in-wine/>

Tannins occur commonly in shrubs and trees. A survey by Bate-Smith and Lerner (1954) showed the distribution of condensed tannins in over 500 species of plants. Likewise, Bate-Smith and Metcalf (1957) observed that 80% of woody perennial dicots and 15% of annual and herbaceous dicots contain tannins. Other surveys of the distribution of tannins have shown that tannins occur commonly in legumes.

Tannins are one of the biomass materials that are cheap and widespread natural polymers extracted from leaves, seeds or barks of plants and have many hydroxyl groups and on drying change to brownish color powder (KHANBABAEE & REE, 2001). The bitterness present in some fruits, chocolate, tea, wine and beverages are also due to presence of some content of tannins (LESSCHAEVE &

NOBLE, 2005). A tannin gel prepared from the tannins by cross-linking has a significant ability to absorb and reduce various metal ions (OGATA *et al.*, 2011). Furthermore, the tannins have a potential for improving soil fertility and productivity as by increasing the rate of organic matter degradation, mineralization and humus formation (KRAUS *et al.*, 2004). There are two types of tannins i.e. *Hydrolyzed tannin* and *Condensed tannin*.

- **Hydrolyzed Tannin**

Hydrolyzed tannins are generally polyol-having carbohydrate (usually D-glucose) as a central core. The hydroxyl groups of the carbohydrate are partly or totally esterified with phenolic groups such as gallic acid as shown in Figure 6 & 7 (3, 4, 5-trihydroxyl benzoic acid) forming the gallotannins (NIEMETZ & GROSS, 2005).

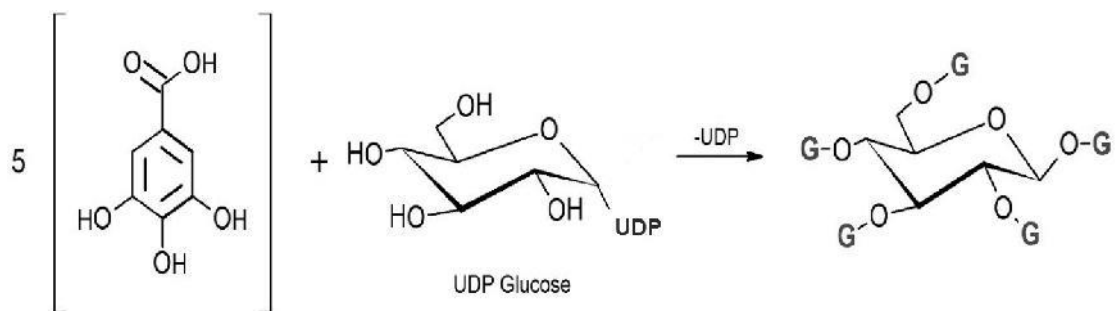


FIGURE 6 – ESTERIFICATION TO URIDINEDIPHOSPHATE GLUCOSE (UDP-GLUCOSE), WHERE G IS GALLYOL MOLECULE

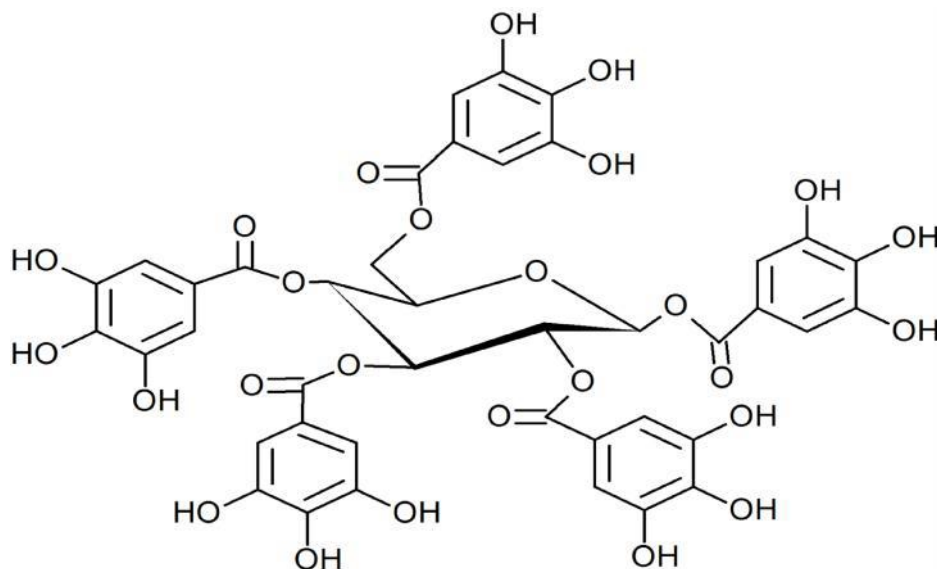


FIGURE 7 – STRUCTURE OF 1,2,3,4,6 PENTAGALLYOL -O-D-GLUCOSE

- **Condensed Tannin**

Condensed tannins are also known as proanthocyanidins (PAs), are polymers of 2 to 50 (or more) flavonoid units that are joined by carbon-carbon bonds, which are not susceptible to being cleaved by hydrolysis. The flavonoids are polyphenolic compound found naturally, significant antioxidant chelating properties. A flavonoid monomer consist of two hydroxylated benzene rings, A and B are link by a three-carbon chain that is part of a heterocyclic C ring (Fig 8). (HAGERMAN, 2002, HE *et al.*, 2008). The most common condensed tannins are flavan-3-ols (-)-epicatechin and (+)-catechin derivatives of flavonoid are shown in Figure 9. Condensed tannin concentration in plant tissue has been shown to vary with many factors. These include plant species, part, plant maturity, growing season and soil fertility (GINER-CHAVEZ *et al.*, 1997). The flavan-3-ol monomer units most frequently linked through either C4/C6 or C4/C8 C–C bonds as in Figure 10 (DIOUF *et al.*, 2013).

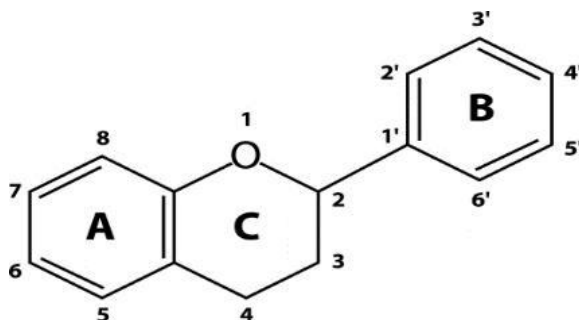


FIGURE 8 – BASIC FLAVONOID RING STRUCTURE AND NUMBERING

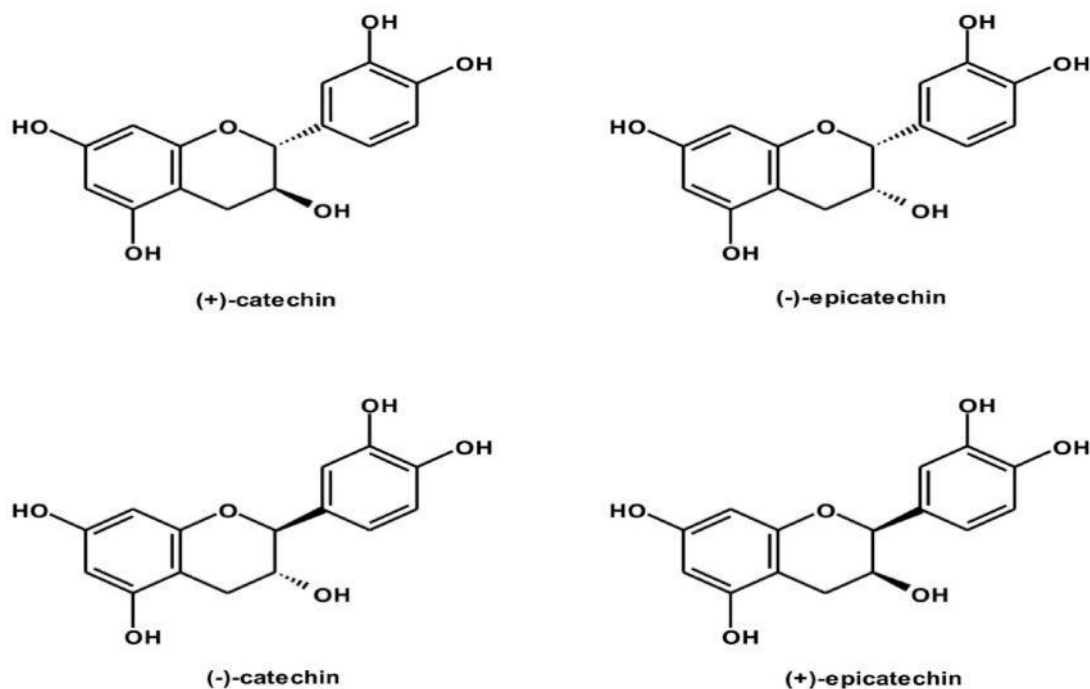


FIGURE 9 – STRUCTURES OF (+)-CATECHIN, (-)-EPICATECHIN, (-)-CATECHIN AND (+)-EPICATECHIN.

SOURCE : Hurst *et al.* 2011

2.9.1. Tannin-Protein Binding

The process of tannin-protein binding is complex and may depend on quantity, structure and size of both tannin and protein. Tannins have a high degree of hydroxylation that offers many possible sites for binding to proteins. Complexes are formed mainly via hydrogen bonding. Proline-rich proteins have been described as particularly reactive with tannins in Figure 11 (CHARLTON *et al.*, 2002). Precipitation increases with size of the complex (DEAVILLE *et al.*, 2007). Tannins are astringent, bitter plant polyphenols that either bind and precipitate or shrink proteins. The astringency from the tannins is that which causes the dry and puckery feeling in the mouth following the consumption of red wine, strong tea, or an unripened fruit (ASHOK & UPADHYAYA, 2012). Astringency plays a significant role in the sensory experience of taste of beverages also has importance in the skincare cosmetic industry (BAJEC & PICKERING, 2008).

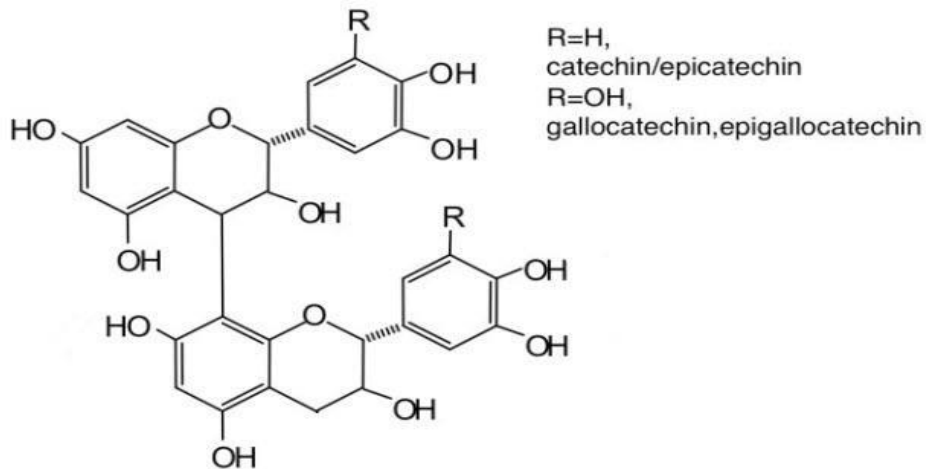


FIGURE 10 – LINKAGES OF C4–C8 OF FLAVONOID MONOMERS
SOURCE :DIOUF et al., 2013

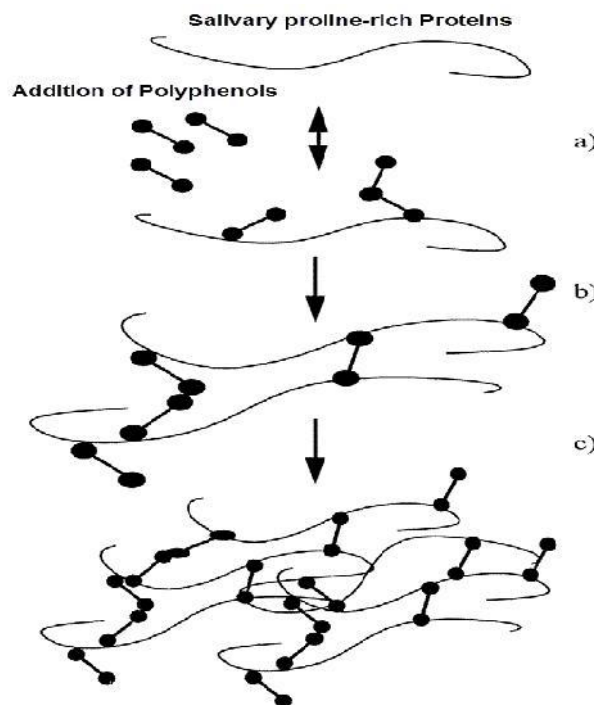


FIGURE 11 – SCHEMATIC REPRESENTATION OF THE STAGES OCCURRING IN
BINDING AND PRECIPITATION OF POLYPHENOLS BY SALIVARY
PROLINE-RICH PROTEINS
SOURCE : CHARLTON et al., 2002.

2.9.2. Tannins in Ruminant Nutrition

Tannins have for a long time been considered harmful in ruminant (animal) nutrition, (MIN *et al.*, 2003). However, certain tannins can prompt important benefits in ruminant nutrition and to the environment. When tannins bind to dietary proteins, they can become 'rumen-escape' proteins, which cannot be degraded by bacterial

enzymes. These proteins pass on to the abomasum of ruminant digestive system, where pH is around 2.5 and complexes may dissociate, also unable dissociate to in some extra stable complex. Moreover, tannins also help to reduce production of methane in ruminants (PATRA & SAXENA, 2010). This is important because extra methane production by domestic ruminants believed to be a major contributor to anthropogenic greenhouse gas emissions (OSKOUÉIAN *et al.*, 2013).

2.9.3. Condensed Tannin from *Acacia mearnsii*

Acacia mearnsii common name Black Wattle (English) acácia-negra (Portuguese) is one of the most planted native Australian plant around the world (Asia, North, Central and South America, Africa (Griffin *et al.*, 2011), often used as a commercial source of tannin or firewood for local populations. This species is also documented as highly invasive, threatening the ecology of a broad range of habitats by competing with indigenous vegetation, replacing grass communities, reducing native biodiversity and increasing water loss from riparian zones. The invasiveness of this species is partly due to its ability to produce large amounts of long-lived seeds which may be triggered to germinate in any harsh conditions (LOWE *et al.*, 2000, RICHARDSON & REJMÁNEK, 2011).

Acacia mearnsii is a round or shapeless tree growing to 3-15 m in height. It is an unarmed, evergreen tree with shallowly ridged branchlets as shown in Figure 12. It grows in wet sclerophyll forest, woodland and coastal scrub and in clay or sandy soils (KODELA, 2012).



FIGURE 12 – IMAGE OF *ACACIA MEARNSII*
SOURCE : <http://www.sciag.ukzn.ac.za/bcs/Photos%20weeds.htm>

The most conspicuous secondary compounds in most species of *Acacia* are proanthocyanidins (CT). The bark of this species often contains 20–40% tannins and bark extracts about 70% proanthocyanidins up to 3000 MW. The proanthocyanidins extracted from *Acacia mearnsii*, mostly constitute a dimer of flavan-3-ols in the combining form of tannin along with some other compounds which are important commercial products. Nowadays, *Acacia mearnsii* is the basis of commercial tannin production in South Africa and Brazil (DUAN *et al.*, 2005, ASSIS & RESENDE, 2011).

2.9.4. Tanfloc

Tanfloc is a tannin-based essentially vegetable originated low molecular weight cationic organic polymer flocculent/coagulant that can be suitable for wastewater treatment applications. Tanfloc is extract from bark of *Acacia*.

The product is manufactured by TANAC, a Brazilian company which has over 260 km² of renewable forests and it is certified with ISO 9002, ISO14001 and NSF accreditation.

Tanfloc acts in colloidal systems neutralizing charges and creating electric bonds between particles, making them unstable, producing flock and causing their sedimentation. Tanfloc does not alter the pH of the water being treated because does not consume the environment's alkalinity and at the same time effective in a pH schedule from 4.5 to 8.0.

Traditional coagulants used in water and wastewater treatment are generally inorganic (typically containing Al³⁺ or Fe³⁺ salts) and therefore can leave residues in the sludge and supernatant. This residue can create problems with sludge and water disposal, interfering with further downstream biological treatment. These products not only add metals to the discharge, but also increase salts (sulfates and chlorides) which in turn can cause further disposal issues.

2.10. Nanoparticles Characterization Techniques

The most significant part of scientific research is characterization, it provides an opportunity to analyze results of experiments and to choose the next step to achieve expected results. Different parameters need different characterization techniques, an efficient analysis strongly depends on how suitable was the technique for certain

parameter. In order to analyze these different properties, it is always necessary to use different kinds of techniques.

2.10.1. X-Ray Diffraction

There are many different methods for measuring structure across this wide range of distances, but the more powerful experimental techniques involve diffraction. s. X-ray diffraction (XRD), conceived by von Laue and the Braggs. X-Ray diffraction is based on a constructive interference of X-ray waves process that is produced in certain space directions (FULTZ & HOWE, 2012). Consider a plane lattice crystal with inter planar distance d . Suppose a beam of X-rays of wavelength λ is incident on the crystal at an angle θ , the beam will be reflected in all possible atomic planes. The path difference between any two reflected waves is equal to the integral multiple of wavelength. From the Figure 13 the ray **P** gets reflected from the surface while the ray **Q** has to undergo some path difference. The extra distance traveled by the ray **Q** is (**BC + CD**). From the diagram either **BC** or **CD** is equal to $d \sin \theta$. So the path difference is

$$d \sin \theta + d \sin \theta = n \lambda$$

$$2 d \sin \theta = n \lambda \quad \text{This is Bragg's law}$$

Here n is the order = 1,2, 3

That means that the waves must be in phase, which happens when their trajectory difference is zero or a whole multiple of wavelengths. The directions in which this phenomenon takes place when applying an X-ray radiation on a material with a periodic atomic structure (SRINIVAS *et al.*) can be predicted by Bragg's law, which establishes that the interference is constructive when the following condition is accomplished as shown in Figure 13;

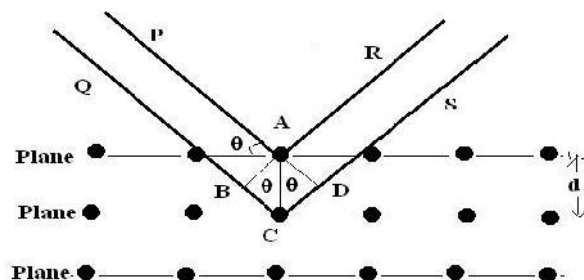


FIGURE 13 – X-RAYS SCATTERING FROM PLANES OF ATOMS EXHIBIT INTERFERENCE EFFECTS LEADING TO SPECIFIC ANGLES WHERE REFLECTIONS ARE OBSERVED. SOURCE : FULTZ & HOWE, 2012

The constructive interferences can be recorded in an X-ray diffractogram in which the diffraction intensity is shown as function of the scattering angle. Each diffractogram is taken using a specific wavelength.

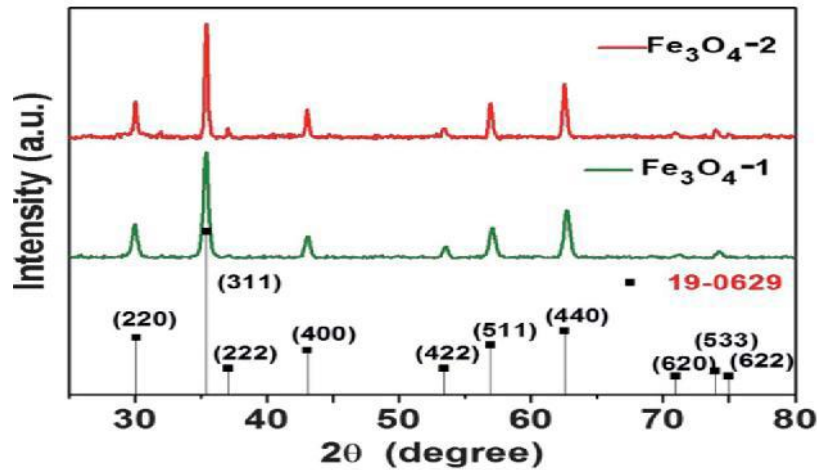


FIGURE 14 – X-RAY POWDER DIRACTION PATTERNS FOR $\text{Fe}_3\text{O}_4^{-1}$ AND $\text{Fe}_3\text{O}_4^{-2}$
SOURCE: NANOPARTICLES (DAR & SHIVASHANKAR, 2014).

The positions of the resulting peaks depend on the interplanar spacing distances. So, the bigger is the distance between identical planes, the smaller is the value of 2θ at which the corresponding peak appears, and vice versa as shown in Figure 14. Thus, by carrying out X-ray diffractions from solid samples, it is possible to identify whether a material is crystalline or not, and in case it is, it is also possible to know which crystal (or mixture of crystals) that we are working with it.

2.10.2. Magnetic Properties

Magnetism, the phenomenon by which materials assert an attractive or repulsive force. It is due to a magnetic field, which is caused by moving electrically charged particles. It is also inherent in magnetic objects such as a magnet. All materials experience magnetism, some more strongly than others. The space surrounding a magnet where a magnetic force is experienced is called a **magnetic field**. The term "magnetic field" simply describes a volume of space where there is a change in energy within that volume. This change in energy can be detected and measured. The location where a magnetic field can be detected exiting or entering a material is called a magnetic pole. Magnetic poles have never been detected in isolation but always occur in pairs, hence the name dipole. Therefore, a dipole is an object that has a magnetic pole on one end and a second, equal but opposite, magnetic pole on the other (WALKER, 2005, PENDRY *et al.*, 2006).

Permanent magnets, made from materials such as iron, experience the strongest effects, known as ferromagnetism. Every magnet has two poles. This is where most of its magnetic strength is most powerful. These poles are called north and south or north-seeking and south seeking poles. A bar magnet can be considered a dipole with a north pole at one end and south pole at the other.

When a material medium is placed in a magnetic field, the medium is magnetized. This magnetization is described by the magnetization vector \mathbf{M} , the dipole moment per unit volume measured in amperes per meter and oersted. Then the total magnetic induction \mathbf{B} in the material is given by:

$$\mathbf{B} = \mathbf{B}_0 + \mu_0 \mathbf{M}$$

where μ_0 is the **relative magnetic permeability** of space and \mathbf{B}_0 is the externally applied magnetic field. The units of \mathbf{B} is Tesla and Wb/m^2

Since the magnetization is induced by the external applied field also called magnetic field strength \mathbf{H} , it can be define also by relationship

$$\mathbf{H} = \mathbf{B} / \mu_0 - \mathbf{M} \text{ or}$$

$$\mathbf{B} = \mu_0 (\mathbf{H} + \mathbf{M})$$

\mathbf{H} and \mathbf{M} will have the same units, amperes/meter.

we may assume that \mathbf{M} is proportional to \mathbf{B} , the magnetic field, i.e.

$$\mathbf{M} = \chi \mathbf{B}$$

Where proportionality constant χ is known as the **magnetic susceptibility** which is defined in low field as the ratio between \mathbf{M} and \mathbf{H} of the medium.

The values of the magnetic susceptibility (χ) and the relative permeability (μ_0) can be used to classify magnetic materials. The materials with negative susceptibility are defined as diamagnetic whereas if the susceptibility and the permeability are small and positive the materials are known as paramagnetic. As for paramagnetic materials, ferromagnetic materials have a positive susceptibility and permeability, but much larger values (REITZ *et al.*, 2008).

The best way to introduce the different types of magnetism is to describe how materials respond to magnetic fields is illustrated in Figure 16 (LESLIE-PELECKY & RIEKE, 1996).

- **Diamagnetic Materials**

These materials when placed in a magnetic field, becomes weakly magnetized in the direction opposite to that of the applied field. There is no permanent dipole moment in each atom. The induced magnetic moment produced in these materials during the application of the external magnetic field decreases the magnetic induction present in the specimen. A material contains a large number of electrons and the orbits are filled. The current that is produced due to movement of electron in an orbit produces magnetic field in a direction at right angles to the plane of the orbit. When placed in a magnetic field, the lines of force tend to avoid the surface. Hence the magnetic moments of all such electron gets cancelled resulting in the net magnetism equal to zero in the material. Susceptibility (χ) of a diamagnetic material is always negative. It does not depend on temperature and the strength of applied magnetic field. Examples are Cadmium, Silver, Bismuth, Tin, Gold, Niobium and compounds like H₂O, NaCl, alcohol etc.

- **Paramagnetic Materials**

Some materials exhibit a magnetization which is proportional to the applied magnetic field in which the material is placed. These materials are said to be paramagnetic and follow Curie's law:

$$\mathbf{M} = C (\mathbf{B} / \mathbf{T})$$

Where **M** is magnetization, **C** is Curie constant, **B** is total magnetic field **T** is temperature.

All atoms have inherent sources of magnetism because electron spin contributes a magnetic moment and electron orbits act as current loops which produce a magnetic field. In most materials the magnetic moments of the electrons cancel, but in materials which are classified as paramagnetic, the cancellation is incomplete. Paramagnetic materials have a net magnetic moment due to the unpaired electron in the partially-filled orbitals. The magnetic moments on neighboring atoms in paramagnetic materials are non-interacts and the temperature causes random orientation of these moments. The application of a magnetic field aligns the magnetic moments partially toward the field direction (CULLITY & GRAHAM, 2011). At low field, the magnetization of paramagnetic materials increases as the magnetic field is increased and the paramagnetic susceptibility is temperature dependent as shown in Figure 15.

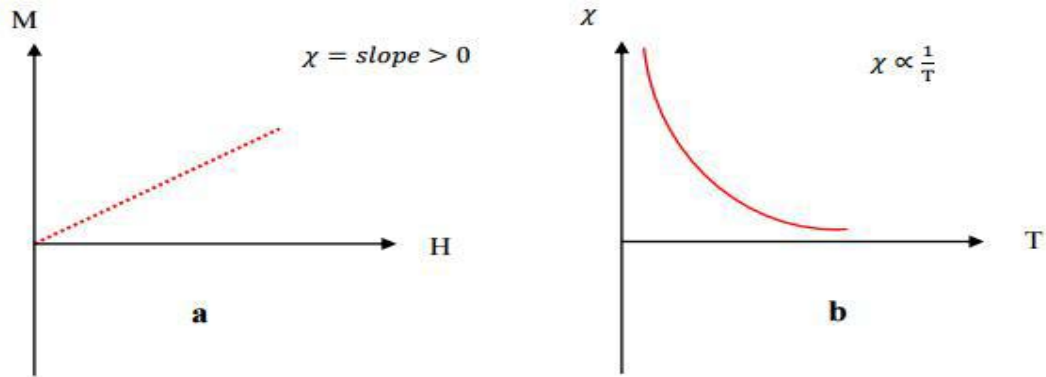


FIGURE 15 – A) THE PARAMAGNETIC MAGNETIZATION AND SUSCEPTIBILITY ARE POSITIVE
 B) THE PARAMAGNETIC SUSCEPTIBILITY IS TEMPERATURE DEPENDENT.
 SOURCE : CULLITY & GRAHAM, 2011

Paramagnetic materials become weakly ionized when placed in a magnetic field in the same direction as that of the applied field. It has permanent dipole moment in each atom. When external magnetic field is applied, the induced magnetic moment is produced which increase the magnetic induction present in the specimen. The orientation of the magnetic moment along the direction of the external field gives rise to paramagnetism. The permanent magnetic moment arises due to orbital motion of electron around the nucleus and spin motion of electron about its own axis. The magnetic moment due to former disappears due to the effect of electric field of the neighboring charges. But the magnetic moment due to electron spin are randomly oriented i(n) the absence of external field. When the external field is applied, the magnetic moments tend to align in the direction of the applied field resulting in large magnetization. But due to the thermal agitation of the atoms the magnetic moments are partially aligned in the direction of the external field resulting in weak magnetization. Susceptibility (χ) is positive and small. When magnetic field is applied to paramagnetic material, it is attracted towards the center of the material.

Examples are Aluminum, Calcium, Oxygen, Platinum, Titanium and Chromium.

- **Ferro Magnetic Materials**

Ferromagnetic materials are strongly magnetized in the direction of the applied magnetic field. It possesses enormous permanent magnetic moment in each atom. When external magnetic field is applied, a large amount of induced magnetic moment is produced which increases the magnetic induction present in the specimen.

The presence of permanent magnetic moments in the atoms or molecules in the specimen gives rise to ferromagnetism as this magnetic moment align themselves in the same direction as that of the external field. The exchange interaction between unpaired electrons of adjacent atoms in the crystal lattice gives rise to local molecular magnetic field resulting in spontaneous magnetization. Magnetic susceptibility (χ) value is large and positive. The temperature dependence of susceptibility for ferromagnetic materials is said to be complex. When magnetic field is applied to a ferromagnetic material, the magnetic lines of force are strongly attracted by the specimen. Ferromagnetic materials exhibit hysteresis. Even if the magnetic field is removed from the material, it retains the magnetism due to spontaneous magnetization. They have permanent dipole moment. Examples are Iron, Cobalt, Nickel.

<u>Ferromagnetic</u> ↓ ↓ ↓ ↓ ↓ ↓	Magnetic moments are aligned.
<u>Antiferromagnetic</u> ↓ ↑ ↓ ↑ ↓ ↑	Zero net magnetic moment at sufficiently low temperatures.
<u>Ferrimagnetic</u> ↓ ↑ ↓ ↑ ↓ ↑	Magnetic moments oppose but do not cancel.
<u>Paramagnetic</u> ↓ ↑ ↑ ↓ ↓ ↑	Random magnetic moments. Magnetic moments will align with an applied magnetic field. Occurs above Curie temperature.

FIGURE 16 – BEHAVIOR OF MAGNETIC FIELD ON DIFFRENT TYPE OF MAGNETIC MATERIALS

SOURCE : http://gravmag.ou.edu/mag_rock/mag_rock.html

SQUID (superconducting quantum interference device), which is a very sensitive magnetometer used to measure extremely refined magnetic fields, is very useful when trying to determine the magnetic behavior of a material . To optimize speed and sensitivity, the MPMS SQUID VSM utilizes some analytic techniques employed by vibrating sample magnetometers (VSMs). Specifically, the sample is vibrated at a known frequency and phase sensitive detection is employed for rapid data collection and spurious signal rejection. The size of the signal produced by a sample is not dependent on the frequency of vibration, but only on the magnetic

moment of the sample, the vibration amplitude and the design of the SQUID detection circuit.

The magnetic hysteresis curve is the curve that displays the relationship between the magnetizing force H and the magnetic flux density B of the material. the magnetization (Fig. 17).

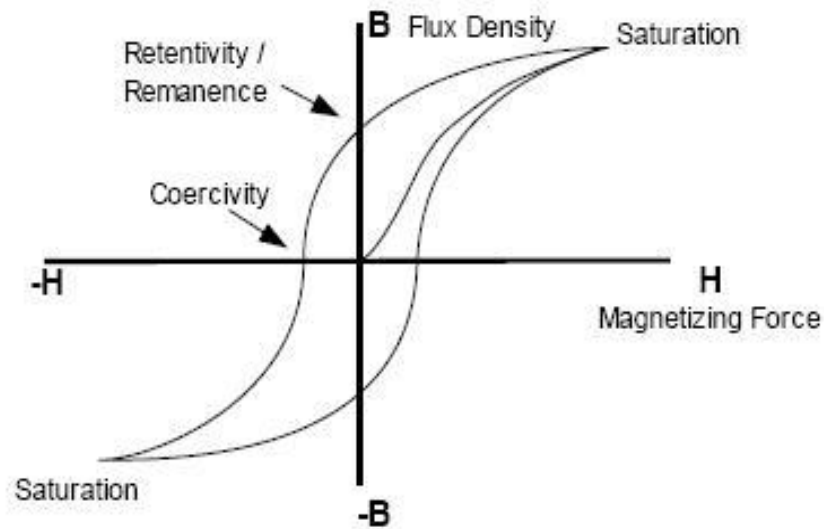


FIGURE 17 – MAGNETIC HYSTERESIS (B-H) LOOP
SOURCE: http://gravmag.ou.edu/mag_rock/mag_rock.html

From the hysteresis loop, a number of primary magnetic properties of a material can be determined:

- **Retentivity** - A measure of the residual flux density corresponding to the saturation induction of a magnetic material. In other words, it is a material's ability to retain a certain amount of residual magnetic field when the magnetizing force is removed after achieving saturation. (The value of B at point b on the hysteresis curve.)
- **Residual Magnetism or Residual Flux** - the magnetic flux density that remains in a material when the magnetizing force is zero. Note that residual magnetism and retentivity are the same when the material has been magnetized to the saturation point. However, the level of residual magnetism may be lower than the retentivity value when the magnetizing force did not reach the saturation level.

- **Coercive Force** - The amount of reverse magnetic field which must be applied to a magnetic material to make the magnetic flux return to zero. (The value of **H** at point c on the hysteresis curve.)

- **Reluctance** - Is the opposition that a ferromagnetic material shows to the establishment of a magnetic field. Reluctance is analogous to the resistance in an electrical circuit.

Superparamagnetic materials have a high saturation magnetization and zero coercivity and remanence, making it to be distinguished from ferromagnetism and paramagnetism as shown in Figure 18.

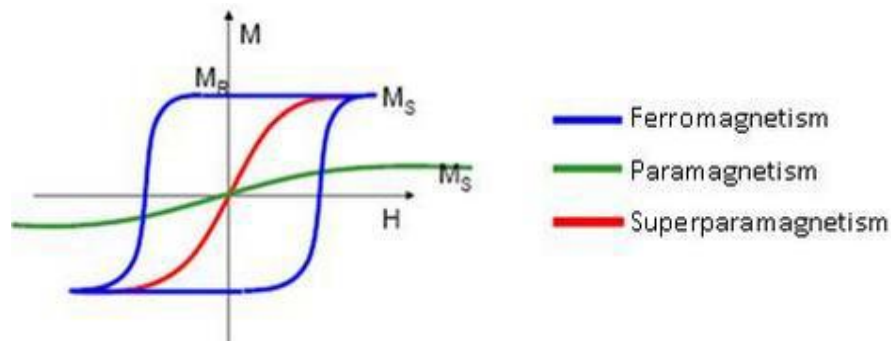


FIGURE 18 – HYSTERESIS LOOPS OF DIFFERENT TYPES OF MATERIALS
SOURCE : http://www.science20.com/mei/blog/blocking_temperature

There are also some other kinds of measurements have commonly been used. The first is called a zero-field-cooled (**ZFC**) and second is called field-cooled (**FC**).

These methods supplies useful information about the magnetic properties of the materials, is based on measuring the magnetization **M** of the sample as a function of Temperature **T**. Basically; it consists of two chief steps: the **ZFC** and the **FC** curves formation, which together leads to a graphic similar to the one shown in Fig. 19 (BURGHOFF *et al.*, 2007).

First of all, the **ZFC** curve is formed by cooling the sample without any magnetic field and then applying a magnetic field small enough (about 50 Oe) to leave the inner magnetic moments of the material unaffected and maintaining it during the further heating process, in which **M** increases until reaching a peak that corresponds to the **T_B** (blocking temperature) of the material. At low temperatures, the thermal energy becomes smaller and the magnetic moments become blocked. This temperature is the blocking temperature **T_B**. Below blocking temperature, superparamagnetic material loses its preferred direction of magnetization in zero

magnetic fields After reaching this point, the **M** decreases as a consequence of a misalignment of the magnetic moments also caused by the increase of the temperature. Generally, the heating process is kept beyond the material's **T_{irr}**, and then the **FC** curve is 'drawn' by cooling again the sample at fixed **H**, which leads to higher values of **M**. The bifurcation temperature **T_{irr}** is at which **ZFC** starts to deviate from **FC** (ZENTKO *et al.*, 2008).

Basically, the difference between two points corresponding to the **FC** and **ZFC** curves at the same **T** may be compared with the difference of two points of the already explained SQUID hysteresis cycle, corresponding to the initial magnetization curve generated when applying a magnetic field for the first time and the **M** obtained for the same value of applied **H**. This comparison may be clearly observed in Fig 19.

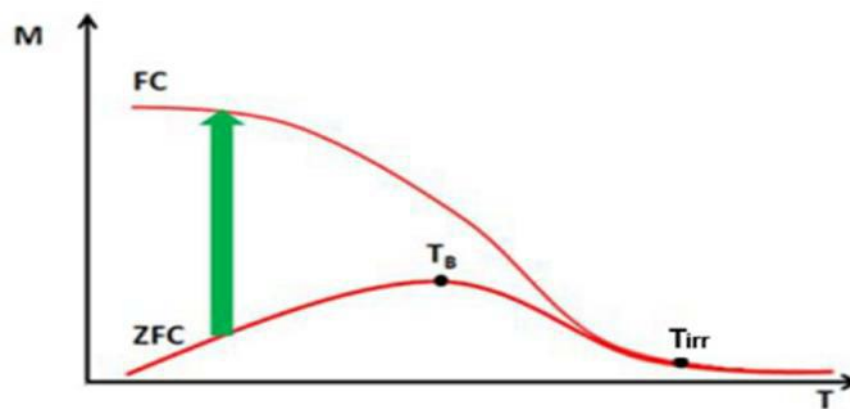


FIGURE 19 – FC-ZFC CURVES PRODUCED WHEN APPLYING A MAGNETIC FIELD.
SOURCE : ÉREZ MIRABET, 2013

The **ZFC** curve allows us to measure the material's blocking temperature, **T_B**, which supplies information about the nanoparticles' distribution size. When combining both **ZFC/FC** curves, on the other hand, it can be determined the magnetic irreversibility range of the material.

2.10.3. EPR Analysis

Electron paramagnetic resonance (EPR) spectroscopy is a powerful tool for investigating paramagnetic species, including organic radicals, inorganic radicals, and triplet states. The basic principles behind EPR are very similar to the more ubiquitous nuclear magnetic resonance (NMR) spectroscopy, except that EPR focuses on the interaction of an external magnetic field with the unpaired electron(s)

in a molecule, rather than the nuclei of individual atoms. EPR has been used to investigate kinetics, mechanisms, and structures of paramagnetic species and along with general chemistry and physics, has applications in biochemistry, polymer science, and geosciences.

EPR spectroscopy can be carried out by either varying the magnetic field and holding the frequency constant or 2) varying the frequency and holding the magnetic field constant (as is the case for NMR spectroscopy). Commercial EPR spectrometers typically vary the magnetic field and holding the frequency constant, opposite of NMR spectrometers (WEIL & BOLTON, 2007).

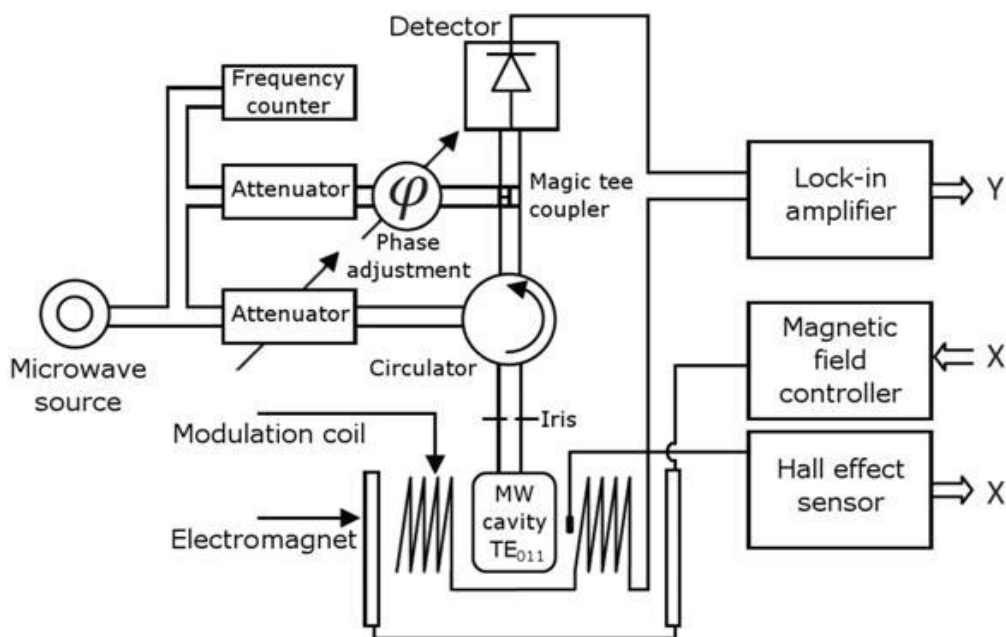


FIGURE 20 – BLOCK DIAGRAMS OF A TYPICAL EPR SPECTROMETER

SOURCE : <http://www.pharmatutor.org/articles/instrumentation-electron-spin-resonance-spectroscopy>

The energy difference between electrons which are in the magnetic spin state $m_s = -\frac{1}{2}$ and those which have $m_s = +\frac{1}{2}$ is

$$\Delta E = g\mu_B B_0 \quad (1)$$

where g is the spectroscopic splitting, μ_B is the Bohr magneton and B_0 is the applied magnetic field as shown in Figure 21 .

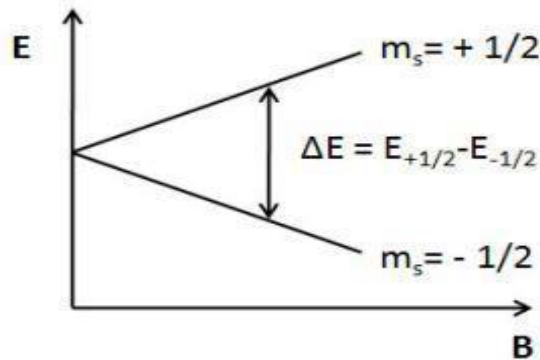


FIGURE 21 – ZEEMANN EFFECT SHOWING ENERGY SPLITTING OF UNPAIRED ELECTRON SPINS IF AN EXTERNAL MAGNETIC FIELD B IS APPLIED

SOURCE: <http://www.pharmatutor.org/articles/instrumentation-electron-spin-resonance-spectroscopy>

$$\frac{n_{upper}}{n_{lower}} = e^{-\frac{\Delta E}{k_B T}} \quad (2)$$

where n_{upper} and n_{lower} are the number of electrons which populate the spin state $m_s = +\frac{1}{2}$ and $-\frac{1}{2}$ respectively, ΔE is the energy difference between the $m_s = +\frac{1}{2}$ and $-\frac{1}{2}$ states, k_B is the Boltzmann constant and T the absolute temperature. According to equation (2), electrons of samples which are subjected to magnetic fields more likely populate the $m_s = -\frac{1}{2}$ spin state. However, they can flip between the two spin states by absorbing and radiating the energy.

Substituting equation (2) with energy as $\Delta E = h\nu$,

where ν is the frequency of the electromagnetic radiation and h the Planck constant. Therefore, if the frequency of the spectrometer is kept constant and the magnetic field is swept, electrons absorb energy.

$$h\nu = g\mu_B B_r \quad (3)$$

where B_r is the resonance magnetic field.

In a characteristic EPR graph in Figure 22, the first derivative of the measured energy absorption is plotted as a function of the applied magnetic field B . Because of the well-defined, sharp transition between the $m_s = -1/2$ and $m_s = +1/2$ state of

free electrons, they result in a sharp characteristic EPR signal with $g = 2.00$ unless there is hyperfine coupling which broadens the signal slightly.

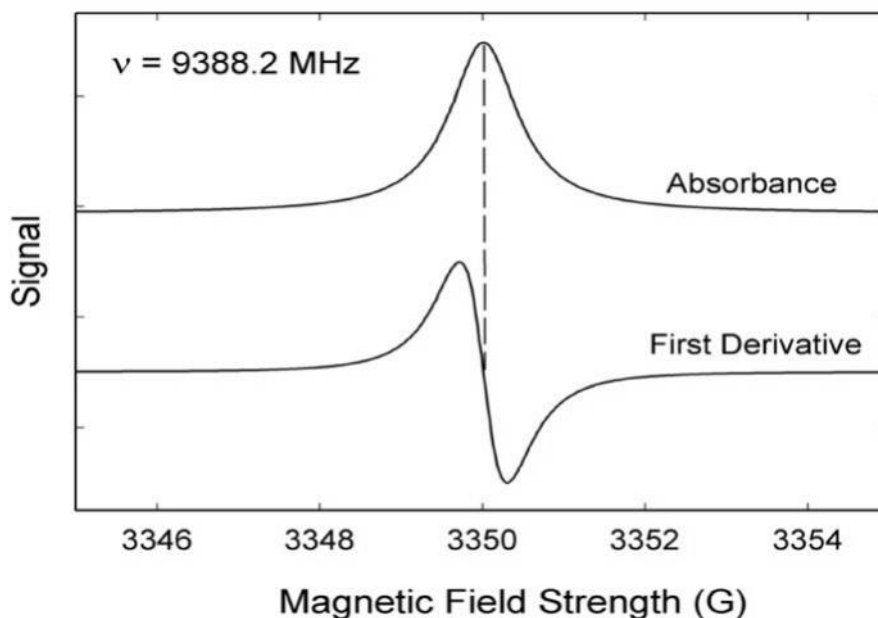


FIGURE 22 – COMPARISON OF ABSORPTION SPECTRUM AND EPR SPECTRUM
 SOURCE: http://chemwiki.ucdavis.edu/Physical_Chemistry/Spectroscopy/Magnetic_Resonance_Spectroscopies/EPR

2.10.4. Scanning Electron Microscope (SEM)

SEM produce images bathing the sample with a focused electron beam which is scanned across an area of the specimen. Once the electrons hit the specimen, some of them lose energy via different mechanisms. This lost energy turns into heat, light or X-ray emission, or other kinds of alternative forms. All the resultant emissions have information about the properties of the sample surface, for instance its composition and form.

2.10.5. Transmission Electron Microscopy (TEMPLETON *et al.*)

In TEM the electron beam is transmitted through the specimen, which lets some electrons get through and scatters others out of the beam. After emerging from the specimen, both scattered and non-scattered electrons carry information about the structure of the specimen, which is magnified by the objective lens of the microscope and can be viewed in some different ways, for instance by projecting the magnified image onto a phosphor-coated viewing screen or recording the image in a CCD

(charge- coupled device) camera and displaying the image on a computer monitor (PARK *et al.*, 2004).

In both of the cases above (SEM and TEM) their resolution power is far greater than light-powered optical microscopes because of electron wavelengths, which are about 100,000 times shorter than photon wavelengths. Every electron microscope uses electromagnetic and electrostatic “lenses” to control and focus the electron beam, generated by an electron gun, to form an image as shown in Figure 23.

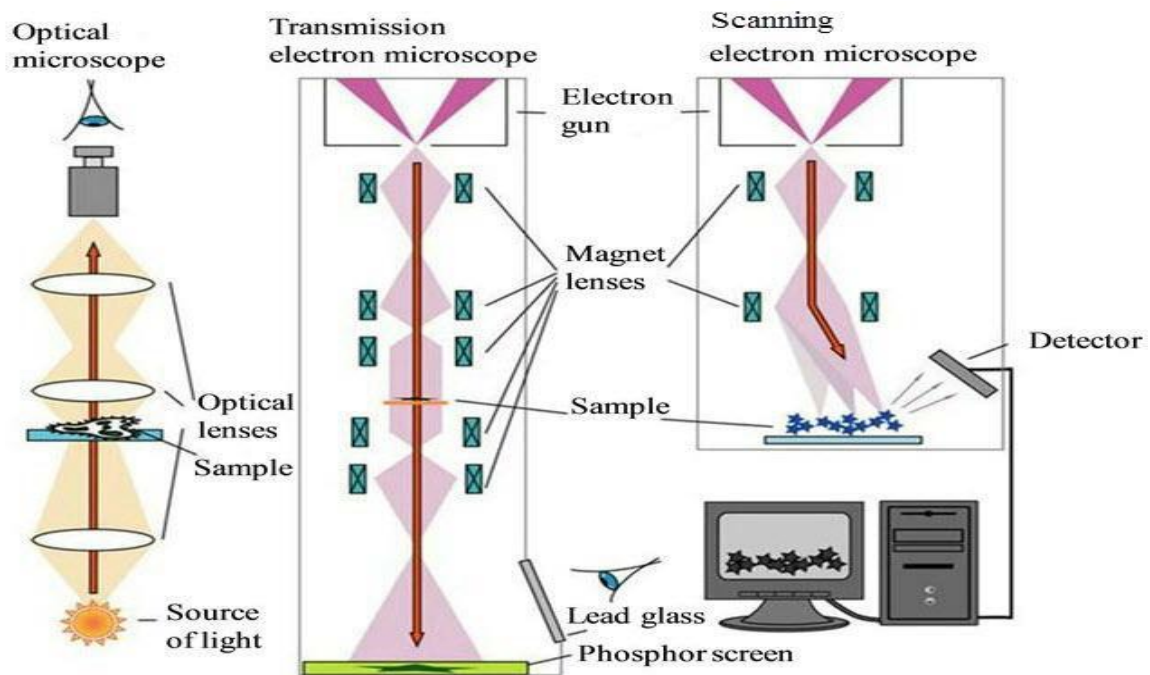


FIGURE 23 – SCHEMATIC OF THE OPTICAL, TRANSMISSION AND SCANNING ELECTRON MICROSCOPES
SOURCE: (ASEYEV *et al.*, 2013)

2.10.6. Thermogravimetric Analysis (TGA)

Thermogravimetric analysis is based on heating a mixture to a high enough temperature so that one or some of the components decompose into a gas, via dissociating themselves into the air. During the whole process, the changes in weight in relation to a temperature are measured under controlled atmosphere. The resulting thermogram shows how the sample mass decreases while temperature increases Fig.24.

Thermogravimetric analyses are useful to determine the composition and purity of a sample. In this vein, this technique uses heat and stoichiometry ratios to determine the percent by mass of different compounds in a mixture.

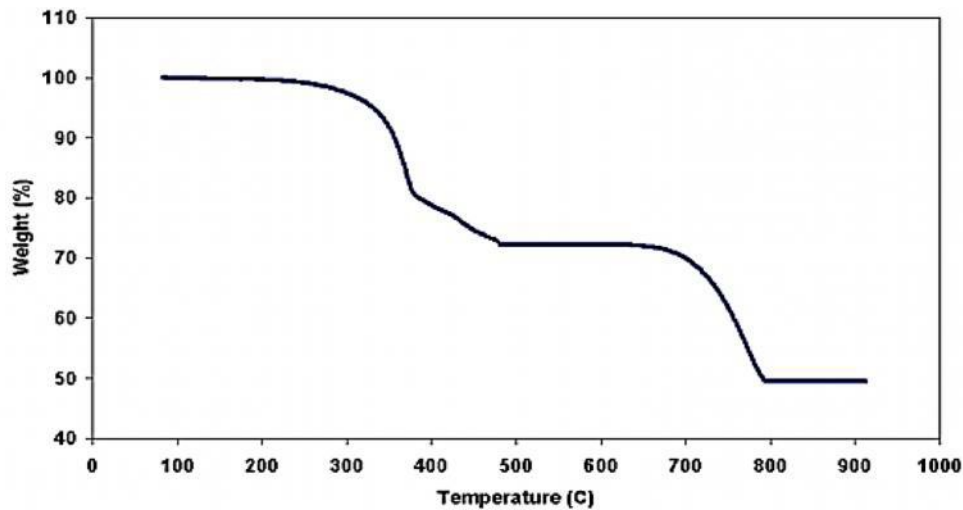


FIGURE 24 – TGA THERMOGRAPH FOR A HYPOTHETICAL MIXTURE

2.11. Sorption Theory

Sorption is the common term used for desorption, absorption and adsorption.

- Sorption : The process by which a substance (sorbate) is sorbed (adsorbed or absorbed) on or in another substance (sorbent).
- Absorption : The process of one material (absorbate) being retained by another (absorbent); this may be the physical solution of a gas, liquid, or solid in a liquid, attachment of molecules of a gas, vapour, liquid, or dissolved substance to a solid surface by physical forces, etc. In spectrophotometry, absorption of light at characteristic wavelengths or bands of wavelengths is used to identify the chemical nature of molecules, atoms or ions and to measure the concentrations of these species.
- Adsorption : An increase in the concentration of a dissolved substance at the interface of a condensed and a liquid phase due to the operation of surface forces. Adsorption can also occur at the interface of a condensed and a gaseous phase.

Adsorption is the physical adherence or bonding of ions and molecules onto the surface of another molecule. The target contaminants for adsorption/absorption

processes are most organic contaminants and selected inorganic contaminants from liquid and gas streams. Activated carbon, alumina and biochar are used most often for the liquid and gas capture of organic materials can remove fluoride and heavy metals. The forager sponge is specifically used to remove heavy metals. Lignin adsorption/sorptive clays treat organic, inorganic and heavy metal contamination within aqueous waste streams. In the subsurface, soil or amendments to soil are often used to sorb contaminants. The complexity of natural geomeedia implies that both broad classes of “sorption” reaction may occur simultaneously. Matter that accumulates at the interface during the adsorption process is termed adsorbate, whereas the surface where it accumulates is called the adsorbent. The term adsorptive refers to any chemical species in the bulk solution that may potentially be adsorbed. In contrast, the terms sorbate, sorbent and sorptive apply in situations where the precise mechanism of solid–liquid transfer is not known and may include surface precipitation or solid state diffusion.

Adsorption involves the interphase accumulation or concentration of substance at surface or interface. The process can occur at an interface between any two phases, such as liquid- liquid, gas- liquid or liquid- solid interphase. Furthermore, adsorption is the binding of a chemical species at phase boundary, such as the surface of suspended particles. The substance thus adsorbed on the surface is called the **adsorbate** and the substance on which it is absorbed is known as **adsorbent**. The term sorption encompasses both processes, while desorption is the reverse process (D BROWSKI, 2001).

The adsorption technique is one of the preferred methods for the removal of heavy metals because of its high efficiency and low cost (Li et al., 2007).

2.11.1. Factors Affecting Adsorption

Molecules of solute are removed from solution and taken up by the sorbent/adsorbent during the process of adsorption. Sorption equilibrium and kinetic are the basic requirements for the design of sorption process. Sorption process depends on the physical and chemical properties of the sorbent, sorbent-sorbate interaction and system conditions. The pH of the solution affects functional groups on the sorbent surface and the properties of sorbed molecules. If the metal ion is used in sorption process, the form of the metal species should be considered to explain sorption mechanism. Sorption rate is strongly influenced by the electrostatic

forces between sorbent and form of metal species. Hence, the contribution from the electrostatic forces should be taken into account in the sorption kinetic analysis.

2.11.2. Kinetic Study of Sorption

The kinetic study of the sorption process used for the removal of chromium determines the rate at which the contaminants are removed from the aqueous media. In this sense, numerous kinetic models have been proposed that are capable of describing the mechanism through which the sorption process takes place. This mechanism is, in most cases, complex and can cause chemical reactions between sorbent functional groups and metal ions, ionic interchange reactions and/or formation of complexes; in addition, mass transfer processes such as the transportation of substances in the liquid phase, diffusion from the liquid phase to the surface of the solid and diffusion in the interior of the macropores and micropores must be taken into consideration.

The kinetics of sorption of Chromium using SPMIOBNPs as solid sorbent were studied, analyzing the effect of the initial concentration of metal and temperature. Pseudo-first order and pseudo-second-order, have been used to represent the kinetics of the process and obtain the main kinetic parameters.

The amount of ions sorbed per unit mass of sorbent was determined according to the following equation:

$$Q_t = \frac{(C_0 - C) \cdot v}{m} \quad (4)$$

where, Q_t is the sorbent capacity of the radical, as mg per gram of sorbent: C_0 , the initial concentration of the sorbate in mgL^{-1} , C , the final/equilibrium concentration of the chromium in mgL^{-1} after contacting with sorbent, v the volume in liters of the solution used in the sorption experiment, and m is the mass of adsorbent in grams.

- **Pseudo-First Order Model**

The pseudo-first order equation (LAGERGREN, 1898, TSENG *et al.*, 2010), is generally expressed as follows:

$$\frac{dq_t}{dt} = k_1(q_e - q_t) \quad (5)$$

By integrating this expression between the limits $t = 0$, $q_t = 0$ and $t = t$, $q_t = q_t$, the equation (5) is obtained:

$$\log (q_e - q_t) = \log q_e - k_1 \cdot t / 2.303 \quad (\text{USEPA-METHOD-7196A})$$

Where q_e and q_t are the sorption capacity at equilibrium and at any time t , respectively, in mg/g, and k_1 is the pseudo-first order rate constant, in min^{-1} .

By plotting the value of $\log((q_e - q_t)/q_e)$ versus t , the value of the rate constant k_1 can be obtained from the slope.

- **Pseudo-Second Order Model**

Pseudo-second order kinetics can be expressed through the following equation (HO & MCKAY, 1999).

$$\frac{dq_t}{dt} = k_2 (q_e - q_t)^2 \quad (\text{USEPA-METHOD-7196A})$$

Where k_2 is the pseudo-second order rate constant, in $\text{g/mg}\cdot\text{min}$.

By integrating this equation between the limits $t = 0$, $q_t = 0$, $t = t$, $q_t = q_t$, the following equation is obtained:

$$\frac{t}{q_t} = \frac{1}{K_2 q_e^2} + \frac{t}{q_e}$$

By plotting t/q_t versus t , the values of q_e and k_2 can be obtained from the slope and the intercept, respectively.

3. OBJECTIVES

3.1. General Objectives

In recent years, biochar, produced by thermal decomposition of biomass and organic material under incomplete supply of oxygen, have received increasing attention as soil amendment. Due to its molecular structure, biochar is chemically and biologically more stable making it more difficult to be converted back to CO₂, as it can store carbon for a longer time (carbon sequestration). On the other hand, biochar contain many chemically reactive groups, such as COOH, OH, ketone, that give biochar a great potential to adsorb toxic substances, such as Al, Mn in acidic soils and As, Cd in heavy metal contaminated soils (BEREK *et al.*). Due to high operational costs, these methods mentioned in the previous section about the treatment of chromium managements have found limited application for example generation of toxic sludge, which Increased overall cost of the process due to treatment, handling, and disposal of sludge therefore, there is a need to explore low cost procedure. Besides these methods which follows sorption of metal ions present in low levels is a promising alternative method to treat industrial wastes mainly because of its low cost and high metal binding capacity (MONSER & ADHOUM, 2002, TAWDE & BHALERAO, 2010, CERQUEIRA *et al.*, 2012, ARAUJO *et al.*, 2013). In this work, we try to develop a new adsorption method using tannin biochar. Different iron oxides (for example, goethite, hematite, maghemite and magnetite) have been used as the metal adsorbent. Iron oxides are present in abundance and diverse form in the earth's crust (CORNELL & SCHWERTMANN, 2003). It is clear that a wide variety of treatment technologies have been implemented for removing Cr(VI) from wastewater. A significant knowledge gap exists for the possible use of these low-cost materials as economically viable sorbents. In this present work, we try to develop a new adsorption method using tannin biochar generated from the low cost wood chips/parts of Acacia tannin rich species is used as sorbent to evaluate their performances for Cr(VI) removal from waste water.

3.2. Specific Objectives

The specific research objectives are as follows:

- Preparation and characterization of superparamagnetic iron oxide biochar nanoparticles (SPMIOBNPs).
- The synthesis process can be done through green synthesis.

- Study the various important properties like particle size and surface of SPMIOBNPs.
- To investigate the removal efficiency of heavy metals and contaminants present in water.
- Identification and comparison of the best results for the removal of hexavalent chromium from aqueous systems using tannin rich content biochar sorbent.
- Investigation of the sorption behavior of Cr(VI) under various experimental conditions of pH and time.

4. MATERIALS AND METHODS

This chapter presents the materials used, methods employed and analytical techniques. All reagents used were high-purity grade from Merck like hydrochloric acid, nitric acid, sodium hydroxide solutions, etc. Highly purified water (Milli-Q system, Millipore) was used to prepare aqueous solutions. The tannin and tanfloc were obtained as a brown powder from TANAC S.A Montenegro -RS- Brazil.

4.1. Chemicals and Reagents

The following chemicals and reagents were used in the experiments.

- Chromium chloride hexahydrate ($\text{CrCl}_3 \cdot 6\text{H}_2\text{O}$)
- Sodium bicarbonate (NaHCO_3)
- Calcium chloride dihydrate ($\text{CaCl}_2 \cdot 2\text{H}_2\text{O}$)
- Potassium dichromate ($\text{K}_2\text{Cr}_2\text{O}_7$)
- Conc. hydrochloric acid 32% (HCl)
- Iron (II) sulphate heptahydrate ($\text{FeSO}_4 \cdot 7\text{H}_2\text{O}$)
Iron (II) /(III) Chloride ($\text{FeCl}_2/\text{FeCl}_3$)
- Diphenylcarbazide (DPC)
- Nitric acid 65% (HNO_3)
- Sodium hydroxide (NaOH)
- 0.01ML^{-1} EDTA Solution
- Water (Milli-Q system, Millipore)
- Distil water

4.2. Experimental Equipments

The following equipments were used in the experiments.

- Electronic balance
- pH meter
- Polyethylene bottles with cover, tube and stoppers (500 -2000 mL)
- Measuring cylinders (5-500 mL)
- Pipettes
- Beakers 100, 250, 500, 1000 and 2000 mL

- Volumetric flasks
- Membrane filters (0.45 μ m, \varnothing 25 mm)
- Syringes with filter heads
- Sampling small polythene bottles.
- Buckets 5, 10 and 20 L capacity.
- Magnetic stirs.
- Mechanical shaker

4.2. Synthesis of SPMIOBNs

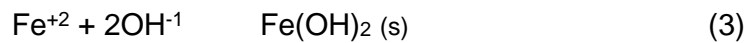
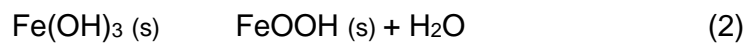
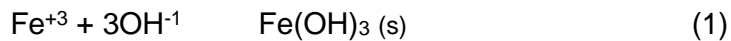
There are several of synthesis methods of SPMIOBNs : water-in-oil microemulsion, polyol, gas deposition, co-precipitation, sol-gel, pyrolysis, thermal decomposition of organic iron precursor, hydrothermal and others. Every method possess specific performance procedure and conditions, and of course nanoparticles of different properties (shape, average, size, size distribution, crystallinity, magnetic properties, dispersibility). In this work two methods with high product quality/synthesis ratio will be compared. These routes are co-precipitation and thermal decomposition.

4.3. Co-precipitation Method of Preparation of (SPMIOBNs)

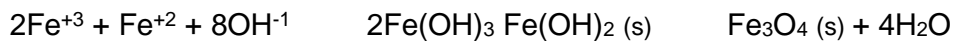
The co-precipitation method is considered as the simplest chemical way to synthesize SPMIOBNs. The SPMIOBNPs were synthesized by a modified co-precipitation method (GUBIN *et al.*, 2005). 200 grams of dry ground tannin biomass screened to 80 mesh were added to 1 L of solution containing ferric chloride and ferrous chloride (80 10^{-3} mol/L of FeCl_3 and 40 10^{-3} mol/L of FeCl_2). Under vigorous magnetic stirring, an aqueous solution of 5 mol/L NaOH is added drop wise to increase the pH of the suspension to 10. The stirring continued for 0.5 h afterward, the formed precipitate was separated by centrifugation at 3000 RPM and with relative centrifugal force with $\text{RCF} = 1811$ g (PENDLETON, 2006, FREI, 2014). Finally, the material was taken to pyrolysis. First, the material is heated to 100 $^{\circ}\text{C}$ for 2 hours, and then the temperature is raised to 400 $^{\circ}\text{C}$ or 700 $^{\circ}\text{C}$, at the rate of 5 $^{\circ}\text{C}/\text{min}$ and kept at this temperature for 6 hours and Figure 25 shown the product obtained. Then the material is removed from the oven, after cooled to the room

temperature and wash with distilled water as shown in the Figure 26, given the name, SPMIOBNs (Superparamagnetic Iron Oxide/Biochar Nanoparticles) (CHEN *et al.*, 2011, KHARISOV *et al.*, 2012). Similar method was used for tanfloc materials also but the synthesis process was complicated.

The co-precipitation method using iron salts containing Fe^{+2} and Fe^{+3} ions, for the formation of SPMIOBNPs at alkaline conditions has been widely studied (GNANAPRAKASH *et al.*, 2007, NYIR -KÓSA *et al.*, 2009, MASCOLO *et al.*, 2013) and the following mechanism was proposed in the equations below:



Giving an overall reaction:



Nanoparticle size, morphology and magnetic properties can be controlled by varying of solution pH, ionic strength, temperature, reaction time, type of salts ferrous and ferric chlorides are most popular (KOESEOGLU *et al.*, 2005).



FIGURE 25 – THE SPMIOBNP AFTER PYROLIS



FIGURE 26 – THE PURE CLEAN SPMIOBNP AFTER WASHING AND DRYING.

4.3.1. Effect of pH on Particle Size of SPMIOBNs

The pH range of the solution throughout the synthesis of SPMIOBNPs should be 8-11 with maintaining molar ratio of $\text{Fe}^{3+} / \text{Fe}^{2+}$ (2:1) under a non-oxidizing condition. The effect of pH on the average particle size of SPMIOBNPs as estimated from the Scherrer equation of the XRD peaks is presented in Fig 27 (MAHDAVI *et al.*, 2013). The figure 27 shows the sizes of SPMIOBNPs reduce with the increase of solution pH when the pH is lower than 11, and also the particle size of SPMIOBNPs increase with the increase of solution pH when the pH is higher than 11. After increasing of the pH solution, the hydrolysis of Fe^{3+} occurred and $\text{Fe}(\text{OH})_3$ was generated in the first step. Then, $\text{Fe}(\text{OH})_2$ was generated as the pH of the reaction system increased, which was attributed to the hydrolysis of Fe^{2+} . Finally, SPMIOBNPs can just be formed as the pH of the solution is further increased. This result shows that the growth of SPMIOBNPs nucleus occurred when the pH of solution is lower than 11, while the growth of Fe_3O_4 nucleus is easier to happen when the pH of solution is higher than 11 (YANG *et al.*, 2014). Therefore the pH of 11 will be selected for the optimum pH in further experiment (MAHDAVI *et al.*, 2013).

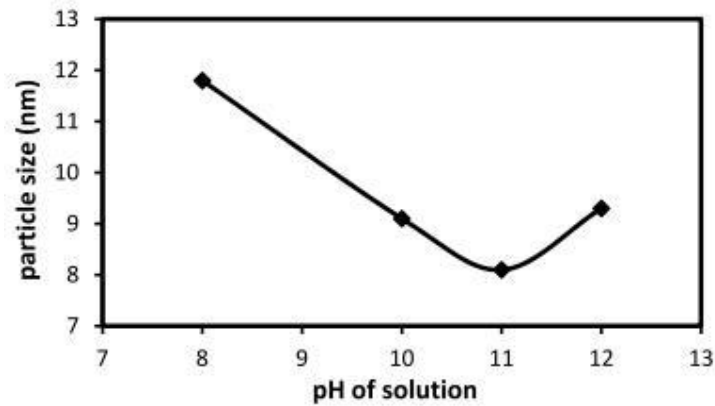


FIGURE 27 – EFFECT OF THE SOLUTION PH ON SIZES OF SPMIOBN
Source: MAHDAVI et al., 2013

4.3.2. Effect of Temperature on Particle Size of SPMIOBNPs

The effect of temperature at the beginning of synthesis on particle size of SPMIONPs was investigated from 25 to 85 °C, previously as show from the XRD results of the work of MAHDAVI (2013). The results in Figure 28 indicated that all the nanoparticles were in spinel structure with face-centered cubic phase (SANTOYO SALAZAR *et al.*, 2011). The intensity of the Bragg peaks increase by increasing the temperature but there is no effect temperature upon the crystal structure of SPMIOBNPs .

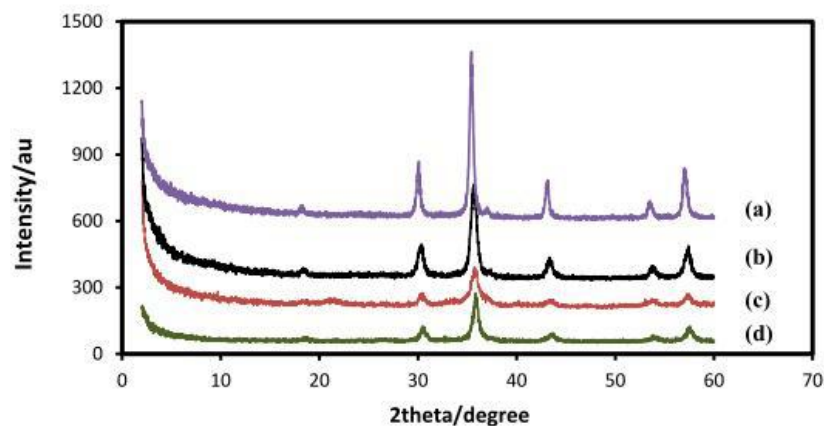


FIGURE 28 – EFFECT OF TEMPERATURE ON PARTICLE SIZE OF SPMIOBNS
SOURCE : MAHDAVI et al., 2013

4.4. Alternative Method of Synthesis

Iron oxide nanoparticles were synthesized by a modified co-precipitation method. Ferric chloride ($\text{FeCl}_3 \cdot 6\text{H}_2\text{O}$, 0.074 g) and ferrous chloride ($\text{FeCl}_2 \cdot 4\text{H}_2\text{O}$, 0.190 g) at a ratio of 2 to 1 were dissolved in 20 mL deionized water, which was then stirred and heated to 60 °C. The solution was bubbled with Argon gas to prevent unwanted oxidation as shown in Figure 29. Subsequently, 10 mL of 2.5 molL⁻¹ NaOH solution was injected at 60 °C and the reaction continued at that temperature for 20 minutes before the flask was removed from heating and stirring. The nanoparticles were then removed from solution by magnetic separation. During synthesis, the concentration and amount of NaOH was varied to control the particle size (UMUT, 2013).

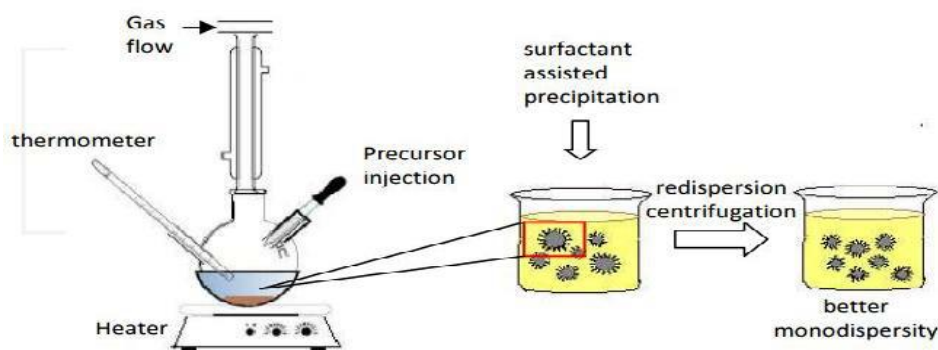


FIGURE 29 – NANOPARTICLE SYNTHESIS BY THERMAL DECOMPOSITION METHOD AND SIZE SELECTION PROCESSES
SOURCE: UMUT 2013.

4.5. Methods Used for Characterization of the Samples

The X-ray diffraction analysis (XRD) examines crystalline material structure, including atomic arrangement and crystallite size of the prepared samples. The XRD analysis of dried ground SPMIOBNPs sample was done in a Philips PW 3020 diffractometer using CuK radiation with electrical parameters of 40 kV and 40 mA. The scanning angles ranged from 3° to 70° (2 θ) at a speed of 2° min⁻¹.

The magnetic properties were analyzed with a vibrating sample magnetometer SQUID (PPMS Evercool II-Quantum Design Inc.). The PPMS SQUID VSM utilizes a superconducting magnet (a solenoid of superconducting wire) to subject samples to magnetic fields up to 7 Tesla (70 KOe). The squid and magnet

is cooled with the help of liquid Helium. Liquid Helium is also used to cool the sample chamber, providing temperature control of samples from 300K down to 10K.

Fourier transform infrared spectroscopy (FTIR) analysis was conducted by using a Bomem B100 spectrometer operating in the transmission mode between 4000 and 400 cm^{-1} , by mixing a pre-dried sample of 3.0 mg with 100 mg KBr discs pressed hydraulically at 10 tons/ m^2 (Specac Ltd, UK). For the base line construction, the analysis was conducted for only the KBr disc as a control (blank).

Thermogravimetric curves were obtained on a Shimadzu, model TGA-50, under nitrogen atmosphere, with a flow of 40 mL min^{-1} at a heating rate of 10 $^{\circ}\text{C min}^{-1}$, in the temperature range 30-900 $^{\circ}\text{C}$ in a platinum crucible, using about 5 mg of each sample.

The surface area (SA) and average pore radius (APR) were determined by multipoint BET analysis of adsorption data points with relative pressures or saturation point P/P_0 of 0.05–0.3. The total pore volume (TPV) was estimated from a single N_2 saturation point at a relative pressure of about 0.99 (LOWELL, 2004). Pore size distribution was constructed by analyzing desorption data points using the BJH method (BARRETT *et al.*, 1950).

EPR spectra were recorded at room temperature on a Bruker EMX spectrometer equipped with an ER-4116 DM Bruker cavity in the range of 8-10 GHz (X-band). Samples were put into the specialized quartz EPR tube under argon.

The transmission electron micrograph (TEMPLETON *et al.*) were taken by using a JEOL JEM-1200 EXII transmission electron microscope (JEOL Ltd., Tokyo, Japan) at an accelerating voltage of 120 kV, the suspension of the samples were dripped to the copper grids, coated with thin Formvar film carefully and then dried under ambient temperature before analyzing in the microscope.

Scanning electron microscopy (SEM) help to understand the external morphology of SPMIOBNPs material with chemical analysis of samples by taking energy-dispersive X-ray spectra (EDXS) using a JEOL JSM-6360LV scanning electron microscope (JEOL Ltd., Tokyo, Japan) at an acceleration voltage of 15 kV.

The model T80 from PG Instruments is a high performance double beam spectrophotometer was used for optical measurements operated at a wavelength of 541 nm.

4.6. Stock and Standard Solutions

Stock solutions and standard solutions containing 1000 mg/L of Cr(III) and Cr(VI) were prepared from chromium chloride hexahydrate ($\text{CrCl}_3 \cdot 6\text{H}_2\text{O}$) and potassium dichromate ($\text{K}_2\text{Cr}_2\text{O}_7$) and used in the experiments. The pH of the model water was adjusted by adding the required amount of hydrochloric acid (HCl) and sodium hydroxide (NaOH) solutions.

4.7. Hexavalent Chromium

Dissolved hexavalent chromium, in the absence of interfering amounts of substances such as molybdenum, vanadium, and mercury, may be determined colorimetrically by reaction with diphenylcarbazide in acid solution. A red violet/purple color of unknown composition is produced (USEPA-METHOD-7196A, 1992). This method may also be applicable to certain domestic and industrial wastes, provided that no interfering substances are present.

Hexavalent chromium is determined by the 1,5-diphenylcarbohydrazide method using a single dry powder formulation called ChromaVer 3™ Chromium Reagent. This reagent contains an acidic buffer combined with 1,5-diphenylcarbohydrazide which reacts to give a purple color when hexavalent chromium is present. The method is applicable to fresh water and wastewater samples. Color development is directly proportional to the amount of hexavalent chromium present. The mechanism of complex formation Cr(VI) with 1,5-diphenylcarbohydrazide is shown in the reaction below in strong acidic medium (ASHLEY *et al.*, 2003, BASU & JOHNSON, 2012).

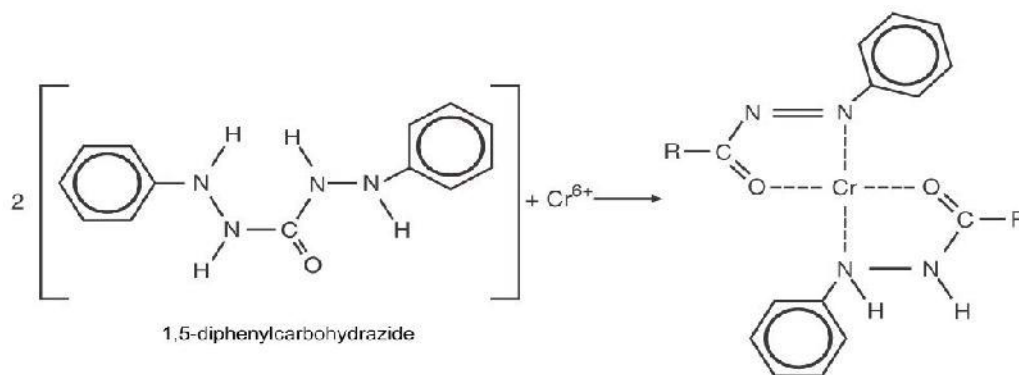


FIGURE 30 – REACTION OF CR(VI) WITH 1,5-DIPHENYLCARBOHYDRAZIDE
SOURCE : ASHLEY *et al.*, 2003

4.8. Total chromium

In the analysis for total chromium, the sample was heated to the boiling point under strong alkaline conditions in the presence of hypobromite. The trivalent chromium was converted to hexavalent chromium. The proper chemical conditions for this oxidation are provided by Chromium 1 Reagent Powder. After the oxidation is complete, excess hypobromite is destroyed by the addition of Chromium 2 Reagent Powder. Then ChromaVer 3 Chromium Reagent, which contains an acidic buffer combined with 1,5-diphenylcarbohydrazide, is added. A purple color develops with an intensity directly proportional to the total chromium concentration. The concentration of hexavalent chromium was determined by molecular absorption spectroscopy after

reaction with 1,5-diphenylcarbazide, using a PG Instruments Model T80+ spectrophotometer operated at a wavelength of 541 nm.

The trivalent chromium can be determined by subtracting the hexavalent chromium test results from the results obtained in the total chromium test.

- **Method for pH Dependence on Sorption of Chromium**

50 mL aliquots of aqueous 10 mg L^{-1} Cr(VI) solution were transferred by pipette into 250 mL glass flasks. A 100 mg portion of SPMIOBNPs was added to each bottle. The pH of the solutions were adjusted to 2, 3, 4 and 5 using 1.0 mol L^{-1} HCl, after which the mixtures were agitated for 120 h and then filtered through $0.45 \mu\text{m}$ Millipore filters. The filtrates were acidified with nitric acid (1:1), and stored in polyethylene containers prior to determination of Cr(VI) and Cr(III). A control was prepared by addition of Cr(VI) solution to the suspension of SPMIOBNPs material. The experiments were performed in triplicate (CERQUEIRA *et al.*, 2012).

- **Influence of time on the Sorption of Chromium**

50 mL aliquots of aqueous 10 mg L^{-1} Cr(VI) solution were transferred by pipette into 250 mL glass flasks. A 100 mg portion of SPMIOBNPs was added to each bottle, and the pH adjusted to pH 2.0 with 1 mol L^{-1} HCl. The suspensions were placed under agitation, and after varying time intervals (between 24 and 120 h)

samples were removed and filtered through 0.45 μm Millipore filters. The filtrates were stored in polyethylene containers, acidified with 1:1 nitric acid, for subsequent determination of Cr(VI) and Cr(III). A blank (control) solution was prepared without the SPMIOBNPs material. The experiments were performed in triplicate (CERQUEIRA *et al.*, 2012).

- **Determination of Cr(VI) and Cr(III) in solution**

The concentrations of Cr(VI) and Cr(III) were determined in the filtrates. The amount of metal that had been removed was determined as the difference between the total amount of chromium added and the amount measured in the filtrate.

5. RESULTS AND DISCUSSION

5.1. Characterization of SPMIOBNPs

It has been emphasized on several occasions that nanoparticles have special properties which make them useful for some different applications. In order to analyze these different properties, it is always necessary to use different kinds of techniques. This chapter is concerned in explaining the basics of the main kinds of techniques used in this thesis to characterize the synthesized SPMIOBNPs.

5.1.1. FTIR Analysis

The Fourier transform infrared (FTIR) spectroscopy a time-saving method and allows the analysis of a relevant amount of composition and structural information to identify functional groups in the specific material. Figure 31 shows the spectrum of tannins showing a strong absorption around 3700 and 3000 cm^{-1} with a wide and strong band centered at 3381 and 3356 cm^{-1} respectively. These bands are assigned to the hydroxyl groups (OH) stretching vibrations and due to the wide variety of hydrogen bonding with the OH group. Also a peak at 2927 cm^{-1} and a small shoulder at 2860 cm^{-1} associated with the symmetric and anti-symmetric C–H stretching vibrations of CH_2 and CH_3 groups respectively (ARSHAD *et al.*, 1969). The peaks at 1720 cm^{-1} is consequence of the carbonyl groups, i.e. C=O, stretching vibration of carboxylic acids and esters structures (STARLIN *et al.*, 2012). The deformation vibration of the C=C aromatic bonds in the phenolic groups absorbs in the region of 1400-1500 cm^{-1} (STUART, 2005). At 760 cm^{-1} shows the result distortion vibration of C=C in benzene rings (SOCRATES, 2004).

Figure 32 represents some of the main characteristic functional groups in the pyrolysed SPMIOBNPs at 400 °C and 700 °C with condensed tannin. The absorption bands at 1480, 1680, and 3350 cm^{-1} normally originates from carbon dioxide and water which generally nanomaterial absorbed from the environment due to their mesoporous structure. The intensity of aromatic behavior decline in the spectrum of SPMIOBNPs 700 due to the loss of organic material poly hydroxyl groups near 1300-1600 cm^{-1} . The peaks at 1000-1400 cm^{-1} are attributed to the C–OH stretching and O–H bending vibrations more distinct in SPMIOBNPs 700 (BAE *et al.*, 2012). The peak present at 850 cm^{-1} attributed the presence of halogen chloro group (WU *et al.*, 2011). A slight small distinct peak at 2365 cm^{-1} can be referred to

surface and bulk O–H groups in magnetite nanoparticle (ROSE *et al.*, 2013). As analyzing the SPMIOBNPs 700 with FTIR and magnetic data in section confirming also the rare amount of organic material compared to SPMIOBNPs 700.

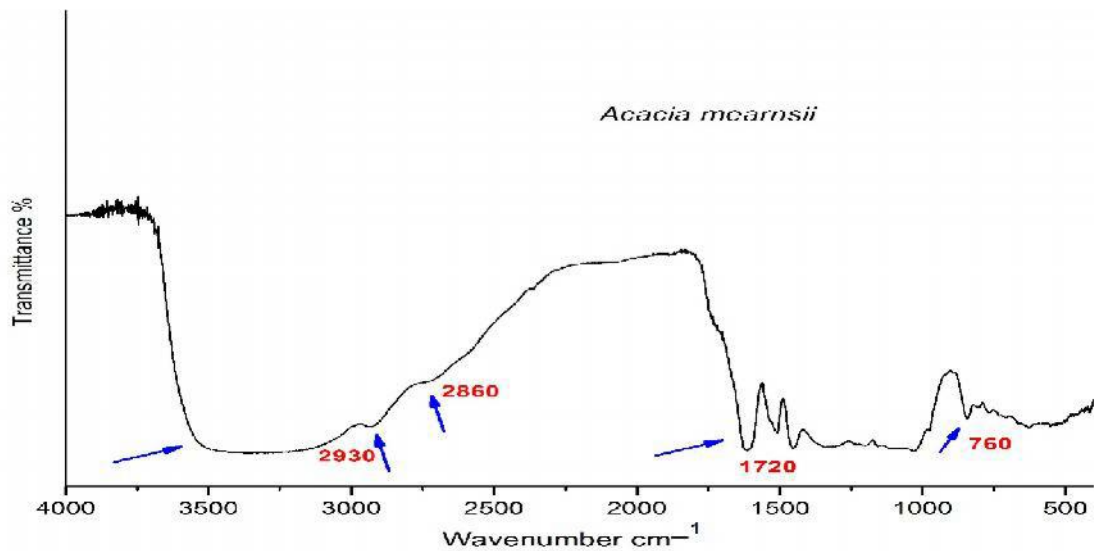


FIGURE 31 – FTIR SPECTRUM OF TANNIN EXTRACT OF ACACIA MEARNsii

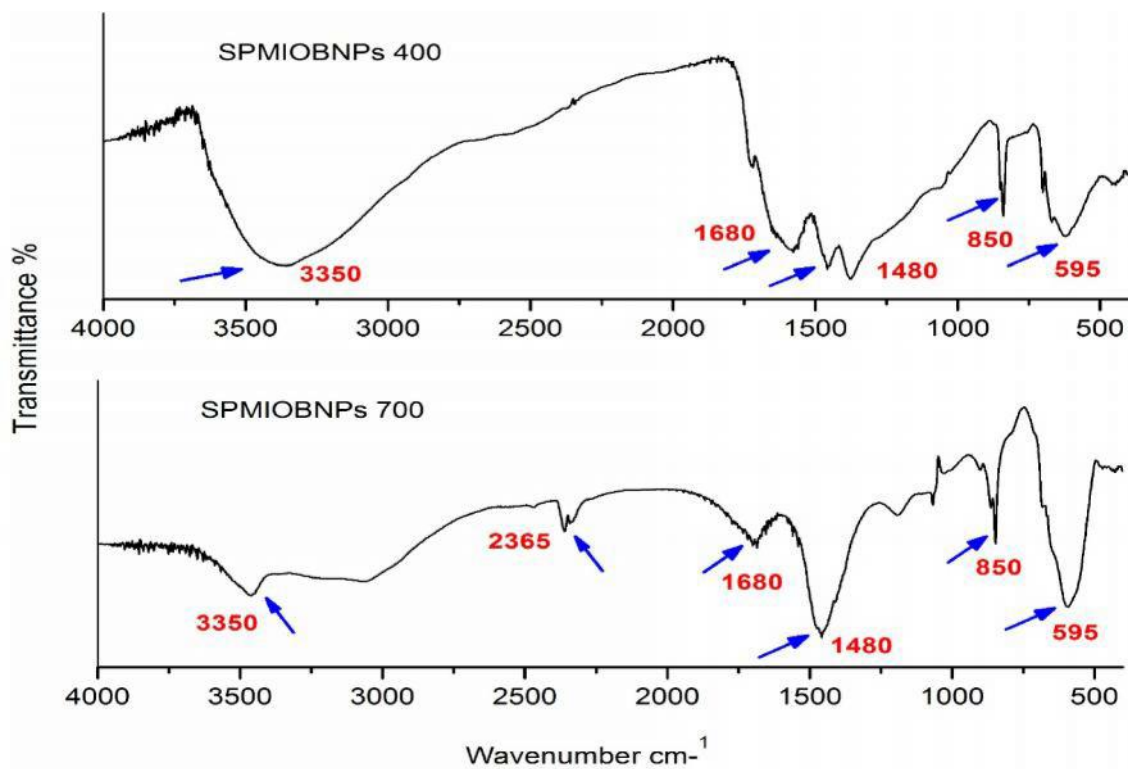


FIGURE 32 – COMPARATIVE FTIR SPECTRUM OF SPMIOBNP 400 AND SPMIOBNP 700

5.1.2. EPR STUDY

Below we can see the EPR spectra of tannin plus FeSO_4 and tannin plus FeCl_2 mixtures (Fig.33, blue spectra) and nano met tanfloc, a zwitterion tannin polymer, and nano met tannin (red and pink spectra, respectively). Both the spectra of tannin mixed with the Fe(II) salts present spectra composed of lines due to the diluted dominions of isolated Fe(III) ions in oxygenated complexes with rhombic distortions ($g = 9.0$ and $g = 4.3$). The two spectra also present a wide and low absorption line with $g = 2.1$, both due a clusters of Fe(III) ions, showing the tannin oxidations capacity of Fe(II) to Fe(III) .

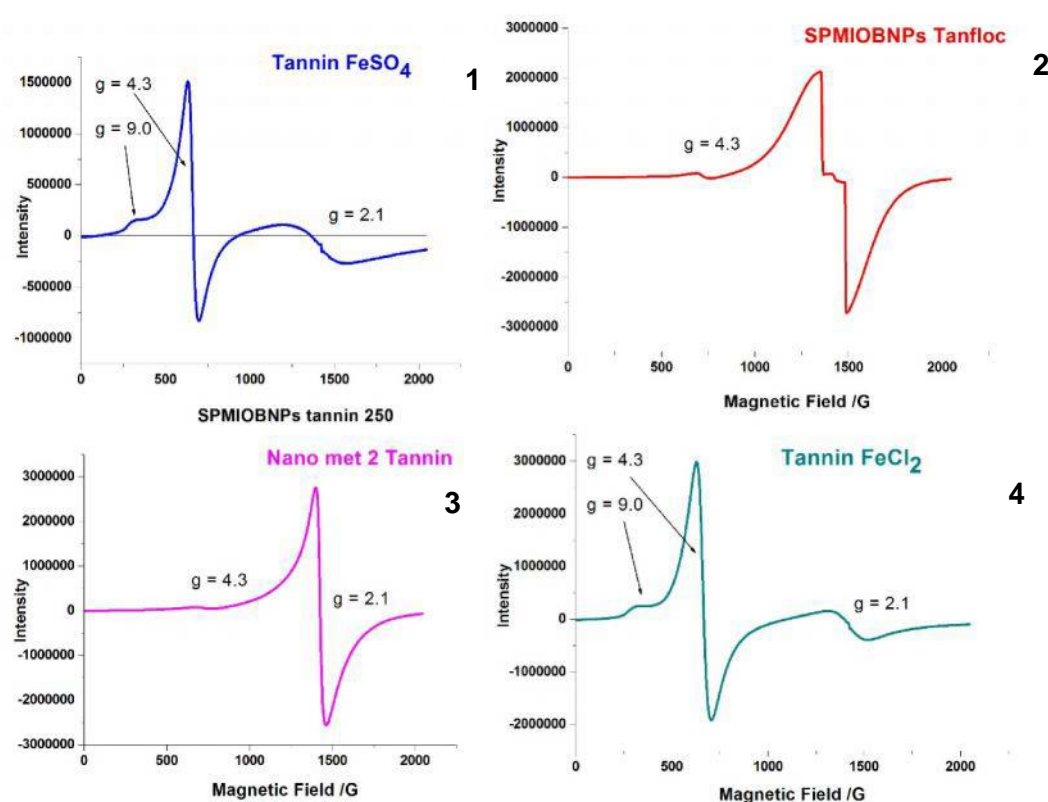


FIGURE 33 – 1.TANNIN FESO4 ; 2.NANO META TANFLOC ; 3. NANO META TANNIN; 4.TANNIN FECL2 .

After heating the tannin Fe(II) mixture to 250 $^{\circ}\text{C}$ the formed SPMIOBNPs shows a high and narrow absorption line at $g = 2.1$. The tannin acted as a template for the superparamagnetic material formation. The tanfloc Fe(II) mixture submitted to the same conditions shows a more intense superparamagnetism. So, the tanfloc, with its zwitterion structure seems to be a more effective template for paramagnetic iron oxide preparation. Tanfloc was not used in the next synthesis in this work

because it was not a good green chemistry preparation precursor. Tanfloc suffer decomposition by heating with liberation of urea vapors. Figure 34 shows the EPR spectra of the SPMIOBNPs obtained by heating tannin and Fe(II)/Fe(III) salts at 400 and 700 0C. The magnetism was so strong that it was impossible to get good EPR spectra even at very low microwaves powers.

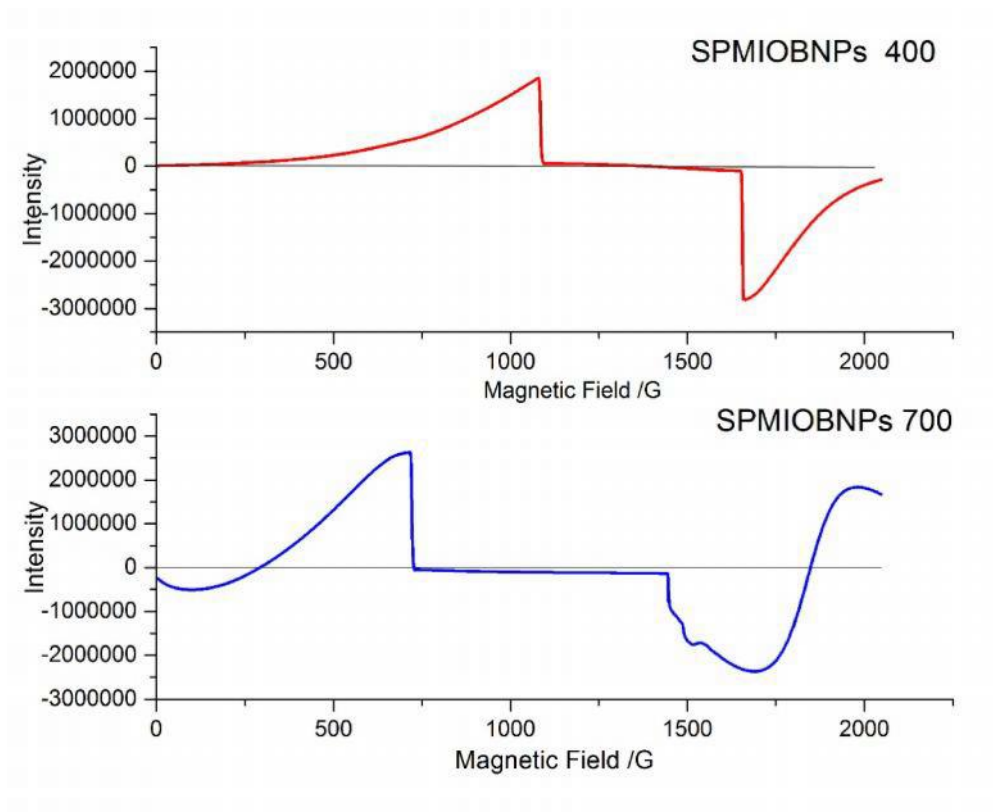


FIGURE 34 – COMPARATIVE EPR SPECTRA BETWEEN THE REFERENCE I.E. SPMIOBNP 700 AND SPMIOBNP 400 RESPECTIVELY.

5.1.3. SEM-EDS of Tannin Extract and SPMIOBNPs

Scanning electron microscopy (SEM) provides detailed high-resolution images of the sample by restoring a focused electron beam against the surface and detecting secondary or backscattered electron signal. An Energy Dispersive X-Ray Analyzer (EDX or EDA) was used to provide elemental identification and quantitative compositional information. The SEM images of pure tannin powder shows that the particles are with irregular shape, large particle size with smooth and fine surface as shown in the Figure 35. The EDX analysis of tannin (Fig. 36 and Table 2 confirming the principle's elements i.e. C, O and Cl are present in greater amount

and also with some amount of Al, K and Ca respectively. The presence of Cu in the spectra is of the metalizing copper was used for analysis.

The SEM micrographs of SPMIOBNPs surface adsorbent in the Figure 37 showing porous surface and crystalline in nature, due to the formation of nanoparticle. The porous shaped structure of SPMIOBNPs best suitable for adsorption after reacting with iron with very fine porous structure even at high magnification best suitable for adsorption. The chemical analysis of SPMIOBNPs 400 showing the presence of Fe in large quantity attributed the formation of magnetic nano composite as shown in the Figure 38 and Table 2.

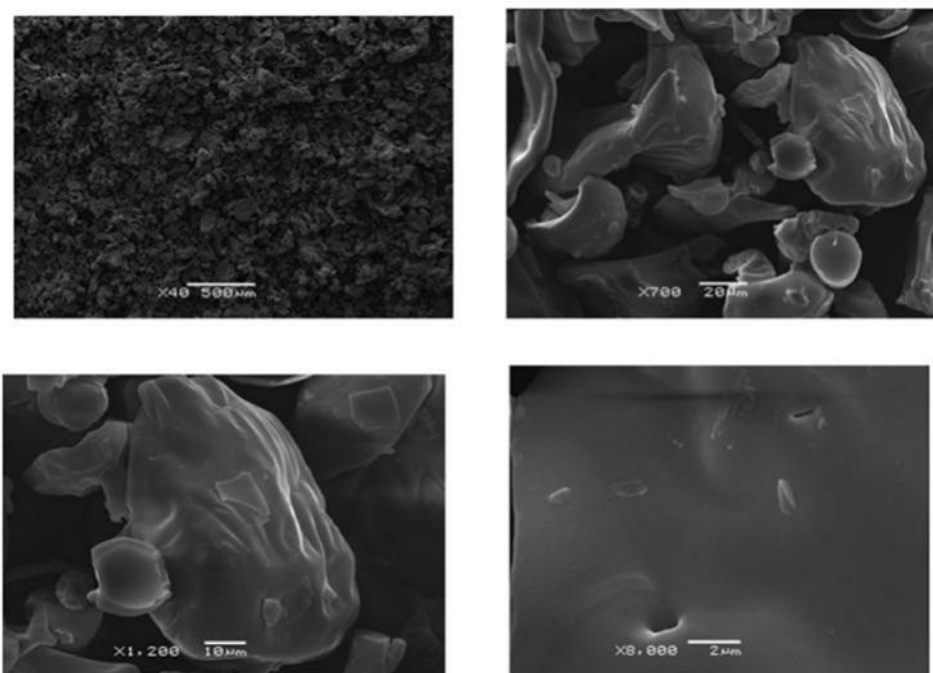


FIGURE 35 – SEM MICROGRAPHS OF PURE TANNIN EXTRACT FROM *ACACIA MEARNIS*

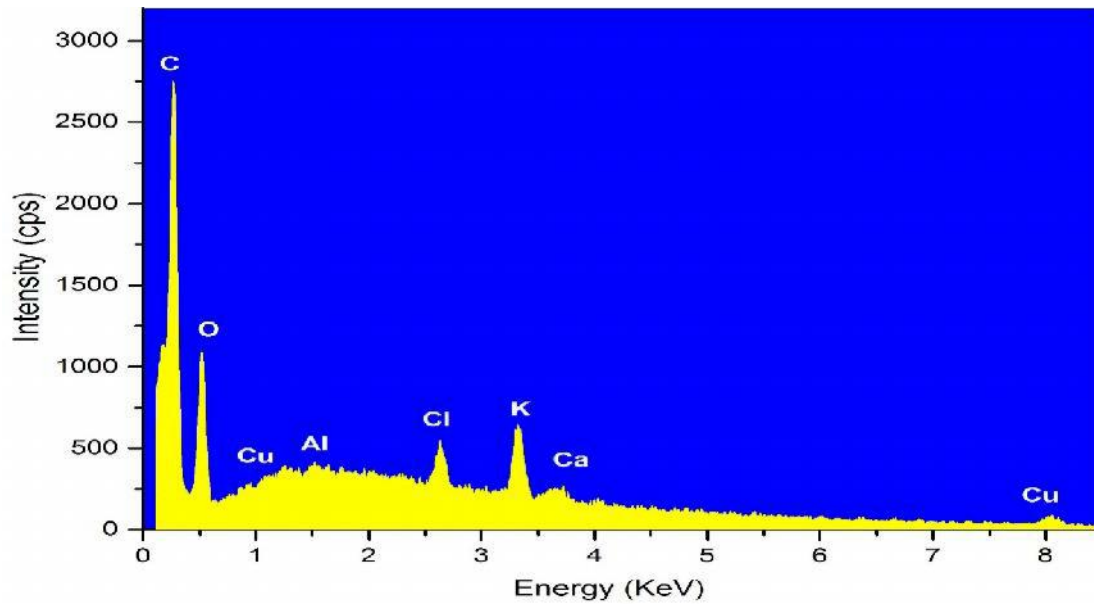


FIGURE 36 – SEM-EDX ANALYSIS OF TANNIN EXTRACT FROM ACACIA MEARNsii

TABLE 2 – QUANTITATIVE ELEMENTAL RESULTS OF TANNIN EXTRACT

<i>Element Line</i>	<i>Net Counts</i>	<i>Weight %</i>	<i>Weight % Error</i>	<i>Atom %</i>
C K	24243	70.24	+/- 0.97	78.42
O K	6617	23.46	+/- 0.64	19.67
Al K	158	0.04	+/- 0.03	0.02
Cl K	3186	1.20	+/- 0.05	0.45
K K	5317	2.32	+/- 0.10	0.79
Ca K	989	0.50	+/- 0.05	0.17
Cu K	800	2.24	+/- 0.41	0.47
Total		100.00		100.00

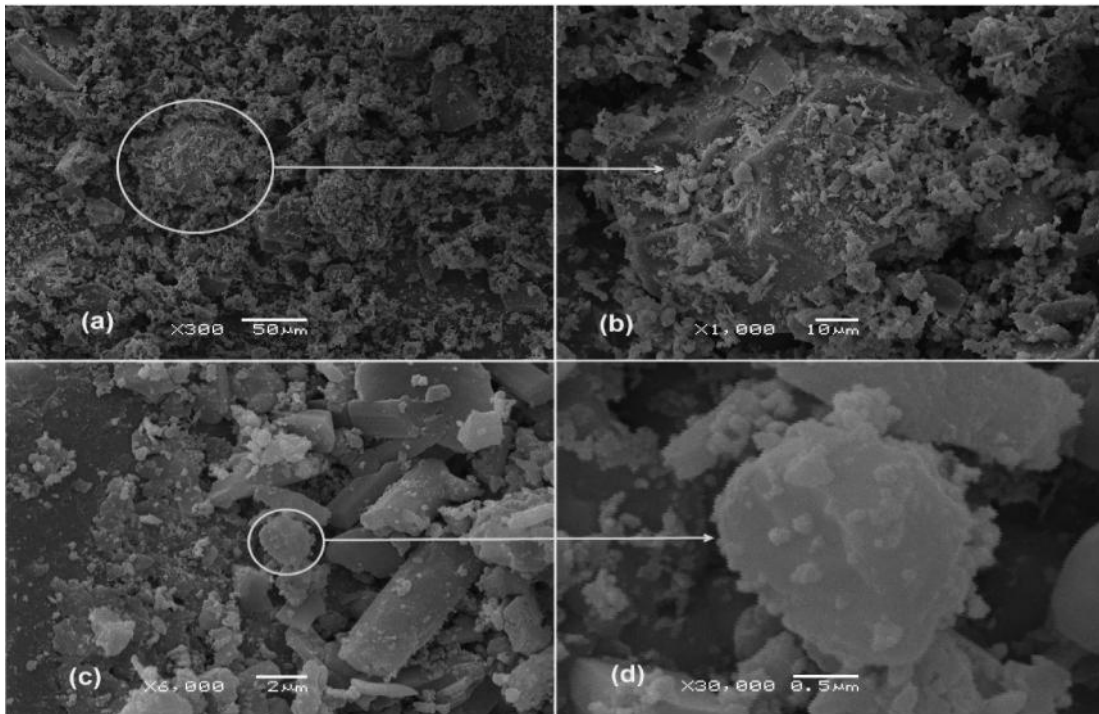


FIGURE 37 – SEM MICROGRAPHS OF SPMIOBNP

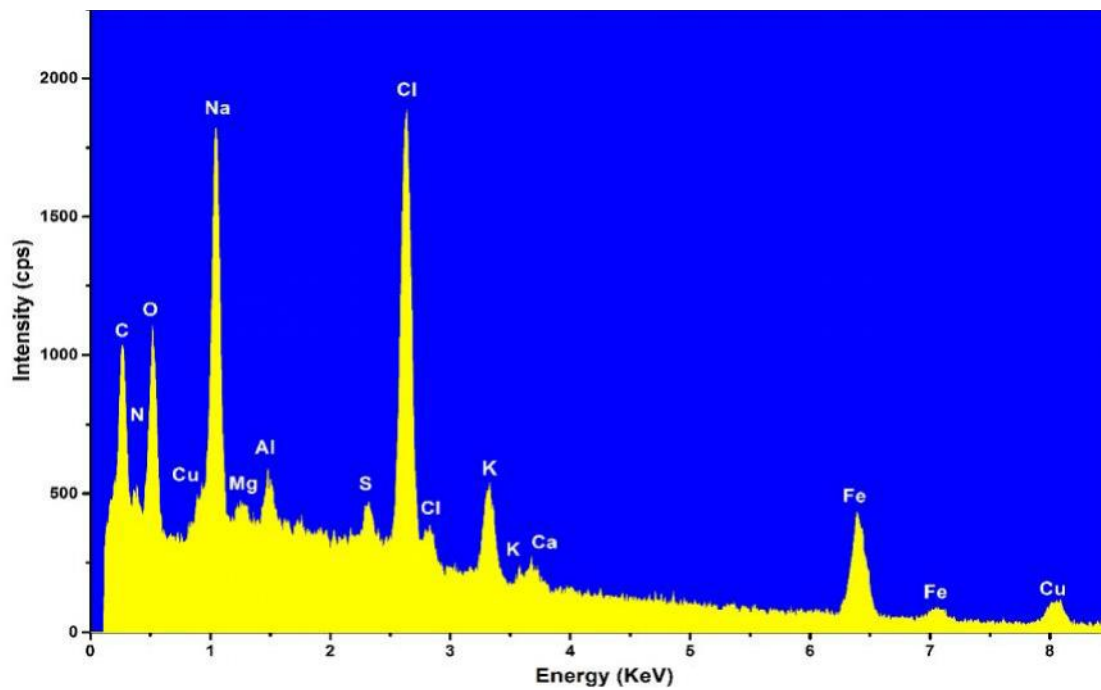


FIGURE 38 – SEM-EDS SPECTRA OF SPMIOBNP

TABLE 3 – QUANTITATIVE ELEMENTAL RESULTS OF SPMIOBNP

Element Line	Net Counts	Weight %	Weight % Error	Atom %	Atom % Error
C K	9602	61.47	+/- 2.92	76.13	+/- 3.62
O K	4236	16.34	+/- 0.39	15.19	+/- 0.37
Na K	5850	4.26	+/- 0.15	2.75	+/- 0.10
Cl K	15613	6.80	+/- 0.12	2.85	+/- 0.05
K K	2829	1.44	+/- 0.11	0.55	+/- 0.04
Fe K	5114	7.82	+/- 0.32	2.08	+/- 0.09
Cu K	593	1.88	+/- 0.26	0.44	+/- 0.06
Total		100.00		100.00	

5.1.4. Transmission Electron Microscopy

TEM is the main characterization technique for a morphologic, structural analysis and size of synthesized nanoparticles. TEM analysis helps further to confirming the formation, size and morphology of magnetic nanoparticles. The micrograph in the Figure 39 supporting the biochar organic matter shell around the particles. The SPMIOBNPs include iron oxide irregular nano-particles with diameter around 25–35 nm having rectangular in shape. These were also accorded with the results obtained from the XRD-analysis (see below). The SPMIOBNPs revealed significant crystal lattice plane while the biomass is in the form of biochar surrounding the particles was amorphous as a result of pyrolysis (MOGHANIAN *et al.*, 2014). The images reveal the formation of highly broad size distribution and random near-spherical shapes, they are stable and separated at certain pH range of a solvent. It is important to note that shape and size are significantly dependent from a homogeneity of the type of method used.

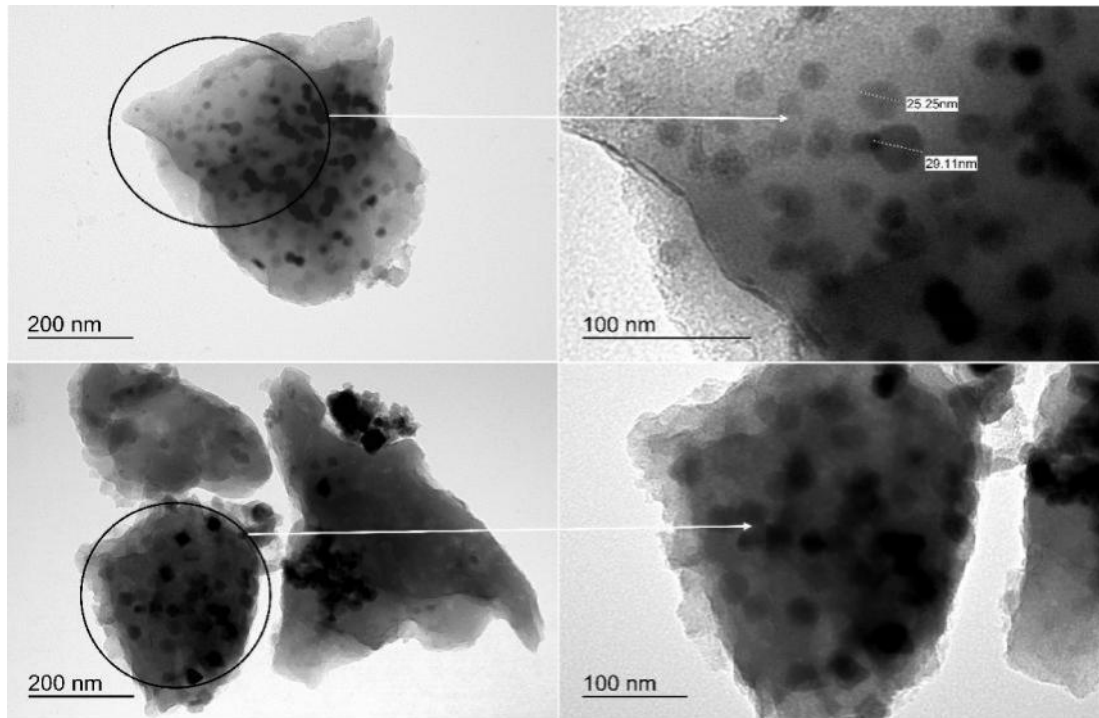


FIGURE 39 – TEM MICROGRAPHS OF SPMIOBNP

5.1.5. XRD Diffraction Analysis

The XRD diffractogram shows that the tannin magnetic nanoparticles are composed of a phase either magnetite or maghemite exhibiting inverse spinel structure with a biochar organic portion as shown TEM images having average diameter around 20-30 nm, which can be a mixture of both as well. The powder XRD analyses (Fig.40) indicated the presence of the pure spinel crystalline phase with the reflections 2 at 18.31, 30.12, 35.48, 37.10, 43.12, 53.48, 57.0, 60.9, 62.5, 65.2, 71.0, 74.06, 78.97, and 86.83 also match well with the file from International Center for Diffraction Data—ICDD card no. 86-1340. The XRD analysis confirms that the adsorbent particles are Face Centered Cubic (FCC) magnetite or maghemite crystals or both as the experimental Miller indices were almost identical with literature values as in the inset of Figure 40 (FJELLVAG *et al.*, 1996, OKUDERA *et al.*, 1996). The XRD analysis can be also widely used for determination of average crystallite size from the full width at half maximum (FWHM) of a diffraction peak using the Scherrer equation as:

$$D = \frac{0.9 \times \lambda}{\beta \times \cos\theta}$$

Where ' λ ' is wave length of X-Ray (CuK = 0.1541 nm or 1.541 Å), ' β ' is FWHM (full width at half maximum) in radians, 0.9 is a constant used for a shape factor, ' θ ' is the diffraction angle and 'D' is particle diameter size (SUN *et al.*, 2004) . The determined results in this work were 27 nm, 31 nm, and 35 nm for magnetite and maghemite nanoparticle (HU *et al.*, 2005, STAROWICZ *et al.*, 2011).

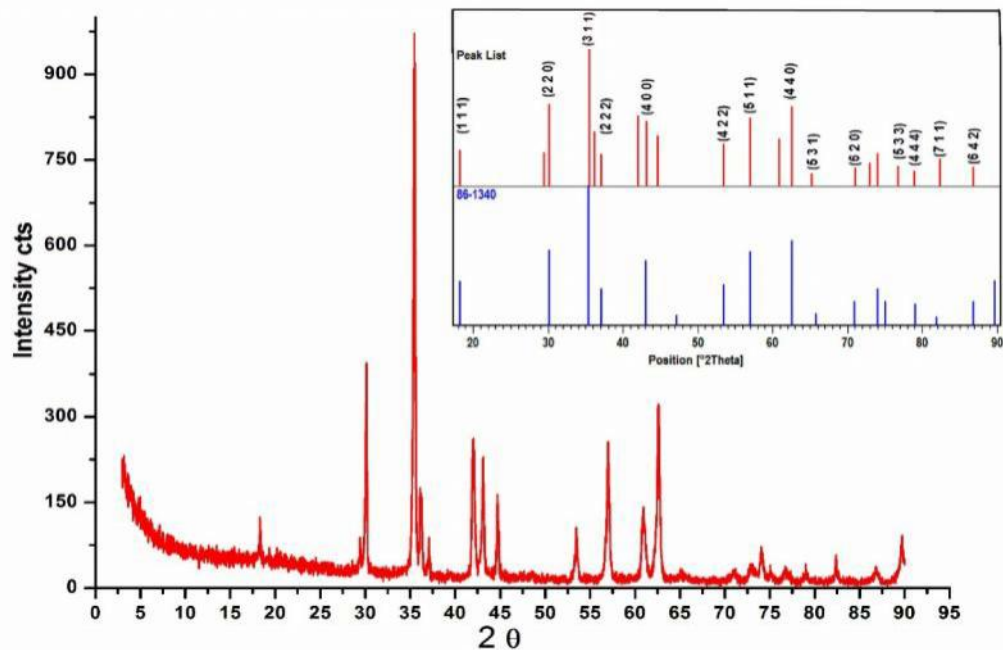


FIGURE 40 – XRD DIFFRACTOGRAM OF THE SPMIOBNP, THE INSET SHOWS SPECIFIC 2 VALUES COMPARED WITH ICDD REFERENCE CARD NO. 86-1340

5.1.6. Thermogravimetric Analysis (TGA)

The TGA/DTG curves of SPMIOBNPs are shown in figure 41. The TGA/DTG analysis was achieved under the Nitrogen atmosphere (ZHAO *et al.*, 2006). There are four derivative peaks in the DTG curve which related to the four mass losses in the curve. The thermal behavior of the material used as adsorbents after pyrolysis lies for the two biomaterials was observed in the region up to 100 °C, a loss of mass in relation to moisture free adsorbed water corresponding to about 5-10 % of the total mass of the sample. There is strong peak decomposition observed in the region 200-400 °C was found for SPMIOBNPs precursor material in the production of magnetic nanoparticles may be associated with natural polyphenolic compounds that form part of its composition. This loss of mass in this temperature range MNPs

400 was observed to be obtained at 400 °C for pyrolysis leading to decomposition of the compounds.

The mass loss observed around 360 °C and 750 °C for the SPMIOBNPs according Magellan et al. (2009) may be related with the reduction of Fe³⁺ magnetite by biochar to Fe²⁺, as observed in the spectrum infrared bands corresponding to Fe–O bond, the reactions presented below:

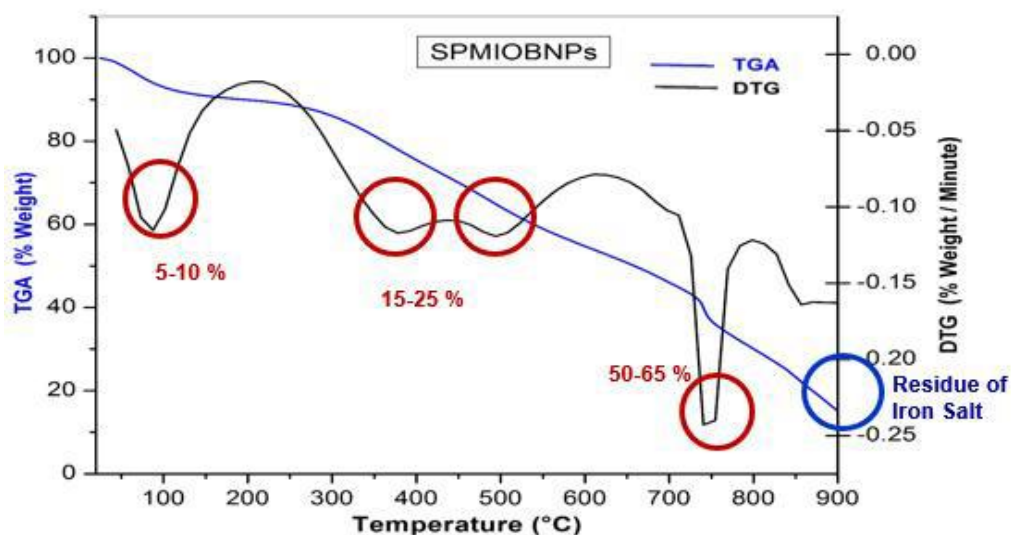
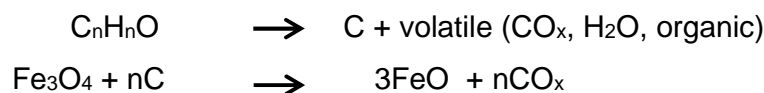


FIGURE 41 – TGA/ DTG ANALYSIS CURVES FOR SPMIOBNP

5.1.7. Magnetic Properties of SPMIOBNPs

The SPMIOBNPs solid samples in vial is magnetic in nature that can show attachment physically with the external magnetic field with neodymium magnet as shown in Figure 42. The magnetization measurement obtained gives the value 32.0 emu/g showing a little bit lower value from the pure Fe₃O₄ nanoparticles reported values, which attributed that the nanoparticles are surrounded by organic shell or core (KOLHATKAR *et al.*, 2013).

The magnetic properties of the SPMIOBNPs were studied using a vibrating sample magnetometer SQUID. The magnetization cycles of a SPMIOBNPs sample measured at 10 K and 300 K are shown in Figure 43 and 44, respectively. The saturation magnetization was 32 emu/g at 300 K. This value is slightly lower than

reported for Fe_3O_4 nanoparticles surrounded by an organic shell, which can lead to a degree of surface disorder and changes in the cation distribution (DARROUDI *et al.*, 2014). The magnetization cycle measured at 10 K revealed a saturation magnetization value of 74 emu/g, as well as hysteretic behavior, as shown in the inset of Figure 43. Non-hysteretic behavior was observed at 300 K, as shown in the inset of Figure 44. The field cooling (FC) and zero field cooling (ZFC) magnetization curves are shown in Figure 45. These measurements were carried out between 10 and 390 K with an applied field cooling of 0.1 T, in order to confirm the superparamagnetism. As the temperature was raised, the ZFC magnetization first increased, and then decreased after reaching a maximum at 120 K. The shoulder clearly observed at around 50 K in the ZFC curve was probably associated with a secondary particle size distribution. The FC magnetization curve showed a maximum at around 120 K, clearly indicating the transition between superparamagnetism and the blocked state (YOON *et al.*, 2011). A progressive increase of the FC magnetization curve when the temperature decreased below 30 K indicated the presence of a small fraction of dispersed magnetic ions in the biochar. The magnetization measurements therefore revealed that the SPMIOBNPs showed superparamagnetic behavior at room temperature (DEMIR *et al.*, 2013, KANDPAL *et al.*, 2013).

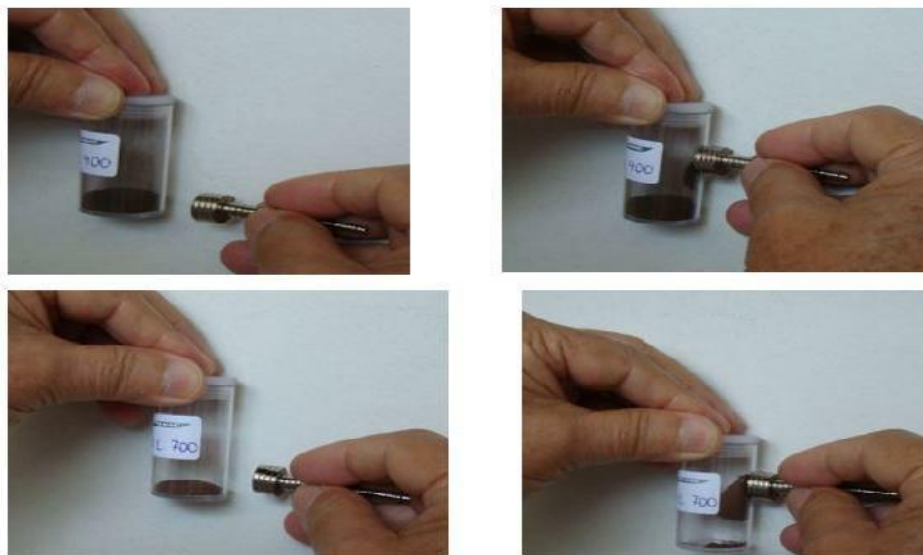


FIGURE 42 –THE ATTRACTION OF SPMIOBNP 400 AND SPMIOBNP 700 UNDER AN EXTERNAL MAGNETIC FIELD

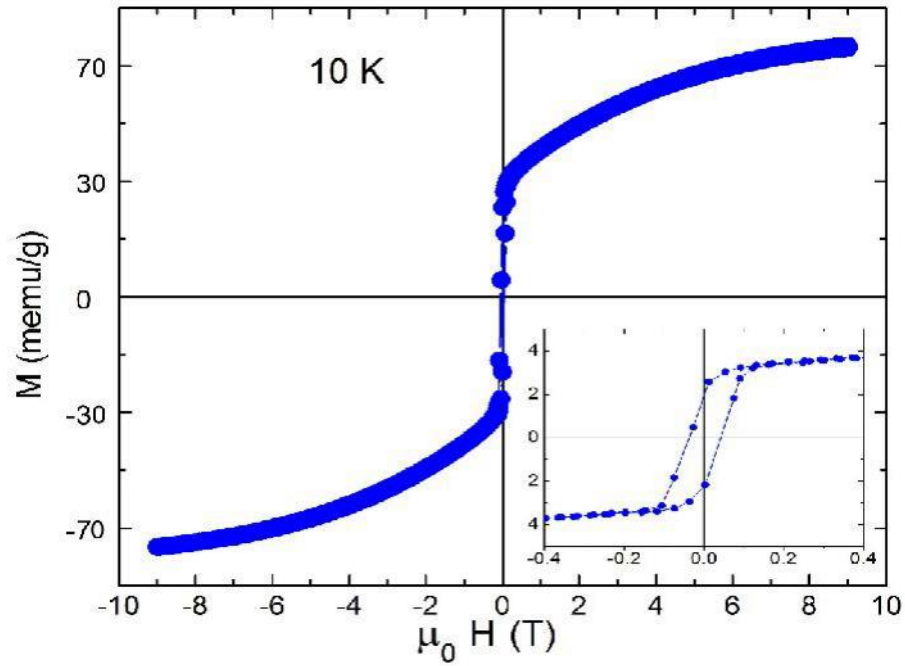


FIGURE 43 – MAGNETIZATION CYCLES OF SPMIOBNP 400 MEASURED AT 10 K.

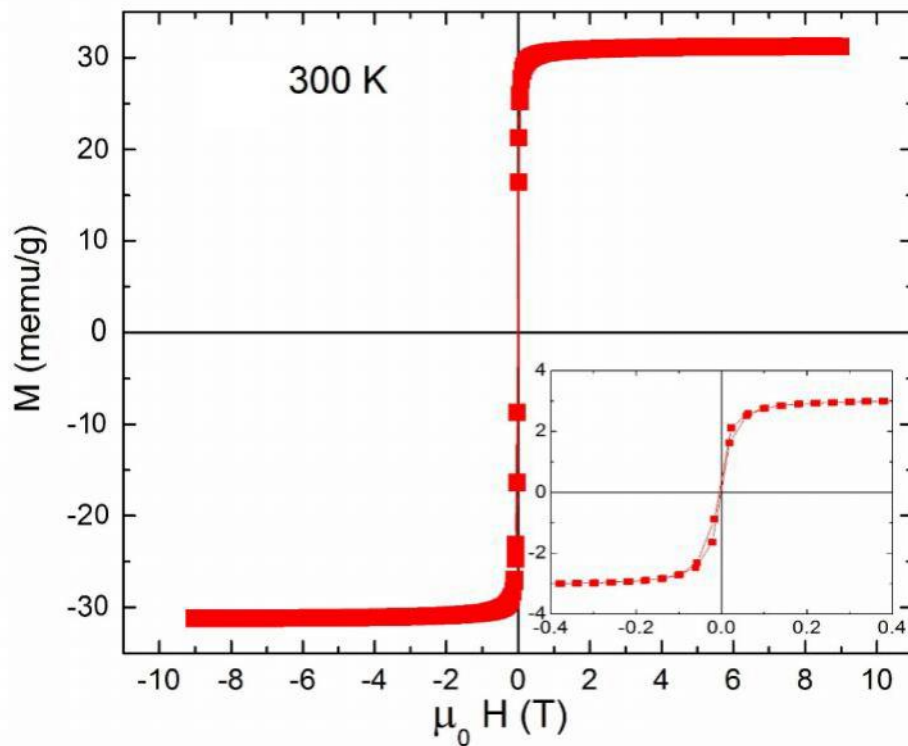


FIGURE 44 – MAGNETIZATION CYCLES OF SPMIOBNP 400 MEASURED AT 300 K.

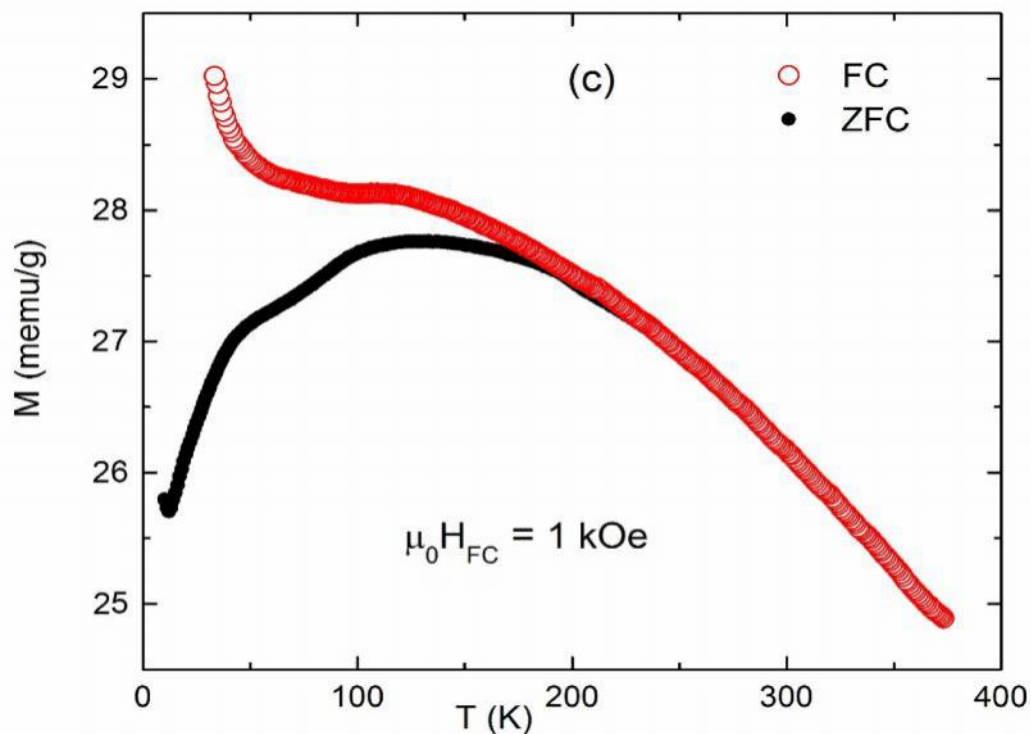


FIGURE 45 – ZERO FIELD COOLING (ZFC) AND FIELD COOLING (FC) MAGNETIZATION CURVES FOR THE SPMIOBNP 400.

5.1.8. BET

Brunauer–Emmett–Teller (BET) nitrogen adsorption-desorption isotherms were recorded for the SPMIOBNPs in order to understand the nature of the surface and pore behavior in possible sorption process. According to the IUPAC classification, the shape of the curves corresponded to a Type III isotherm with H3 hysteresis loop in the Figure 46 (NAGASHANMUGAM & SRINIVASAN, 2011). This type of isotherm reflects co-operative adsorption, with the molecules that have already been adsorbed acting to enhance the adsorption of other molecules. In this situation, adsorbent-adsorbate interactions are less important than adsorbate-adsorbate interactions (BANSAL & GOYAL, 2005). The pores are micropores in size, exist in the form of multilayer and also shows deviation from Langmuir model (WANG *et al.*, 2012). The H3 hysteresis loop is associated with the filling and emptying of the mesopores by capillary condensation, favoring good adsorption at high P/P_0 ratios, with plate-like particles giving rise to slit-shaped pores. The surface area of the SPMIOBNPs was $5.602 \text{ m}^2/\text{g}$. The total volume of pores was $7.445 \times 10^{-3} \text{ cc/gram}$ at $P/P_0 = 0.989894$, and the average pore radius was 2.658 \AA . All the calculations were based on the BJH method (BARRETT *et al.*, 1950).

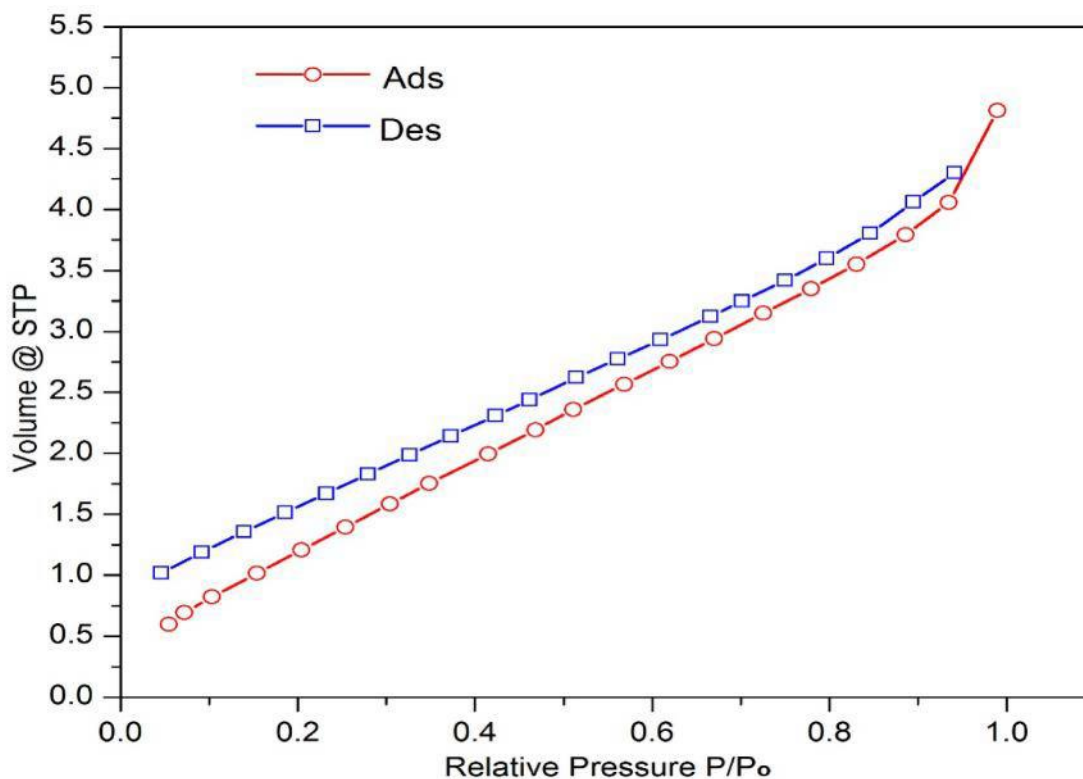


FIGURE 46 – BET ISOTHERM OF THE SPMIOBNPs 400 NITROGEN ADSORPTION (CIRCLES) AND DESORPTION (SQUARES).

5.2. Chromium Removal Results

5.2.1. FTIR Analysis of SPMIOBNPs and SPMIOBNPs 400 Loaded with Cr(VI)

The FTIR spectrum was used to identify some of the main characteristic functional groups changes in the before and after loading the Cr(VI) to the pyrolyzed SPMIOBNPs. The broad band observed at 3410 cm^{-1} in the Figure 47 (a) indicated the presence of stretching mode of hydroxyl groups (OH) and adsorbed water but the effect little bit minimize in loaded sample in the Figure 47 (b) suggesting the complexation of Cr(III) with phenolate groups formed by the displacement of protons by the trivalent chromium (CHEN et al., 2011, WANG et al., 2013). These hydroxyl groups in aromatic rings enable the tannins to form Ferric-Tannate complexes in the form of Fe_3O_4 nanoparticles which further showing practical applications (BANDEKAR et al., 1995, OMOIKE, 2008). A distinct absorptions peaks can be seen in the region of 3145 cm^{-1} referring C–H stretching vibration from aromatic rings. The peaks around 1670 cm^{-1} in the spectrum of SPMIOBNPs corresponds to the C=C aromatic skeletal stretching vibrations with aromatic carbons. The peaks at

1000–1300 cm^{-1} in both of the spectra are attributed to the CH_3 asymmetric vibration, C–OH stretching and OH bending vibrations (WENG *et al.*, 2013). The peak at 1485 cm^{-1} corresponds to symmetric stretch of C=O in the Figure 47 (a) are observed similarly asymmetric stretch of C=O observed at 1570 cm^{-1} in the Figure 47 (b) (DEMIR *et al.*, 2013). The peak near at wavenumber 600 cm^{-1} in both of the spectra is attributed to the characteristic absorption band of Fe–O from Fe_3O_4 structure (HUANG *et al.*, 2009). Some slight change of peaks were observed in the spectra of SPMIOBNPs loaded by chromium, in the regions including 1670-700 cm^{-1} and 3450-2800 cm^{-1} which confirmed that Cr(III) and/or Cr(VI) was complexes and reduced by certain functional groups including carboxyl, amide, and sulfonate present in SPMIOBNPs (BAHAFID *et al.*, 2011). The new peaks present at 750-850 cm^{-1} indicating Cr(III) and at a wavenumber 840-900 cm^{-1} attributing Cr(VI) adsorbed on SPMIOBNPs (HOLMAN *et al.*, 1999).

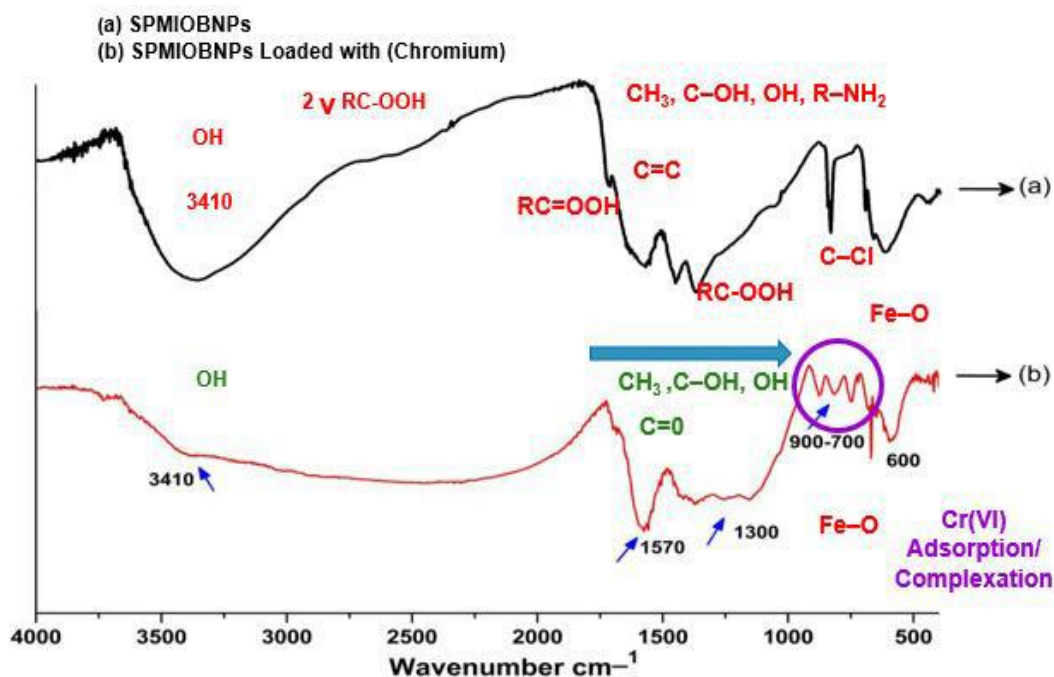


FIGURE 47 – FTIR SPECTRUM OF SPMIOBNP 400 (A) , FTIR SPECTRUM OF SPMIOBNP 400 LOADED WITH HEXAVALENT CHROMIUM (B).

5.2.2. SEM EDS and XPS analysis of SPMIOBNPs and SPMIOBNPs Loaded with Cr(VI)

Scanning electron micrographs at different magnification of the SPMIOBNPs 400 surface adsorbent showing porous surface and crystalline in shape in the Figure 48 (A & B). The SEM micrographs of chromium loaded SPMIOBNPs clearly indicated the presence of new shiny bulky particles produced over the surface of metal loaded adsorbents indicating presence of chromium layer on the surface. It can be observed from the Figure

48 (C & D).that the surface morphology shows changes also having different texture with decrease in porosity, increase in luster.

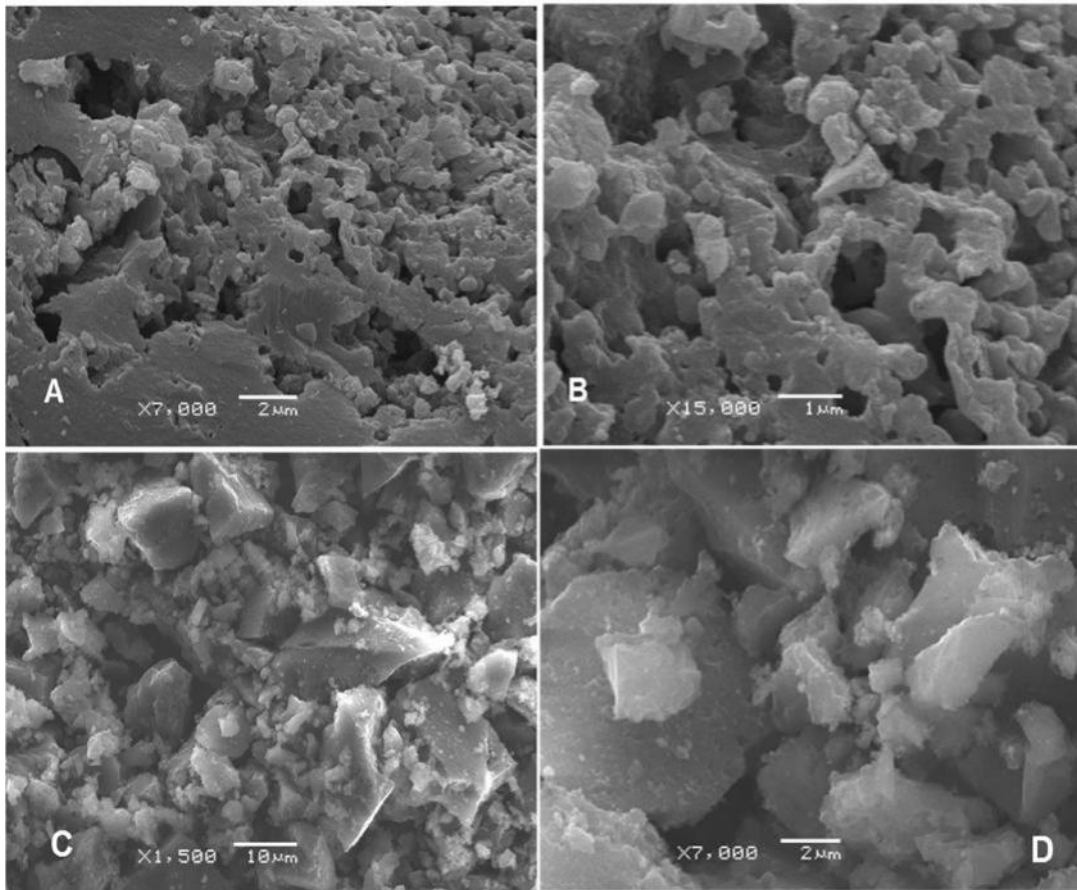


FIGURE 48 – (A), (B) SEM MICROGRAPHS OF SPMIOBNP 400 AND (C), (D) SPMIOBNP 400 LOADED WITH HEXAVALENT CHROMIUM

The EDS of SPMIOBNPs shows Fe and Cl as shown in the Figure 49 in greater content due to the formation of magnetic nanoparticle. The principle's elements i.e. C, O and Cl are according to their order of occurrence as with the increasing of pure carbon content due biochar formation, the Cu present in the spectra is of the sample metalizing copper used for analysis of SEM. The chromium presence was also confirmed by the peak at 0.5 & 5.4 keV in the EDS spectra of loaded SPMIOBNPs in the Figure 50 (GANDHIA *et al.*, 2010, MULANI *et al.*, 2013).

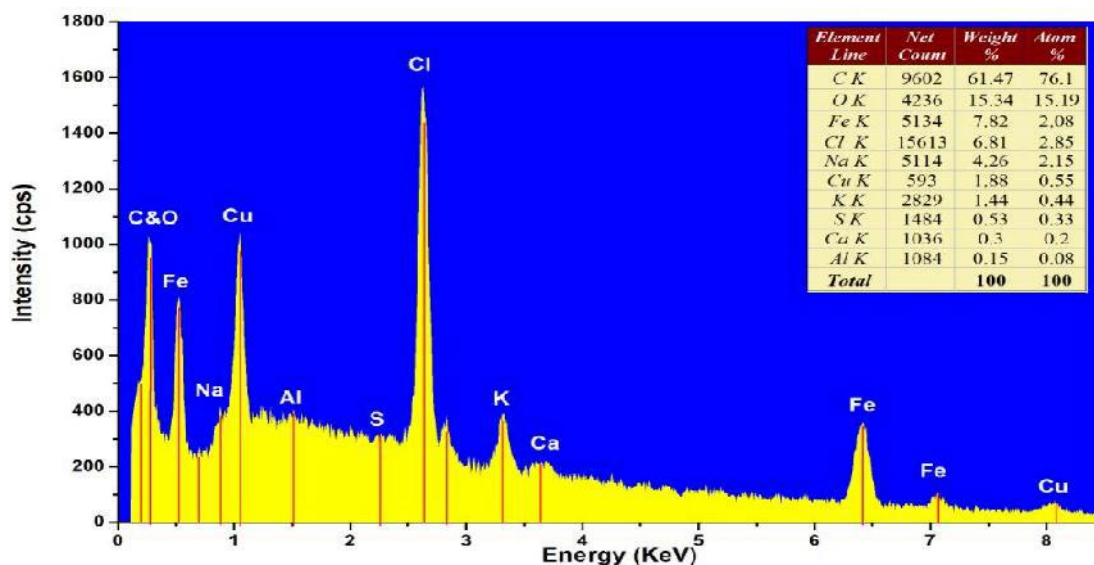


FIGURE 49 – SEM-EDS SPECTRA OF SPMIOBNP 400 WITH QUANTITATIVE TABLE INSERTED.

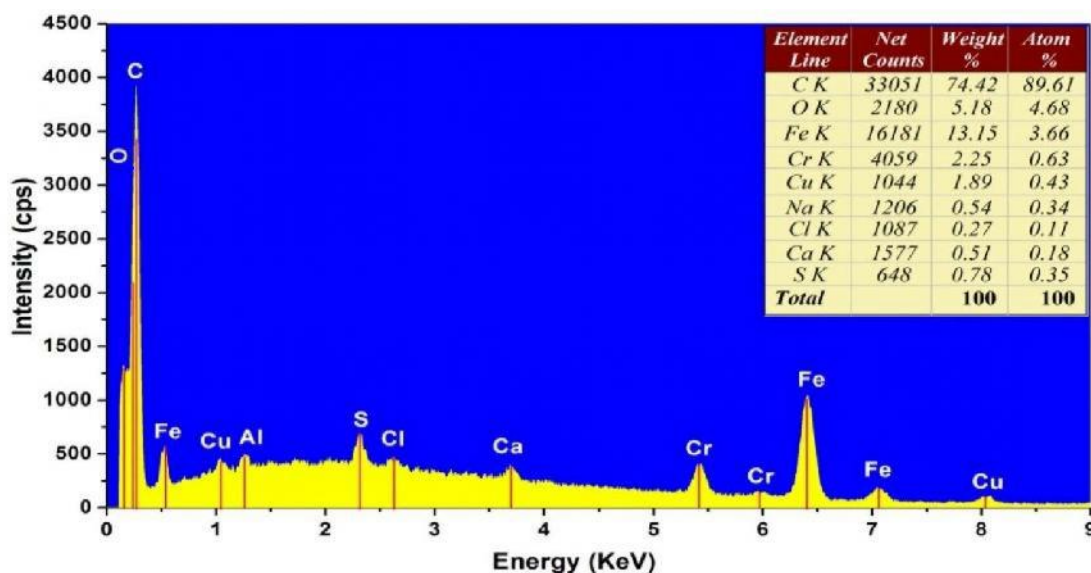


FIGURE 50 – SEM-EDS SPECTRA OF SPMIOBNP 400 LOADED WITH HEXAVALENT CHROMIUM QUANTITATIVE TABLE INSERTED

XPS (X-Ray Photoelectron Spectroscopy) is well established as a powerful tool for the structural characterization of material surfaces and surface reaction products. The method was used here to detect the chemical form of chromium adsorbed by the SPMIOBNPs surface. The structural components can be identified for both of the components. The C 1s peak, main peak at 288.0 eV shows a higher proportion constituting aromatic nature. Oxygen (O 1s) is bonded to the organic and inorganic fractions of SPMIOBNPs showed by

535.0 eV and Fe and Cu also showed on 714.0 eV and 933.0 eV respectively in the Figure 51 (CERQUEIRA *et al.*, 2012). The peak at 577.25 eV e 579.73 eV in the Figure 52 & 53 (magnified) can be attributed to presence of chromium as confirmed the adsorption by SPMIOBNPs from Cr(VI) solution (BUBERT *et al.*, 2000). According to the detail work done by Biesinger and his co-worker which showed that the peak at 577.25 eV showing Cr(III) and e 579.73 eV is Cr(VI) (BIESINGER *et al.*, 2004). There is a difference of intensity peaks in the two levels as the Cr(III) showing almost all of the Cr(III).

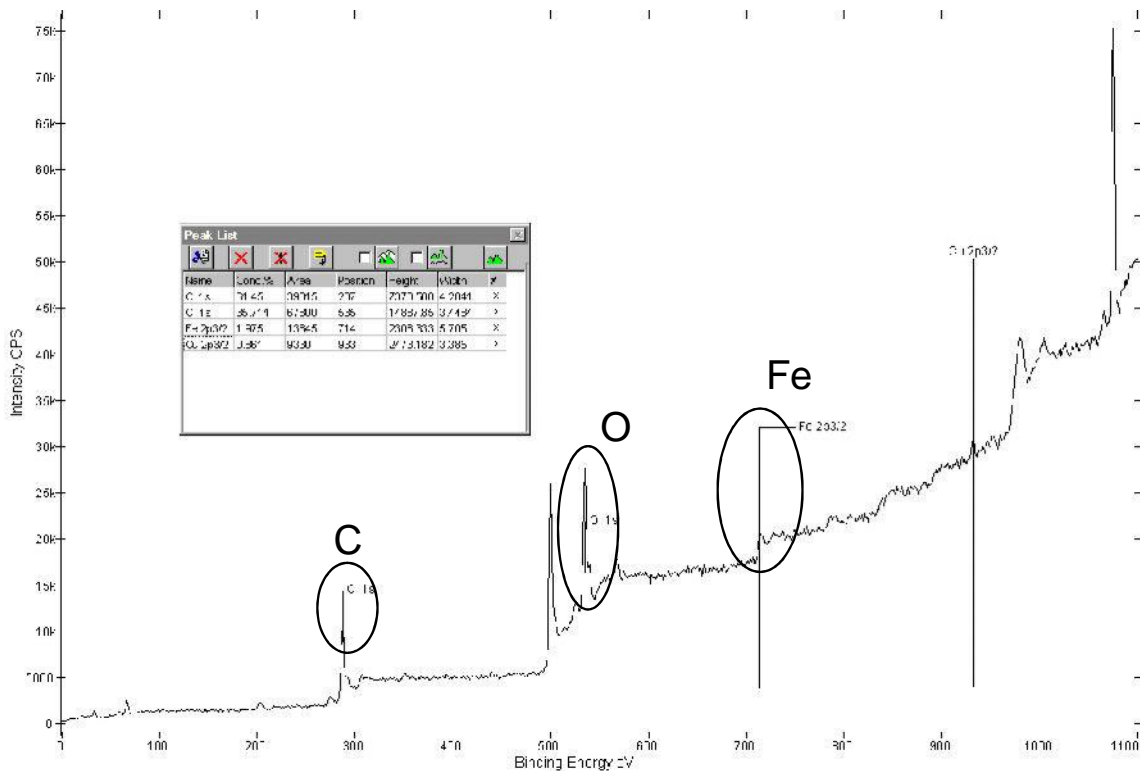


FIGURE 51 – XPS CORE LEVEL SPECTRA OF SPMIOBNP 400

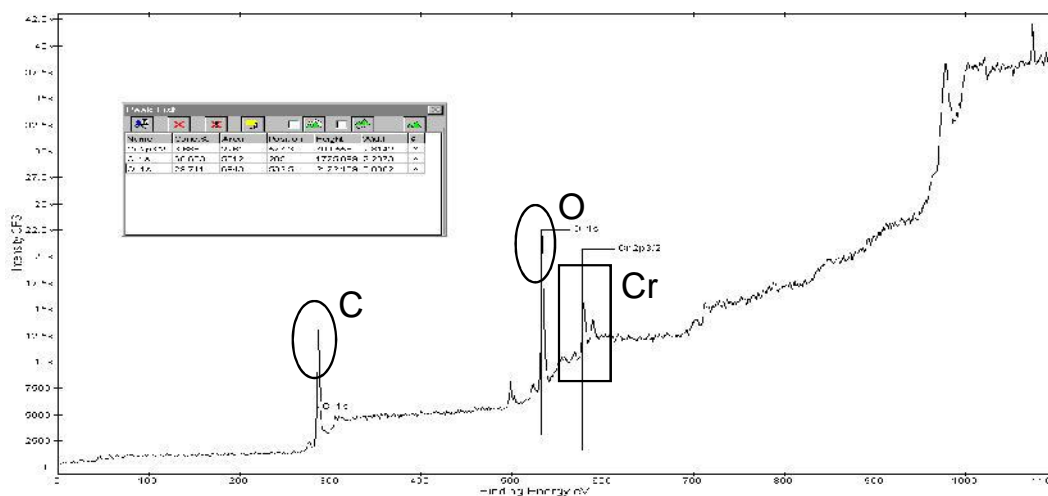


FIGURE 52 – XPS CORE LEVEL SPECTRA OF SPMI0BNP 400 LOADED WITH HEXAVALENT CHROMIUM

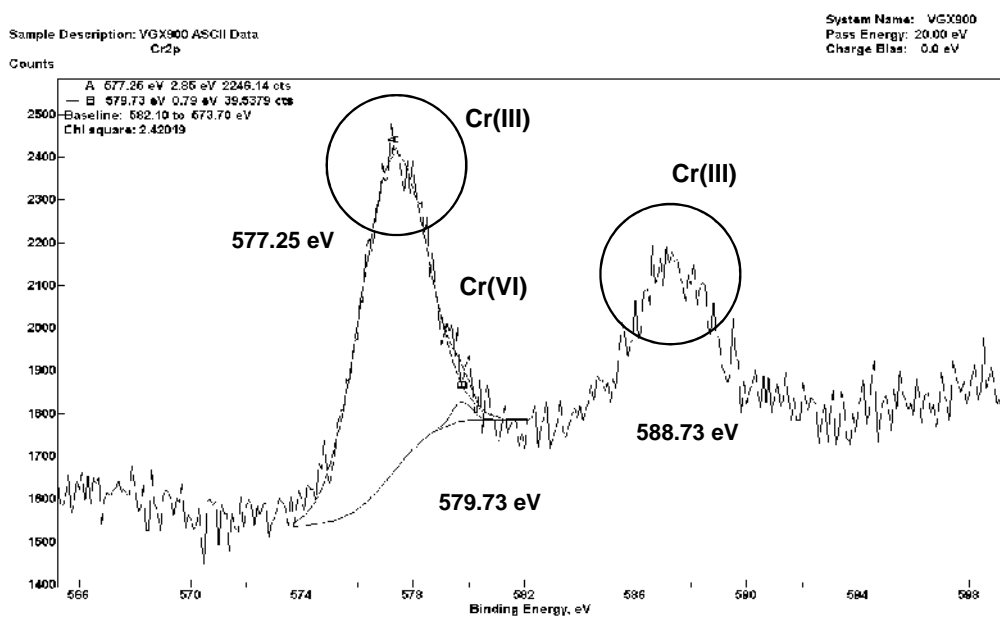


FIGURE 53 – MAGNIFIED XPS CORE LEVEL SPECTRA OF SPMI0BNP 400 LOADED WITH HEXAVALENT CHROMIUM

5.2.3. Quantitative Analysis of Hexavalent Chromium

5.2.3.1. Influence of pH on the reduction/removal of Cr(VI)

In general adsorption of anion is favored at $\text{pH} < \text{pH}_{\text{Pcz}}$. At very low pH, chromium ions exist in the form of HCrO_4^- , at higher pH up to 6 different forms such as $\text{Cr}_2\text{O}_7^{2-}$, HCrO_4^- and $\text{Cr}_3\text{O}_{10}^{2-}$ coexists of which HCrO_4^- leads. As the pH increases equilibrium shifted from HCrO_4^- to CrO_4^{2-} and $\text{Cr}_2\text{O}_7^{2-}$. The SPMI0BNPs follows the

similar pattern having greater value of pH_{PCZ} i.e. 9.6 as shown in Figure 54. The point of zero charge (PZC) or the isoelectric point is defined as the pH at which the surface of the sorbent has a neutral charge. The PZC is a significant property and shows the electrical neutrality of the adsorbent and surface at a specific value of pH (PANNEERSELVAM *et al.*, 2011). The adsorption of Cr(VI) studied by the SPMIOBNPs at varying pH values, such as 1.0, 2.0, 3.0, 4.0, 5.0, 6.0 and 7.0. Increase in adsorption capacity was observed from pH 1.0 through 4.0 ; However, further increase in the pH value form 4.0 through 7.0 resulted in decrease in reduction capacity of Chromium Fig. 55.

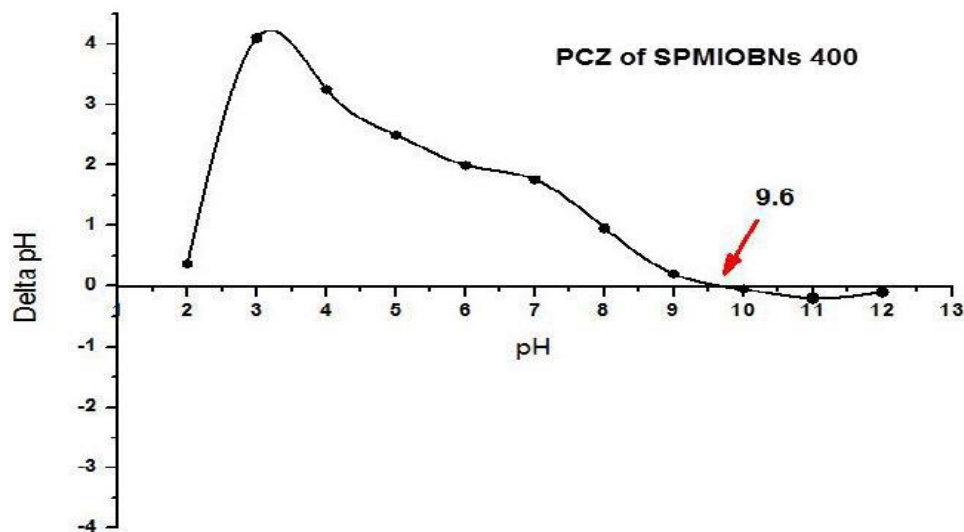


FIGURE 54 –THE POINT OF ZERO CHARGE (PZC) OF SPMIOBNP 400

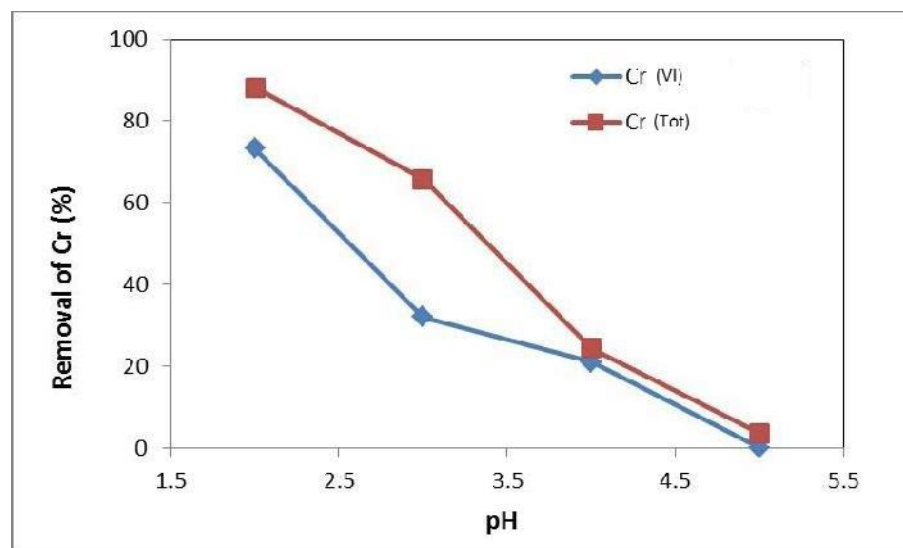


FIGURE 55 – PERCENTAGE REMOVAL OF HEXAVALENT CHROMIUM BY SPMIOBNP 400 AT PH 2 TO 5

TABLE 4 – CONCENTRATIONS OF CHROMIUM (MEAN ± SD) AFTER ADSORPTION BY SPMIOBNP AT DIFFERENT PH VALUES (T = 25 ± 0.2 °C; M = 100 MG OF ADSORBENT).

pH	Cr (Total) (mg L ⁻¹)	Cr (VI) (mg L ⁻¹)	Cr (III) (mg L ⁻¹)
Initial Conc:		11.93	
2	3.18 ± 0.16	1.41 ± 0.54	1.77 ± 0.56
3	8.11 ± 0.77	4.09 ± 0.15	4.02 ± 0.78
4	9.42 ± 0.12	9.02 ± 0.01	0.40 ± 0.12
5	11.93 ± 0.30	11.50 ± 0.17	0.43 ± 0.34

TABLE 5 – PERCENTAGE REMOVAL OF CHROMIUM IN 120 HOURS

pH	Cr (VI) %	Cr (Total) %	Cr (III) %
2	73.3	88.2	14.8
3	32.0	65.7	33.7
4	21.0	24.4	3.4
5	0.0	3.6	3.6

TABLE 6 – PERCENTAGE REMOVAL OF CHROMIUM

Time (h)	Cr (VI) %	Cr(Total) %	Cr(III) %
24	50.0	56.8	6.9
48	57.1	67.8	10.7
72	58.4	73.0	14.6
96	71.0	79.9	8.8
120	70.1	86.7	16.7

5.2.4. Kinetic Study

The percentage quantity of chromium sorbed by using SPMIOBNPs magnetic nanoparticles formed from tannin biomass material was calculated from the equation (1) below:

$$(\%)\text{Removal} = \frac{(C_0 - C_f)}{C_0} \cdot 100 \quad (2)$$

Where C_0 represents the initial concentration of chromium dissolved, C_f is the final concentration in solution after contact with the adsorbent i.e. 100 mg used.

TABLE 7 – QUANTITATIVE TABLE OF INITIAL VERSAS FINAL CONCENTRATION OF CHROMIUM SPECIES AT DIFFERENT TIME INTERVAL

Time (h)	Initial Conc $C_0=10.63 \text{ mgL}^{-1}$ $v=50\text{mL}$			Ads	Ads	Ads
	Cr(VI) in filter C_f mgL^{-1}	Cr(tot) in filter C_f mgL^{-1}	Cr(III) in filter C_f mgL^{-1}	Cr(tot) C_0-C_f mgL^{-1}	Cr(VI) C_0-C_f mgL^{-1}	Cr(III) $[C_0-C_{\text{tot}}+Cr(VI)]$ mgL^{-1}
24	5.32	4.59	0.73	6.04	5.31	0.73
48	4.56	3.42	0.62	7.21	6.07	0.62
72	4.42	2.87	0.94	7.76	6.21	0.98
96	3.18	2.14	1.55	8.49	7.45	1.55
120	3.08	1.41	1.77	9.22	7.55	1.77
132	3.01	1.38	1.80	9.25	7.62	1.78
144	2.97	1.36	1.81	9.27	7.66	1.80

TABLE 8 – PERCENTAGE REMOVAL OF CHROMIUM

Time(h)	%Removal Total Cr	%Removal Cr(VI)	%Removal Cr(III)
24	56.80	49.45	6.86
48	67.80	57.10	5.80
72	73.0	58.41	9.21
96	79.86	70.00	14.58
120	86.73	71.02	16.65
132	87.0	71.68	16.74
144	87.2	71.72	16.93

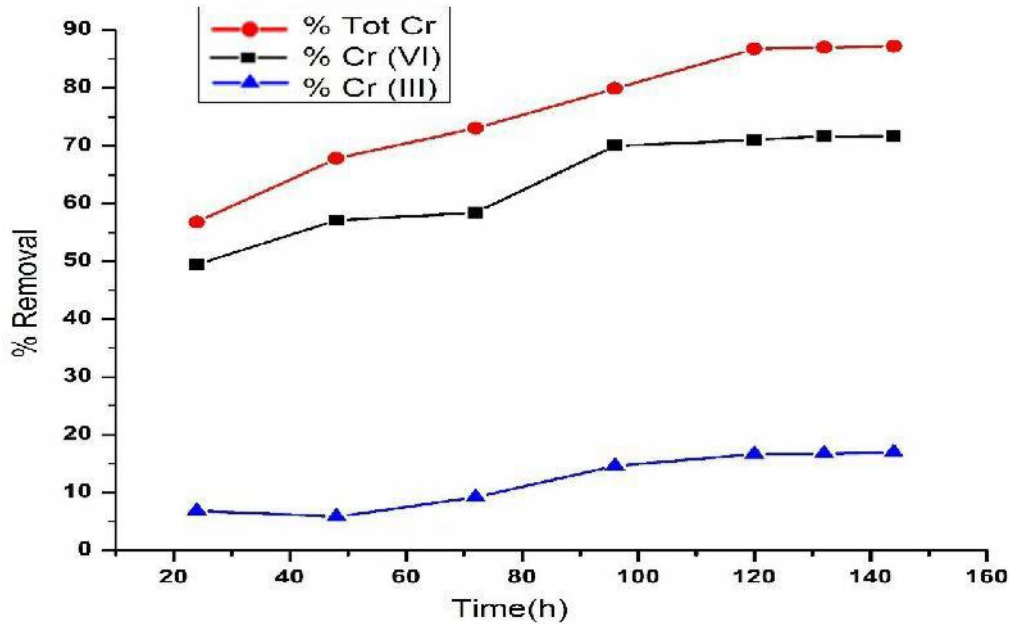


FIGURE 56 – COMPARASON OF ALL THE CHROMIUM SPECIES REMOVED WITH TIME

The comparison plot of all the chromium species was shown in the figure 56 which demonstrate the high removal sorption of harmful hexavalent specie and total chromium and less content of trivalent chromium. Various kinetic models have solids adsorption established for the understanding of the kinetics of adsorption kinetic models are pseudo-first order and pseudo-second order, the most used (TAN *et al.*, 2007).

To determine the amount of adsorbed in the adsorbent in mg g^{-1} , the difference between the initial and final concentrations of solutions obtained after use of the line of analytical curves of equation and Equation (2), was calculated below:

$$q_t = \frac{(C_0 - C) \cdot v}{m} \quad (2)$$

where Q_t is the sorbent capacity of the radical of equilibrium, as mg per gram of sorbent: C_0 , the initial concentration of the sorbate in mgL^{-1} , C is the final/equilibrium concentration of the chromium in mgL^{-1} after contacting with sorbent, v the volume in liters of the solution used in the sorption experiment, and m is the mass of adsorbent in grams.

The data for the adsorption of chromium with SPMIOBNPs of tannin extract were tested with the model of pseudo-first-order Lagergren (LAGERGREN, 1898,

HO, 2006) for the liquid-solid adsorption system in 1898. The Lagergren rate equation is one of the most widely used sorption rate equations for the sorption of a solute from a liquid solution (HAMDAOUI, 2006, GUPTA & RASTOGI, 2008). It may be represented:

$$\frac{dq_t}{dt} = k(q_e - q_t)$$

$$\log\left(\frac{q_e}{q_e - q_t}\right) = \frac{k}{2.303}t$$

$$\log(q_e - q_t) = \log q_e - k.t/2,303$$

Where q_e and q_t are amounts of Chromium adsorbed at initial and final concentration respectively; t (hours) is the time used in the study; k_1 (min^{-1}). After this we have to determine the concentration at equilibrium (q_e) and q_t i.e. the value of first one minus the value of maximum last one is a constant of first-order can be obtained by the slope of the log plot $\log(q_e - q_t)$ vs. t .

TABLE 9 – DETERMINATION OF Q VALUE

V = 50mL	q_t	q_t	q_t	$\log(q_e - q_t)$	$\log(q_e - q_t)$	$\log(q_e - q_t)$
Time (h)	Cr(tot) mg g^{-1}	Cr(VI) mg g^{-1}	Cr(III) mg g^{-1}	Cr(tot)	Cr(VI)	Cr(III)
24	3.02	2.65	0.36	0.20	0.07	0.62
48	3.60	3.03	0.31	0.01	-0.09	0.58
72	3.88	3.10	0.49	-0.12	-0.13	0.54
96	4.24	3.72	0.77	-0.40	-0.95	0.53
120	4.60	3.77	0.88	-1.52	-1.22	0.41
132	4.62	3.81	0.89	-2	-1.69	0.40
144	4.63	3.83	0.9	0	0	0.40

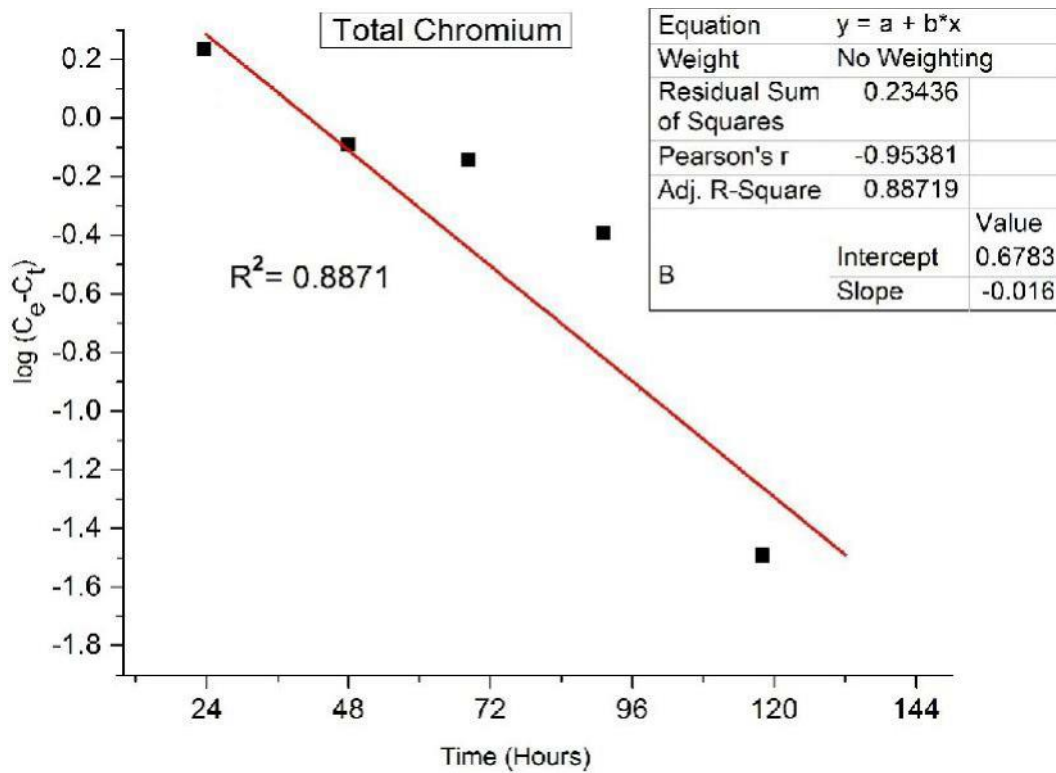


FIGURE 57 – FIRST ORDER PLOT OF TOTAL CHROMIUM ADSORPTION

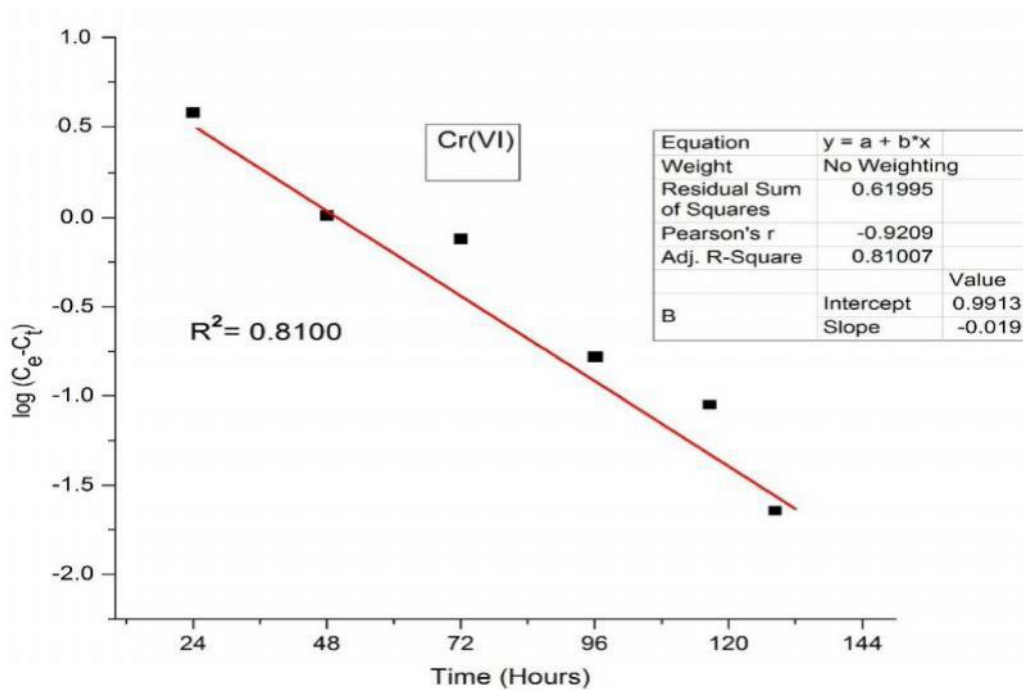


FIGURE 58 – FIRST ORDER PLOT OF HEXAVALENT CHROMIUM ADSORPTION

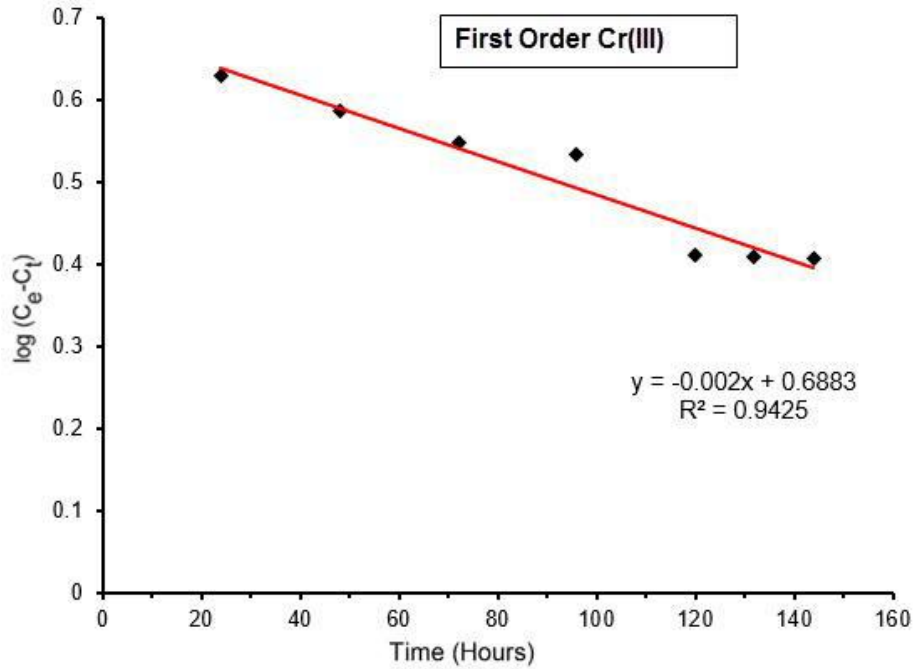


FIGURE 59 – FIRST ORDER PLOT OF TRIVALENT CHROMIUM ADSORPTION

For second order

$$t/q_t = 1/k \cdot q_e + t/q_e \quad (4)$$

Where q_e and q_t are amount (mg L^{-1}) in equilibrium in the experimental time (min) respectively; k_2 (g/mg min) is the rate constant for pseudo-second order. Both q and k_2 , were calculated from the slope of t/q_t vs t .

TABLE 10 – CONVERTING TIME AND CONCENTRATION DATA t/q_t

Time	q Cr(tot)	t/q_t Cr(tot)	q Cr(VI)	t/q_t Cr(VI)	q Cr(III)	t/q_t Cr(III)
24	3.02	7.94	2.65	9.05	0.36	65.87
48	3.60	16	3.03	15.84	0.76	63.26
72	3.88	18.55	3.10	23.22	1.09	66.12
96	4.24	22.66	3.72	25.80	1.22	78.80
120	4.60	26.08	3.77	31.83	2.05	58.62
132	4.62	28.57	3.81	34.64	2.06	63.97
144	4.63	31.10	3.83	37.59	2.08	69.35

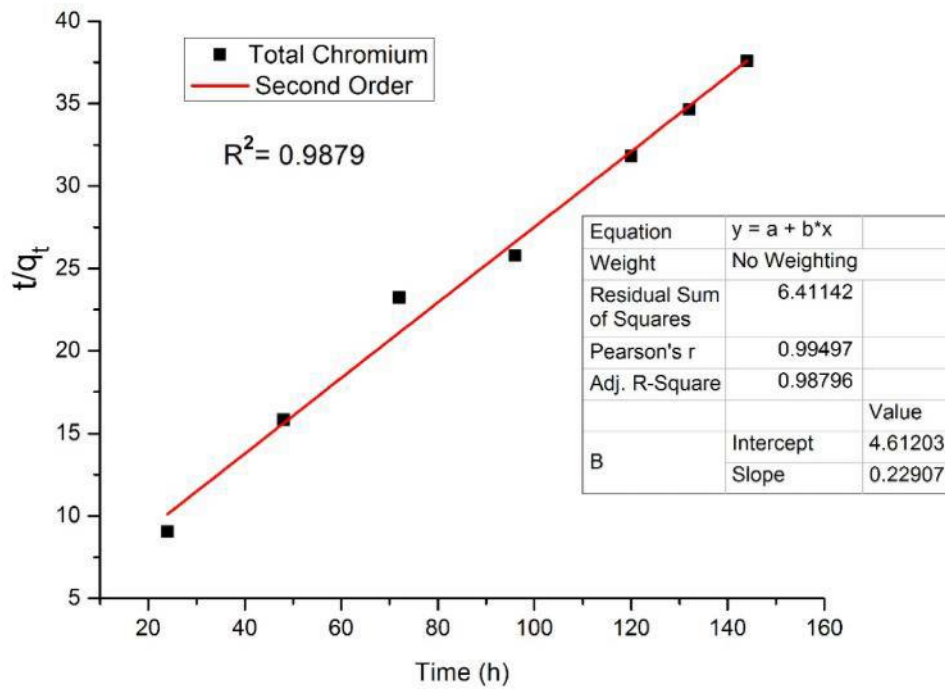


FIGURE 60 – SECOND ORDER PLOT OF TOTAL CHROMIUM

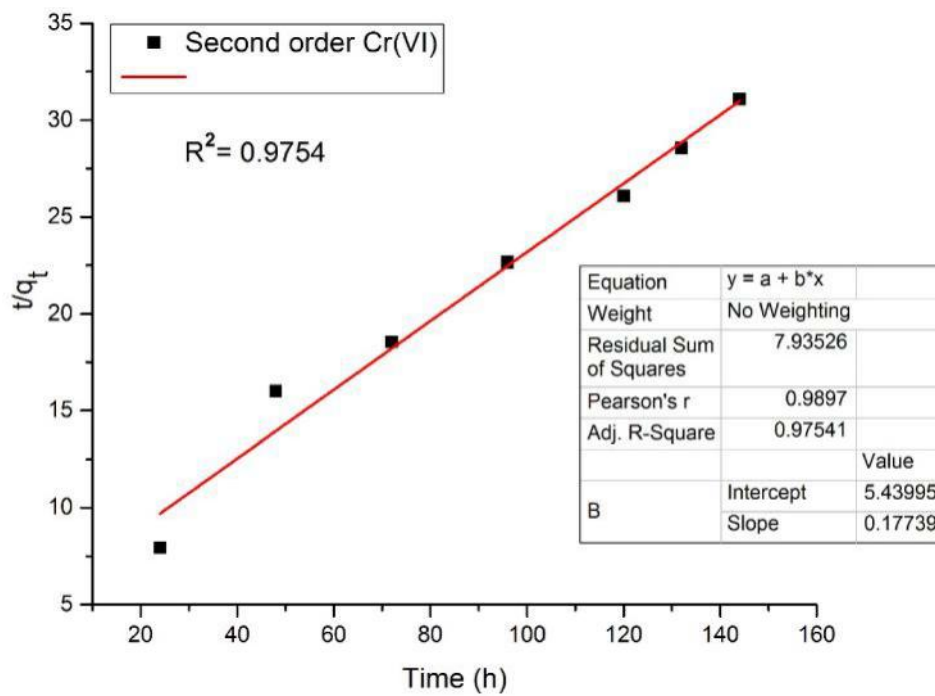


FIGURE 61 – SECOND ORDER PLOT OF HEXAVALENT CHROMIUM ADSORPTION

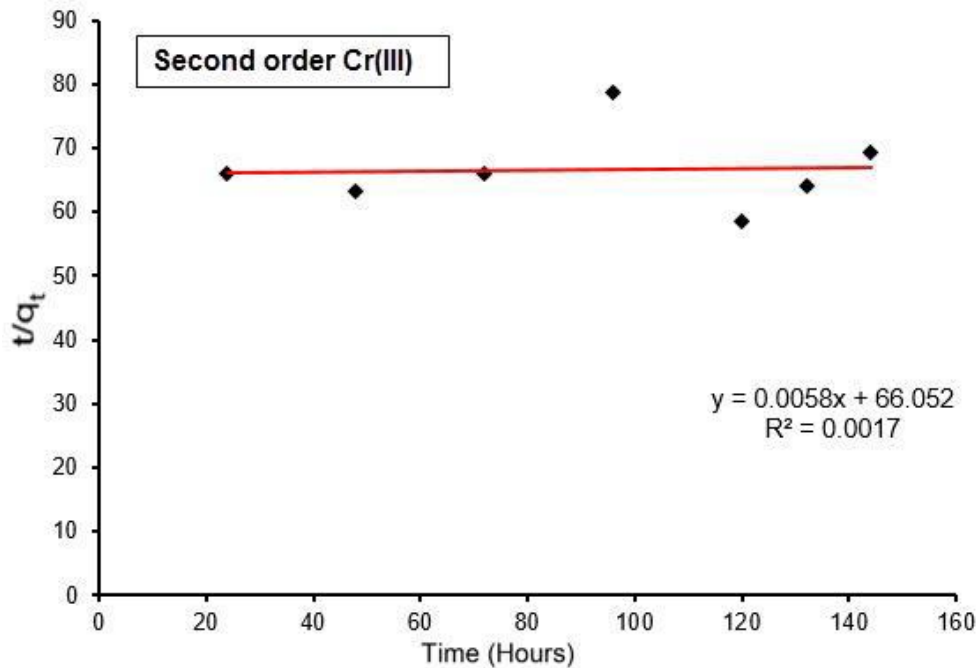


FIGURE 62 – SECOND ORDER PLOT OF TRIVALENT CHROMIUM ADSORPTION

TABLE 11 – ALL RESULTS AND KINETIC CONSTANTS

	Pseudo-First Order				Pseudo-Second order			
	$q_{e(\text{exp})}$	$q_{e(\text{calc})}$	k_1	R^2	$q_{e(\text{exp})}$	$q_{e(\text{calc})}$	k_2	R^2
Cr(Tot)	9.27	5.01	0.04	0.887	7.66	8.13	0.023	0.975
Cr(VI)	7.66	9.80	0.04	0.810	4.63	5.63	0.032	0.989
Cr(III)	1.80	4.63	0.0048	0.942	4.32	5.02	0.0048	.0017

All the results to the model implied that the removal of Cr (VI) by SPMIOBNPs was closer to chemisorptions, i.e., a new chemical species were generated at the sorbent surface with the help of the pyrolyzed supporting biochar surface in the presence of iron (WU *et al.*, 2009). Furthermore, the sorption capacity obtained from pseudo-second- order equation fitting result was consistent with the experimental.

6. CONCLUSIONS

This thesis investigated the synthesis and characterization of SPMIOBNPs. The SPMIOBNPs have been prepared by co-precipitation method with tannin extract paralyzing temperatures at 400 C. The average diameter of magnetite nanoparticles is 20-35 nm and well monodisperse. SPMIOBNPs Iron oxide nanoparticles were applied for removal of Cr(VI) from wastewater shown high efficiency. The synthesis method of SPMIOBNPs was very simple, one pot process and also compatible with the green chemistry. The green method in the present study has many advantageous features for synthesis magnetite nanoparticles, it is economical and environmentally friendly, non-toxic products treatment and size-controlled magnetite nanoparticles at minor conditions. The SPMIOBNPs were then characterized using multiple methods in order to determine the diameter, size, crystal structure, chemical content SPMIOBNPs using BET revealed high porous multilayer surface area to volume ratio that increased removal efficiency of chromium. The results showed that Cr(VI) adsorption on SPMIOBNPs was dependent on lower pH of the solution i.e. 2 this illustrate that SPMIOBNPs can adsorb/remove Cr(VI) better in an acidic pH range and most of the hexavalent chromium removed/reduced at this pH value. Second order kinetic model shows that 'Chemisorption' took place during the adsorption process i.e. a new chemical species were produced at the adsorbent surface.

6.1 Suggestions For Future Work

- Due to the availability of a huge number of adsorbents on the adsorption for heavy metals there is need to develop eco-friendly and economically sustainable adsorbents.
- Need more efforts to better the adsorption capacity of magnetic iron oxide nanoparticles and apply this method to the removal of heavy metals in large scale. Thus, more research is recommended.
- Core-shell SPMIOBNPs synthesized during this work also need more attention for further functionalization and biocompatibility studies.
- This research mainly focused on the synthesis of SPMIOBNPs, characterization of the ability of SPMIOBNPs to remove Cr(VI) or to reduce

Cr(VI) to a less toxic Cr(III) chromium. Another important point to consider are other competing contaminants and the ability of SPMIOBNPs to degrade them. Industrial effluent can contain a broad range of various contaminants especially hydrocarbons with halogen functional groups, so it is vital to determine the efficiency of SPMIOBNPs against them.

- Due to extra superparamagnetic behavior of SPMIOBNPs there is a possibility to investigate the SPMIOBNPs treating the oil spill problem.

REFERENCES

<Adams - 2011 - CHEMICALS IN DRINKING WATER (Cr VI) Public Health Goal for Hexavalent Chromium (Cr VI) in Drinking Water.pdf>. v.,

AHARONI, Y.; GILBOA, N.; SILANIKOVE, N. Models of suppressive effect of tannins. Analysis of the suppressive effect of tannins on ruminal degradation by compartmental models. **Animal Feed Science and Technology**, v. 71, p.251-267, 1998.

AHMAD, M.; RAJAPAKSHA, A.U.; LIM, J.E.; ZHANG, M.; BOLAN, N.; MOHAN, D.; VITHANAGE, M.; LEE, S.S.; OK, Y.S. Biochar as a sorbent for contaminant management in soil and water: a review. **Chemosphere**, v. 99, p.19-33, 2014.

AKBAL, F.; CAMCI, S. Treatment of metal plating wastewater by electrocoagulation. **Environmental Progress & Sustainable Energy**, v. 31, p.340-350, 2011.

AL-JABARI, M.; ABUALFAILAT, M.; SHAHEEN, S. Treating Leather Tanning Wastewater with Stone Cutting Solid Waste. **Clean-Soil Air Water**, v. 40, p.206-210, 2012.

ANASTAS, P.T.; WARNER, J.C., **Green chemistry: theory and practice**. Oxford university press, 2000.

ARAUJO, B.R.; REIS, J.O.; REZENDE, E.I.; MANGRICH, A.S.; WISNIEWSKI, A., JR.; DICK, D.P.; ROMAO, L.P. Application of termite nest for adsorption of Cr(VI). **Journal of Environmental Management**, v. 129, p.216-223, 2013.

ARSHAD, M.; BEG, A.; SIDDIQUI, Z.A. Infrared spectroscopic investigation of tannins. **Die Angewandte Makromolekulare Chemie**, v. 7, p.67-78, 1969.

ASEYEV, S.A.; WEBER, P.M.; ISCHENKO, A.A. Ultrafast Electron Microscopy for Chemistry, Biology and Material Science. v., 2013.

ASHLEY, K.; HOWE, A.M.; DEMANGE, M.; NYGREN, O. Sampling and analysis considerations for the determination of hexavalent chromium in workplace air. **Journal of Environmental Monitoring**, v. 5, p.707-716, 2003.

ASHOK, P.K.; UPADHYAYA, K. Tannins are astringent. **J Pharmacognosy Phytochem**, v. 1, p.45-50, 2012.

ASHOK, P.K.; UPADHYAYA, K. Tannins are Astringent **Journal of Pharmacognosy and Phytochemistry**, v. 1, p.45-50, 2012.

ASSIS, T.F.; RESENDE, M.D.V.D. Genetic improvement of forest tree species. **Crop Breeding and Applied Biotechnology**, v. 11, p.44-49, 2011.

ATSDR. Agency for Toxic Substances and Disease Registry (ATSDR). 2012. Toxicological profile for Chromium. Atlanta, GA: U.S. Department of Health and Human Services, Public Health Service., v., 2012.

BACCILE, N.; BABONNEAU, F.; THOMAS, B.; CORADIN, T. Introducing ecodesign in silica sol-gel materials. **Journal of Materials Chemistry**, v. 19, p.8537-8559, 2009.

BAE, H.; AHMAD, T.; RHEE, I.; CHANG, Y.; JIN, S.-U.; HONG, S. Carbon-coated iron oxide nanoparticles as contrast agents in magnetic resonance imaging. **Nanoscale Res Lett**, v. 7, p.44, 2012.

BAHAFID, W.; H. SAYEL, N.; JOUTEY, T.; GHACHTOULI, N.E. Removal mechanism of hexavalent chromium by a novel strain of pichia anomala isolated from industrial effluents of fez. **Environmental Science and Engineering**, v. 5, p.980-991, 2011.

BAJEC, M.R.; PICKERING, G.J. Astringency: mechanisms and perception. **Critical Reviews in Food Science and Nutrition**, v. 48, p.858-875, 2008.

BAKER, S.; RAKSHITH, D.; KAVITHA, K.S.; SANTOSH, P.; KAVITHA, H.U.; RAO, Y.; SATISH, S. Plants: Emerging as Nanofactories towards Facile Route in Synthesis of Nanoparticles. **BiolImpacts : BI**, v. 3, p.111-117, 2013.

BANDEKAR, J.; SETHNA, R.; KIRSCHNER, M. Quantitative determination of sulfur oxide species in white liquor by FT-IR. **App Spectroscopy**, v. 49, p.1577-1582, 1995

BANSAL, R.C.; GOYAL, M., **Activated Carbon Adsorption** CRC Press Florida, 2005.

Periodic Table of Elements-Chromium (Cr) J.K. Barbalace, inc. Available from: <<http://EnvironmentalChemistry.com/yogi/periodic/Cr.html>>. Accessed: March 2014.

BARCELOUX, D.G. Chromium. **Journal of Toxicology-Clinical Toxicology**, v. 37, p.173-194, 1999.

BARRETT, E.P.; JOYNER, L.G.; HALEND, P.P. The Determination of Pore Volume and Area Distributions in Porous Substances. I. Computations from Nitrogen Isotherms. **Journal of the American Chemical Society**, v. 73, p.373-380, 1950.

BARRETT, E.P.; JOYNER, L.G.; HALEND, P.P. The Determination of Pore Volume and Area Distributions in Porous Substances. I. Computations from Nitrogen Isotherms **Journal of the American Chemical Society**, v. 73, p.373-380, 1950.

BASU, A.; JOHNSON, T.M. Determination of hexavalent chromium reduction using Cr stable isotopes: isotopic fractionation factors for permeable reactive barrier materials. **Environmental Science & Technology**, v. 46, p.5353-5360, 2012.

BECQUER, T.; QUANTIN, C.; SICOT, M.; BOUDOT, J.P. Chromium availability in ultramafic soils from New Caledonia. **Science of the Total Environment**, v. 301, p.251-261, 2003.

BEECHER, G.R. Overview of dietary flavonoids: nomenclature, occurrence and intake. **Journal of Nutrition**, v. 133, p.3248S-3254S, 2003.

BEREK, A.K.; HUE, N.; AHMAD, A. Beneficial Use of Biochar To Correct Soil Acidity. v.,

BIESINGER, M.C.; BROWN, C.; MYCROFT, J.R.; DAVIDSON, R.D.; MCINTYRE¹, N.S. X-ray photoelectron spectroscopy studies of chromium compounds. **Surface and Interface Analysis**, v. 36, p.1550–1563, 2004.

BRACMORT, K., **Biochar: examination of an emerging concept to mitigate climate change**. Congressional Research Service, 2010.

BUBERT, H.; LAMBERT, J.; BURBA, P. Structural and elemental investigations of isolated aquatic humic substances using X-ray photoelectron spectroscopy. **Journal of Analytical Chemistry**, v. 368, p.274–280, 2000.

BURGHOFF, M.; HARTWIG, S.; KILIAN, W.; VORWERK, A.; TRAHMS, L. SQUID systems adapted to record nuclear magnetism in low magnetic fields. **Applied Superconductivity, IEEE Transactions on**, v. 17, p.846-849, 2007.

CERQUEIRA, S.C.A.; ROMÃO, L.P.C.; LUCAS, S.C.O.; FRAGA, L.E.; SIMÕES, M.L.; HAMMER, P.; LEAD, J.R.; MANGONI, A.P.; MANGRICH, A.S. Spectroscopic characterization of the reduction and removal of chromium (VI) by tropical peat and humin. **Fuel**, v. 91, p.141-146, 2012.

CHARLTON, A.J.; BAXTER, N.J.; KHAN, M.L.; MOIR, A.J.; HASLAM, E.; DAVIES, A.P.; WILLIAMSON, M.P. Polyphenol/peptide binding and precipitation. **Journal of Agricultural and Food Chemistry**, v. 50, p.1593-1601, 2002.

CHAUDHARY, A.J.; GOSWAMI, N.C.; GRIMES, S.M. Electrolytic removal of hexavalent chromium from aqueous solutions. **Journal of Chemical Technology and Biotechnology**, v. 78, p.877-883, 2003.

CHEN, B.; CHEN, Z.; LV, S. A novel magnetic biochar efficiently sorbs organic pollutants and phosphate. **Bioresource Technology**, v. 102, p.716-723, 2011.

CHEN, S.; YUE, Q.; GAO, B.; LI, Q.; XU, X. Removal of Cr(VI) from aqueous solution using modified corn stalks: Characteristic, equilibrium, kinetic and thermodynamic study. **Chemical Engineering Journal**, v. 168, p.909-917, 2011.

CHERTOK, B.; MOFFAT, B.A.; DAVID, A.E.; YU, F.; BERGEMANN, C.; ROSS, B.D.; YANG, V.C. Iron oxide nanoparticles as a drug delivery vehicle for MRI monitored magnetic targeting of brain tumors. **Biomaterials**, v. 29, p.487-496, 2008.

CORNELL; SCHWERTMANN, **The Iron Oxides: Structure, Properties, Reactions, Occurrences and Uses**. © WILEY-VCH Weinheim, 2003.

CROMER BERMAN, S.M.; WALCZAK, P.; BULTE, J.W. Tracking stem cells using magnetic nanoparticles. **Wiley Interdisciplinary Reviews: Nanomedicine and Nanobiotechnology**, v. 3, p.343-355, 2011.

CULLITY, B.D.; GRAHAM, C.D., **Introduction to magnetic materials**. John Wiley & Sons, 2011.

D BROWSKI, A. Adsorption—from theory to practice. **Advances in Colloid and Interface Science**, v. 93, p.135-224, 2001.

DAI, J.; REN, F.; TAO, C. Adsorption of Cr(VI) and speciation of Cr(VI) and Cr(III) in aqueous solutions using chemically modified chitosan. **International Journal of Environmental Research and Public Health**, v. 9, p.1757-7070, 2012.

DANIEL, R.; ANJANEYULU, Y.; KRUPADAM, R.J. Cr (VI) Removal from electroplating industrial effluents: A greener and cheaper method. **Zastita Materijala**, v. 50, p.13-18, 2009.

DAR, M.I.; SHIVASHANKAR, S.A. Single crystalline magnetite, maghemite, and hematite nanoparticles with rich coercivity. **RSC Advances**, v. 4, p.4105-4113, 2014.

DARROUDI, M.; HAKIMI, M.; GOODARZI, E.; OSKUEE, R.K. Superparamagnetic iron oxide nanoparticles (SPIONs) Green preparation, characterization and their cytotoxicity effects. v. 40, p.14641–14645, 2014.

DAS, A.P.; SINGH, S. Occupational health assessment of chromite toxicity among Indian miners. **Indian Journal of Occupational and Environmental Medicine**, v. 15, p.6-13, 2011.

DEAVILLE, E.R.; GREEN, R.J.; MUELLER-HARVEY, I.; WILLOUGHBY, I.; FRAZIER, R.A. Hydrolyzable tannin structures influence relative globular and random coil protein binding strengths. **Journal of Agricultural and Food Chemistry**, v. 55, p.4554-4561, 2007.

DEMIR, A.; TOPKAYA, R.; BAYKAL, A. Green synthesis of superparamagnetic Fe₃O₄ nanoparticles with maltose: Its magnetic investigation. **Polyhedron**, v. 65, p.282-287, 2013.

DHAL, B.; THATOI, H.; DAS, N.; PANDEY, B. Chemical and microbial remediation of hexavalent chromium from contaminated soil and mining/metallurgical solid waste: a review. **Journal of Hazardous Materials**, v. 250, p.272-291, 2013.

DHAL, B.; THATOI, H.N.; DAS, N.N.; PANDEY, B.D. Chemical and microbial remediation of hexavalent chromium from contaminated soil and mining/metallurgical solid waste: a review. **Journal of Hazardous Materials**, v. 250-251, p.272-291, 2013.

DIOUF, P.N.; TIBIRNA, C.M.; GARCÍA-PÉREZ, M.-E.; ROYER, M.; DUBÉ, P.; STEVANOVIC, T. Structural Elucidation of Condensed Tannin from *Picea mariana* Bark. v., 2013.

DOANE, P.H.; MBUGUA, D.M. Analysis of condensed tannins: a review. **Animal Feed Science and Technology**, v. 91, p.21-40, 2001.

DORNIANI, D.; HUSSEIN, M.Z.; KURA, A.U.; FAKURAZI, S.; SHAARI, A.H.; AHMAD, Z. Preparation of Fe₃O₄ magnetic nanoparticles coated with gallic acid for drug delivery. **Int J Nanomedicine**, v. 7, p.5745-5756, 2012.

DUAN, W.; OHARA, S.; HASHIDA, K.; MAKINO, R. Condensed tannins from steamed *Acacia mearnsii* bark. **Holzforschung**, v. 59, p.289-294, 2005.

EPA. In situ treatment of soil and ground water contaminated with chromium. A technical resource guide **U.S. Environmental Protection Agency**, v. 625, 2000.

FAUCONNIER, N.; PONS, J.; ROGER, J.; BEE, A. Thiolation of maghemite nanoparticles by dimercaptosuccinic acid. **Journal of Colloid and Interface Science**, v. 194, p.427-433, 1997.

FENG, X.; WU, Z.; CHEN, X. Removal of metal ions from electroplating effluent by EDI process and recycle of purified water. **Separation and Purification Technology**, v. 57, p.257-263, 2007.

FJELLVAG, H.; GRØNVOLD, F.; STØLEN, S. On the Crystallographic and Magnetic Structures of Nearly Stoichiometric Iron Monoxide. v. 124, p.52-57, 1996.

FREI, M. Centrifugation basics Report Sigma-Aldrich. v. 5, 2014.

FULTZ, B.; HOWE, J.M., **Transmission electron microscopy and diffractometry of materials**. Springer Science & Business Media, 2012.

GANDHIA, M.R.; VISWANATHAN, N.; SANKARAN MEENAKSHIA. Adsorption mechanism of hexavalent chromium removal using amberlite IRA 743 resin. **Ion Exchange Letters**, v. 3, p.25-35, 2010.

GINER-CHAVEZ, B.I.; VAN SOEST, P.J.; ROBERTSON, J.B.; LASCANO, C.; REED, J.D.; PELL, A.N. A method for isolating condensed tannins from crude plant extracts with trivalent ytterbium. **Journal of the Science of Food and Agriculture**, v. 74, p.359-368, 1997.

GNANAPRAKASH, G.; MAHADEVAN, S.; JAYAKUMAR, T.; KALYANASUNDARAM, P.; PHILIP, J.; RAJ, B. Effect of initial pH and temperature of iron salt solutions on formation of magnetite nanoparticles. **Materials Chemistry and Physics**, v. 103, p.168-175, 2007.

GUBIN, S.P.; KOKSHAROV, Y.A.; KHOMUTOV, G.B.; YURKOV, G.Y. Magnetic nanoparticles preparation, structure. properties. **Russian chemical reviews**, v. 74, p.489 – 520, 2005.

GUPTA, V.; RASTOGI, A. Sorption and desorption studies of chromium (VI) from nonviable cyanobacterium *Nostoc muscorum* biomass. **Journal of Hazardous Materials**, v. 154, p.347-354, 2008.

GWINN, M.R.; VALLYATHAN, V. Nanoparticles: Health Effects—Pros and Cons. **Environmental Health Perspectives**, v. 114, p.1818-1825, 2006.

A Tannin Chemistry © Ann E. Hagerman Miami, 2002. Available from: <<http://www.users.miamioh.edu/hagermae/>>. Accessed: November 2013.

HAMDAOUI, O. Batch study of liquid-phase adsorption of methylene blue using cedar sawdust and crushed brick. **Journal of Hazardous Materials**, v. 135, p.264-273, 2006.

HASLAM, E., **Plant polyphenols vegetable tannins revisited chemistry and pharmacology of natural products**. . Cambridge University Press, Cambridge, 1989.

HE, F.; PAN, Q.H.; SHI, Y.; DUAN, C.Q. Biosynthesis and genetic regulation of proanthocyanidins in plants. **Molecules**, v. 13, p.2674-2703, 2008.

HERVAS, G.; FRUTOS, P.; SERRANO, E.; MANTECON, A.R.; GIRALDEZ, F.J. Effect of tannic acid on rumen degradation and intestinal digestion of treated soya bean meals in sheep. **Journal of Agricultural Science**, v. 135, p.305-310, 2000.

HO, Y.-S. Review of second-order models for adsorption systems. **Journal of Hazardous Materials**, v. 136, p.681-689, 2006.

HO, Y.-S.; MCKAY, G. Pseudo-second order model for sorption processes. **Process Biochemistry**, v. 34, p.451-465, 1999.

HOLMAN, H.N.; PERRY, D.L.; MARTIN, M.C.; LAMBLE, G.M.; MCKINNEY, W.R.; HUNTER-CEVERA, J.C. Real time characterization of biogeochemical reduction of Cr(VI) on basalt surfaces by SR-FTIR imaging. **Geomicrobiology Journal**, v. 16, p.307–324, 1999.

HU, J.; CHEN, G.; LO, I.M. Removal and recovery of Cr(VI) from wastewater by maghemite nanoparticles. **Water Research**, v. 39, p.4528-4536, 2005.

HUANG, X.; ZHUANG, J.; CHEN, D.; LIU, H.; TANG, F.; YAN, X.; MENG, X.; ZHANG, L.; REN, J. General strategy for designing functionalized magnetic microspheres for different bioapplications. **Langmuir**, v. 25, p.11657-11663, 2009.

ILIAS, M.; RAFIQULLAH, I.M.; DEBNATH, B.C.; MANNAN, K.S.B.; HOQ, M.M. Isolation and characterization of chromium (VI)-reducing bacteria from tannery effluents. **Indian journal of microbiology**, v. 51, p.76-81, 2011.

JAIN, M.; GARG, V.K.; KADIRVELU, K. Chromium(VI) removal from aqueous system using Helianthus annuus (sunflower) stem waste. **Journal of Hazardous Materials**, v. 162, p.365-372, 2009.

Jefferson Lab. Available from: <http://education.jlab.org/itselemental/ele024.html>. Accessed: April 2014.

JEFFERY, S.; BEZEMER, T.M.; CORNELISSEN, G.; KUYPER, T.W.; LEHMANN, J.; MOMMER, L.; SOHI, S.P.; VOORDE, T.F.; WARDLE, D.A.; GROENIGEN, J.W. The way forward in biochar research: targeting trade-offs between the potential wins. **GCB Bioenergy**, v. 7, p.1-13, 2015.

JIANG, H.-M.; YANG, T.; WANG, Y.-H.; LIAN, H.-Z.; HU, X. Magnetic solid-phase extraction combined with graphite furnace atomic absorption spectrometry for speciation of Cr (III) and Cr (VI) in environmental waters. **Talanta**, v. 116, p.361-367, 2013.

KABATA-PENDIAS, A., **Trace elements in soils and plants**. CRC press, 2010.

KABATA-PENDIAS, A.; MUKHERJEE, A.B., **Trace Elements from Soil to Human**. © Springer-Verlag Berlin Heidelberg New York, 2007.

KABAY, N.; ARDA, M.; SAHA, B.; STREAT, M. Removal of Cr(VI) by solvent impregnated resins (SIR) containing aliquat 336. **Reactive and Functional Polymers**, v. 54, p.103-115, 2003.

KANDPAL, N.D.; SAH, N.; LOSHALI, R.; JOSHI, R.; PRASAD, J. Co-precipitation method of synthesis and characterization of iron oxide Nanoparticles. **Journal of Scientific & Industrial Research**, v. 73, p.87-90, 2013.

KARLSSON, H.L.; CRONHOLM, P.; GUSTAFSSON, J.; MOLLER, L. Copper oxide nanoparticles are highly toxic: a comparison between metal oxide nanoparticles and carbon nanotubes. **Chemical Research in Toxicology**, v. 21, p.1726-1732, 2008.

KARN, B. The Road to Green Nanotechnology. **Journal of Industrial Ecology**, v. 12, p.263-266, 2008.

KHANBABAEE, K.; REE, T.V. Tannins Classification and Definition, . **Nat. Prod. Rep**, v. 18, p.641-649, 2001.

KHARISOV, B.I.; DIAS, H.V.R.; KHARISSOVA, O.V.; VAZQUEZ, A.; PENA, Y.; GOMEZ, I. Solubilization, dispersion and stabilization of magnetic nanoparticles in water and non-aqueous solvents: recent trends. **RSC Advances**, v. 4, p.45354-45381, 2014.

KHARISOV, B.I.; RASIKA DIAS, H.V.; KHARISSOVA, O.V.; MANUEL JIMÉNEZ-PÉREZ, V.; OLVERA PÉREZ, B.; MUÑOZ FLORES, B. Iron-containing nanomaterials: synthesis, properties, and environmental applications. **RSC Advances**, v. 2, p.9325, 2012.

KIM, S.D.; PARK, K.S.; GU, M.B. Toxicity of hexavalent chromium to *Daphnia magna*: influence of reduction reaction by ferrous iron. **Journal of Hazardous Materials**, v. 93, p.155-164, 2002.

PlantNET - FloraOnline Available from: <<http://plantnet.rbgsyd.nsw.gov.au/cgi-bin/NSWfl.pl?page=nswfl&lvl=sp&name=Acacia~mearnsii>>. Accessed: Dec 2014.

KOESEOGLU, Y.; KAVAS, H.; AKTAS, B. Size effects on magnetic properties of Fe₃O₄ nanoparticles. v., 2005.

KOLHATKAR, A.G.; JAMISON, A.C.; LITVINOV, D.; WILLSON, R.C.; LEE, T.R. Tuning the Magnetic Properties of Nanoparticles. **Int J Mol Sci**, v. 14, p.15977-16009, 2013.

KRAUS, T.E.C.; ZASOSKI, R.J.; DAHLGREN, R.A. Fertility and pH effects on polyphenol and condensed tannin concentrations in foliage and roots. **Plant and Soil**, v. 262, p.95-109, 2004.

KURNIAWAN, T.A.; CHAN, G.Y.S.; LO, W.-H.; BABEL, S. Physico-chemical treatment techniques for wastewater laden with heavy metals. **Chemical Engineering Journal**, v. 118, p.83-98, 2006.

LAGERGREN, S. About Theory of So-Called Adsorption of Soluble Substances. **K. Sven. Vetenskapsakad. Handl.**, v. 24 p.1, 1898.

LEHMANN, J. A handful of carbon. **Nature**, v. 447, p.143-144, 2007.

LEHMANN, J.; GAUNT, J.; RONDON, M. Bio-char sequestration in terrestrial ecosystems—a review. **Mitigation and adaptation strategies for global change**, v. 11, p.395-419, 2006.

LESLIE-PELECKY, D.L.; RIEKE, R.D. Magnetic properties of nanostructured materials. **Chemistry of Materials**, v. 8, p.1770-1783, 1996.

LESSCHAEVE, I.; NOBLE, A.C. Polyphenols: factors influencing their sensory properties and their effects on food and beverage preferences. **American Society for Clinical Nutrition**, v. 81, p. 330S-335S, 2005.

LI, X.-Q.; ELLIOTT, D.W.; ZHANG, W.-X. Zero-valent iron nanoparticles for abatement of environmental pollutants: materials and engineering aspects. **Critical Reviews in Solid State and Materials Sciences**, v. 31, p.111-122, 2006.

LOWE, S.; BROWNE, M.; BOUDJELAS, S.; DE POORTER, M., **100 of the world's worst invasive alien species: a selection from the global invasive species database**. Invasive Species Specialist Group Auckland,, New Zealand, 2000.

LOWELL, S., **Characterization of porous solids and powders: surface area, pore size and density**. Springer, 2004.

M. AWWAD, A.; M. SALEM, N. A Green and Facile Approach for Synthesis of Magnetite Nanoparticles. **Nanoscience and Nanotechnology**, v. 2, p.208-213, 2013.

MACHALA, L.; ZBORIL, R.; GEDANKEN, A. Amorphous Iron (III) Oxide A Review. **The Journal of Physical Chemistry B**, v. 111, p.4003-4018, 2007.

MAHDAVI, M.; AHMAD, M.B.; HARON, M.J.; NAMVAR, F.; NADI, B.; RAHMAN, M.Z.; AMIN, J. Synthesis, surface modification and characterisation of biocompatible magnetic iron oxide nanoparticles for biomedical applications. **Molecules**, v. 18, p.7533-7548, 2013.

MAIER-HAUFF, K.; ROTHE, R.; SCHOLZ, R.; GNEVECKOW, U.; WUST, P.; THIESEN, B.; FEUSSNER, A.; VON DEIMLING, A.; WALDOEFNER, N.; FELIX, R. Intracranial thermotherapy using magnetic nanoparticles combined with external beam radiotherapy: results of a feasibility study on patients with glioblastoma multiforme. **Journal of Neuro-Oncology**, v. 81, p.53-60, 2007.

MANGRICH, A.; ANGELO, L.; MANTOVANI, K. 2013. Biochar Produced from Chemical Oxidation of Charcoal. Pp. 997-1001. *Functions of Natural Organic Matter in Changing Environment*. Springer.

MARTINEZ, S.A.; RODRIGUEZ, M.G. Dynamical modeling of the electrochemical process to remove Cr (VI) from wastewaters in a tubular reactor. **Journal of Chemical Technology and Biotechnology**, v. 82, p.582-587, 2007.

MASCOLO, M.C.; PEI, Y.; RING, T.A. Room Temperature Co-Precipitation Synthesis of Magnetite Nanoparticles in a Large pH Window with Different Bases. **Materials**, v. 6, p.5549-5567, 2013.

MAURI, R.; SHINNAR, R.; D'AMORE, M.; GIORDANO, P.; VOLPE, A. Solvent extraction of chromium and cadmium from contaminated soils. **American Institute of Chemical Engineers (AIChE)**, v. 47, p.509-512, 2001.

MAURICE, J. Tannery pollution threatens health of half-million Bangladesh residents. **Bulletin of The World Health Organization**, v. 79, p.78-79, 2001.

MEI, B.; PURYEAR, J.D.; NEWTON, R.J. Assessment of Cr tolerance and accumulation in selected plant species. **Plant and Soil**, v. 247, p.223-231, 2002.

MIN, B.; BARRY, T.; ATTWOOD, G.; MCNABB, W. The effect of condensed tannins on the nutrition and health of ruminants fed fresh temperate forages: a review. **Animal Feed Science and Technology**, v. 106, p.3-19, 2003.

MODY, V.V.; SIWALE, R.; SINGH, A.; MODY, H.R. Introduction to metallic nanoparticles. **Journal of Pharmacy and Bioallied Sciences**, v. 2, p.282, 2010.

MOGHANIAN, H.; MOBINIKHALEDI, A.; BLACKMAN, A.G.; SAROUGH-FARAHANI, E. Sulfanilic acid-functionalized silica-coated magnetite nanoparticles as an efficient, reusable and magnetically separable catalyst for the solvent-free synthesis of 1-amido- and 1-aminoalkyl-2-naphthols. **RSC Advances**, v. 4, p.28176-28185, 2014.

MOHAN, D.; PITTMAN, C.U., JR. Activated carbons and low cost adsorbents for remediation of tri- and hexavalent chromium from water. **Journal of Hazardous Materials**, v. 137, p.762-811, 2006.

MOHAN, D.; RAJPUT, S.; SINGH, V.K.; STEELE, P.H.; PITTMAN JR, C.U. Modeling and evaluation of chromium remediation from water using low cost bio-char, a green adsorbent. **Journal of Hazardous Materials**, v. 188, p.319-333, 2011.

MOHAN, D.; SINGH, K.P.; SINGH, V.K. Removal of hexavalent chromium from aqueous solution using low-cost activated carbons derived from agricultural waste materials and activated carbon fabric cloth. **Industrial & Engineering Chemistry Research**, v. 44, p.1027-1042, 2005.

MONSER, L.; ADHOUM, N. Modified activated carbon for the removal of copper, zinc, chromium and cyanide from wastewater. **Separation and Purification Technology**, v. 26, p.137-146, 2002.

Merchant Research & Consulting, Ltd. Available from: <http://mcgroup.co.uk/news/20120509/chromium-output-remains-stably-high-kazakhstan.html>. Accessed: May 2014.

MULANI, K.; DANIELS, S.; RAJDEO, K.; TAMBE, S.; CHAVAN, N. Adsorption of Chromium(VI) from Aqueous Solutions by Coffee Polyphenol-Formaldehyde/Acetaldehyde Resins. **Journal of Polymers**, v. 2013, p.11, 2013.

MURRAY, K.J.; MOZAFARZADEH, M.L.; TEBO, B.M. Cr(III) Oxidation and Cr toxicity in cultures of the manganese(II)-oxidizing pseudomonas putida strain GB-1. **Geomicrobiology Journal**, v. 22, p.151-159, 2005.

NAGASHANMUGAM, K.B.; SRINIVASAN, K. Removal of chromium (VI) from aqueous solution by chemically modified gingelly oil cake carbon. **Indian Journal of Chemical Technology**, v. 18, p.207-219, 2011.

NAMASIVAYAM, C.; RANGANATHAN, K. Waste Fe(III)/Cr(III) hydroxide as adsorbent for the removal of Cr(VI) from aqueous solution and chromium plating industry wastewater. **Environmental Pollution**, v. 82, p.255-261, 1993.

NICOLINI, J.; KHAN, M.Y.; MATSUI, M.; CÔCCO, L.C.; YAMAMOTO, C.I.; LOPES, W.A.; DE ANDRADE, J.B.; PILLON, C.N.; ARIZAGA, G.G.C.; MANGRICH, A.S. Evaluation of PAH contamination in soil treated with solid by-products from shale pyrolysis. **Environmental Monitoring and Assessment**, v. 187, p.1-10, 2015.

NIEMETZ, R.; GROSS, G.G. Enzymology of gallotannin and ellagitannin biosynthesis. **Phytochemistry**, v. 66, p.2001-2011, 2005.

NYIR -KÓSA, I.; NAGY, D.C.; PÓSFAL, M. Size and shape control of precipitated magnetite nanoparticles. **European Journal of Mineralogy**, v. 21, p.293-302, 2009.

O'NEILL, B.; GROSSMAN, J.; TSAI, M.; GOMES, J.; LEHMANN, J.; PETERSON, J.; NEVES, E.; THIES, J.E. Bacterial community composition in Brazilian anthrosols and adjacent soils characterized using culturing and molecular identification. **Microbial Ecology**, v. 58, p.23-35, 2009.

OECD. Environmental Outlook to 2030. **Organisation for Economic Co-operation and Development (OECD)**, v., 2008.

OGATA, T.; MORISADA, S.; OINUMA, Y.; SEIDA, Y.; NAKANO, Y. Preparation of adsorbent for phosphate recovery from aqueous solutions based on condensed tannin gel. **Journal of Hazardous Materials**, v. 192, p.698-703, 2011.

OKUDERA, H.; KIHARA; MATSUMOTO, T. Temperature Dependence of Structure Parameters in Natural Magnetite: Single Crystal X-ray Studies from 126 to 773 K **Acta Cryst.**, v. B52, p.450-457, 1996.

OMOIKE, A. Synthesis and Characterization of Tannic Acid Functionalized Magnetic Nanoparticles. **American Chemical Society**, v. 8, p.90-107, 2008.

OSKOU EIAN, E.; ABDULLAH, N.; OSKOU EIAN, A. Effects of Flavonoids on Rumen Fermentation Activity, Methane Production, and Microbial Population. **BioMed Research International**, v. 2013, p.349129, 2013.

OZER, A.; ALTUNDOGAN, H.S.; ERDEM, M.; TUNMEN, F. A study on the Cr (VI) removal from aqueous solutions by steel wool. **Environmental Pollution**, v. 97, p.107-112, 1997.

PADILLA, A.P.; TAVANI, E.L. Treatment of an industrial effluent by reverse osmosis. **Desalination**, v. 126, p.219-226, 1999.

PANG, Y.; ZENG, G.; TANG, L.; ZHANG, Y.; LIU, Y.; LEI, X.; LI, Z.; ZHANG, J.; LIU, Z.; XIONG, Y. Preparation and application of stability enhanced magnetic nanoparticles for rapid removal of Cr(VI). **Chemical Engineering Journal**, v. 175, p.222-227, 2011.

PANNEERSELVAM, P.; MORAD, N.; TAN, K.A. Magnetic nanoparticle (Fe₃O₄) impregnated onto tea waste for the removal of nickel(II) from aqueous solution. **Journal of Hazardous Materials**, v. 186, p.160-168, 2011.

PARK, K.; KITTELSON, D.B.; MCMURRY, P.H. Structural properties of diesel exhaust particles measured by transmission electron microscopy (TEM): Relationships to particle mass and mobility. **Aerosol Science and Technology**, v. 38, p.881-889, 2004.

PATRA, A.K.; SAXENA, J. A new perspective on the use of plant secondary metabolites to inhibit methanogenesis in the rumen. **Phytochemistry**, v. 71, p.1198-1222, 2010.

PEARSON, R.G. Hard and Soft Acids and Bases. **Journal of the American Chemical Society**, v. 85, p.3533-3539, 1963.

PENDLETON, M. Descriptions of melissopalynological methods involving centrifugation should include data for calculating Relative Centrifugal Force (RCF) or should express data in units of RCF or gravities (g). **Grana**, v. 45, p.71-72, 2006.

PENDRY, J.B.; SCHURIG, D.; SMITH, D.R. Controlling electromagnetic fields. **Science**, v. 312, p.1780-1782, 2006.

PERKAS, N.; KOLTYPIN, Y.; PALCHIK, O.; GEDANKEN, A.; CHANDRASEKARAN, S. Oxidation of cyclohexane with nanostructured amorphous catalysts under mild conditions. **Applied Catalysis A: General**, v. 209, p.125-130, 2001.

PICKARD, M.; CHARI, D. Enhancement of magnetic nanoparticle-mediated gene transfer to astrocytes by 'magnetofection': effects of static and oscillating fields. **Nanomedicine: Nanotechnology, Biology, and Medicine**, v. 5, p.217-232, 2010.

PUGH, C.T.; PALMER, T.T.; CARR, P.A. A study of significant variables and their effects on the analysis of hexavalent chromium. **Journal of Chemical Health and Safety**, v. 15, p.25-28, 2008.

REEDER, R.J.; SCHOONEN, M.A.A.; LANZIROTTI, A. Metal Speciation and Its Role in Bioaccessibility and Bioavailability. **Reviews in Mineralogy and Geochemistry**, v. 64, p.59-113, 2006.

REITZ, J.R.; MILFORD, F.J.; CHRISTY, R.W., **Foundations of electromagnetic theory**. Addison-Wesley Publishing Company, 2008.

RENGARAJ, S.; JOO, C.K.; KIM, Y.; YI, J. Kinetics of removal of chromium from water and electronic process wastewater by ion exchange resins: 1200H, 1500H and IRN97H. **Journal of Hazardous Materials**, v. 102, p.257-275, 2003.

RICHARDSON, D.M.; REJMÁNEK, M. Trees and shrubs as invasive alien species – a global review. **Diversity and Distributions**, v. 17, p.788-809, 2011.

ROSE, P.A.; PRASEETHA, P.; BHAGAT, M.; ALEXANDER, P.; ABDEEN, S.; CHAVALI, M. Drug embedded PVP coated magnetic nanoparticles for targeted killing of breast cancer cells. **Technology in Cancer Research & Treatment**, v. 12, p.463-472, 2013.

ROSEMANN, N. 2005. Drinking Water Crisis in Pakistan and the Issue of Bottled Water. Bern Switzerland.

ROWBOTHAM, A.L.; LEVY, L.S.; SHUKER, L.K. Chromium in the environment: an evaluation of exposure of the UK general population and possible adverse health effects. **Journal of Toxicology and Environmental Health-Part B-Critical Reviews**, v. 3, p.145-178, 2000.

SANTOYO SALAZAR, J.; PEREZ, L.; DE ABRIL, O.; TRUONG PHUOC, L.; IHIAWAKRIM, D.; VAZQUEZ, M.; GRENECHE, J.-M.; BEGIN-COLIN, S.; POURROY, G. Magnetic Iron Oxide Nanoparticles in 10–40 nm Range: Composition in Terms of Magnetite/Maghemite Ratio and Effect on the Magnetic Properties. **Chemistry of Materials**, v. 23, p.1379-1386, 2011.

SANTOYO SALAZAR, J.; PEREZ, L.; DE ABRIL, O.; TRUONG PHUOC, L.; IHIAWAKRIM, D.; VAZQUEZ, M.; GRENECHE, J.-M.; BEGIN-COLIN, S.; POURROY, G. Magnetic Iron Oxide Nanoparticles in 10– 40 nm Range: Composition in Terms of Magnetite/Maghemite Ratio and Effect on the Magnetic Properties. **Chemistry of Materials**, v. 23, p.1379-1386, 2011.

SHANKER, A.K.; CERVANTES, C.; LOZA-TAVERA, H.; AVUDAINAYAGAM, S. Chromium toxicity in plants. **Environment International**, v. 31, p.739-753, 2005.

SHARMA, S.K.; PETRUSEVSKI, B.; AMY, G. Chromium removal from water: a review. **Journal of Water Supply: Research and Technology—AQUA**, v. 57, p.541, 2008.

SMITH, B.; SWAIN, **Flavonoid compounds comparative biochemistry**. Academic Press, New York, 1962.

SOCRATES, G., **Infrared and Raman characteristic group frequencies: tables and charts**. John Wiley & Sons, 2004.

SOHI, S.; KRULL, E.; LOPEZ-CAPEL, E.; BOL, R. A review of biochar and its use and function in soil. **Advances in agronomy**, v. 105, p.47-82, 2010.

SRINIVAS, P.R.; PHILBERT, M.; VU, T.Q.; HUANG, Q.; KOKINI, J.L.; SAOS, E.; CHEN, H.; PETERSON, C.M.; FRIEDL, K.E.; MCDADE-NGUTTER, C. Nanotechnology research: applications in nutritional sciences. **The Journal of Nutrition**, v. 140, p.119-124, 2010.

SRINIVASARAO, C.; GOPINATH, K.; VENKATESH, G.; DUBEY, A.; WAKUDKAR, H.; PURAKAYASTHA, T.; PATHAK, H.; JHA, P.; LAKARIA, B.; RAJKHOWA, D. Use of biochar for soil health management and greenhouse gas mitigation in India:

Potential and constraints. **Central Research Institute for Dryland Agriculture, Hyderabad, Andhra Pradesh. 51p**, v., 2013.

STARLIN, T.; RAGAVENDRAN, P.; RAJ, C.A.; PERUMAL, P.C.; GOPALAKRISHNAN, V.K. Element and functional group analysis of *Ichnocarpus frutescens* R.Br(Apocynaceae). **International Journal of Pharmacy and Pharmaceutical Sciences**, v. 4, p.343-345, 2012.

STAROWICZ, M.; STAROWICZ, P.; ZUKROWSKI, J.; PRZEWOZNIK, J.; LEMANSKI, A.; KAPUSTA, C.; BANAS, J. Electrochemical synthesis of magnetic iron oxide nanoparticles with controlled size. **Journal of Nanoparticle Research**, v. 13, p.7167-7176, 2011.

STUART, B., **Infrared spectroscopy**. Wiley Online Library, 2005.

SUN, Y.-K.; MA, M.; ZHANG, Y.; GU, N. Synthesis of nanometer-size maghemite particles from magnetite. **Colloids and Surfaces A: Physicochemical and Engineering Aspects**, v. 245, p.15-19, 2004.

TAN, I.; HAMEED, B.; AHMAD, A. Equilibrium and kinetic studies on basic dye adsorption by oil palm fibre activated carbon. **Chemical Engineering Journal**, v. 127, p.111-119, 2007.

TANG, S.C.; LO, I.M. Magnetic nanoparticles: essential factors for sustainable environmental applications. **Water Research**, v. 47, p.2613-2632, 2013.

TAWDE, S.P.; BHALERAJ, S.A. Adsorption of chromium (VI) from an aqueous solution using *Azadirachta indica*. A. juss. (neem) and activated charcoal: A comparative study. **Biological Forum - An International Journal**, v. 2, p.4-10, 2010.

TEMPLETON, D.M.; ARIESE, F.; CORNELIS, R.; DANIELSSON, L.-G.; MUNTAU, H.; VAN LEEUWEN, H.P.; LOBINSKI, R. Guidelines for terms related to chemical speciation and fractionation of elements. Definitions, structural aspects, and methodological approaches (IUPAC Recommendations 2000). **Pure and Applied Chemistry**, v. 72, 2000.

TSENG, R.-L.; WU, F.-C.; JUANG, R.-S. Characteristics and applications of the Lagergren's first-order equation for adsorption kinetics. **Journal of the Taiwan Institute of Chemical Engineers**, v. 41, p.661-669, 2010.

UFPR. Programa de Pós-graduação em Química v.,

UMUT, E. Surface Modification of Nanoparticles Used in Biomedical Applications. **Modern Surface Engineering Treatments**, v. 1, p.185-208, 2013.

US-Census Bureau - World Population_ 1950-2050 Available from: <http://www.census.gov/population/international/data/idb/worldpopgraph.php>. Accessed: Jan 2015.

USEPA-METHOD-7196A. EPA-Method-7196A. **United State Environmental Protection Agency**, v., 1992.

- WALKER, S.M., **Magnetism**. Lerner Publications, 2005.
- WANG, G.; CHANG, Q.; HAN, X.; ZHANG, M. Removal of Cr(VI) from aqueous solution by flocculant with the capacity of reduction and chelation. **Journal of Hazardous Materials**, v. 248-249, p.115-121, 2013.
- WANG, W.; LIU, P.; ZHANG, M.; HU, J.; XING, F. The Pore Structure of Phosphoaluminate Cement. v., 2012.
- WATERMAN, P.G.; MOLE, S., **Analysis of phenolic plant metabolites** Blackwell Scientific Publication, Oxford, 1994.
- WEIL, J.A.; BOLTON, J.R., **Electron paramagnetic resonance: elementary theory and practical applications**. John Wiley & Sons, 2007.
- WEINSTEIN, J.S.; VARALLYAY, C.G.; DOSA, E.; GAHRAMANOV, S.; HAMILTON, B.; ROONEY, W.D.; MULDOON, L.L.; NEUWELT, E.A. Superparamagnetic iron oxide nanoparticles: diagnostic magnetic resonance imaging and potential therapeutic applications in neurooncology and central nervous system inflammatory pathologies, a review. **Journal of Cerebral Blood Flow and Metabolism**, v. 30, p.15-35, 2010.
- WENG, X.; HUANG, L.; CHEN, Z.; MEGHARAJ, M.; NAIDU, R. Synthesis of iron-based nanoparticles by green tea extract and their degradation of malachite. **Industrial Crops and Products**, v. 51, p.342-347, 2013.
- WHO--Chromium in drinking water guidelines for drinking water quality**
Available from:
<<http://www.who.int/watersanitationhealth/dwq/chemcals/chromium.pdf>>.
Accessed: Dec 2013.
- WU, F.-C.; TSENG, R.-L.; HUANG, S.-C.; JUANG, R.-S. Characteristics of pseudo-second-order kinetic model for liquid-phase adsorption: A mini-review. **Chemical Engineering Journal**, v. 151, p.1-9, 2009.
- WU, S.; DUAN, N.; WANG, Z.; WANG, H. Aptamer-functionalized magnetic nanoparticle-based bioassay for the detection of ochratoxin a using upconversion nanoparticles as labels. **Analyst**, v. 136, p.2306-2314, 2011.
- YANG, X.-C.; SHANG, Y.-L.; LI, Y.-H.; ZHAI, J.; FOSTER, N.R.; LI, Y.-X.; ZOU, D.; PU, Y. Synthesis of Monodisperse Iron Oxide Nanoparticles without Surfactants. **J Nanomater**, v. 2014, p.5, 2014.
- YAVUZ, C.T.; MAYO, J.; WILLIAM, W.Y.; PRAKASH, A.; FALKNER, J.C.; YEAN, S.; CONG, L.; SHIPLEY, H.J.; KAN, A.; TOMSON, M. Low-field magnetic separation of monodisperse Fe₃O₄ nanocrystals. **Science**, v. 314, p.964-967, 2006.
- YOON, T.-J.; LEE, H.; SHAO, H.; WEISSLEDER, R. Highly magnetic core-shell nanoparticles with unique magnetization mechanism. **Angewandte Chemie (International Ed. in English)**, v. 50, p.4663-4666, 2011.
- ZENTKO, A.; KAVECANSKY, V.; MIHALIK, M.; MATAS, S.; MITRÓOVÁ, Z.; ZENTKOVÁ, M.; MARYSKO, M.; JAGLICIC, Z. Magnetic relaxation and memory

effect in nickel-chromium cyanide nanoparticles. **Acta Physica Polonica-Series A General Physics**, v. 113, p.511-514, 2008.

ZHAO, S.; LEE, D.K.; KIM, C.W.; CHA, H.G.; KIM, Y.H.; KANG, Y.S. Synthesis of Magnetic Nanoparticles of Fe₃O₄ and CoFe₂O₄ and Their Surface Modification by Surfactant Adsorption. **BULLETIN-KOREAN CHEMICAL SOCIETY**, v. 27, p.237, 2006.

ZHENG, W.; SHARMA, B.; RAJAGOPALAN, N. Using biochar as a soil amendment for sustainable agriculture. v., 2010.

7. APPENDICES

Publications

- NICOLINI, J.; KHAN, M.Y.; MATSUI, M.; CÔCCO, L.C.; YAMAMOTO, C.I.; LOPES, W.A.; DE ANDRADE, J.B.; PILLON, C.N.; ARIZAGA, G.G.C.; MANGRICH, A.S. Evaluation of PAH contamination in soil treated with solid by-products from shale pyrolysis. **Environmental Monitoring and Assessment**, v. 187, p.1-10, 2015.
- YOUNAS, M.K.; MANGRICH, A.S.; GRASEL, F.S.; MATTOSO, N.; MOSCA, D.H. Green chemistry preparation of superparamagnetic nanoparticles containing Fe₃O₄ cores in biochar. **Journal of Analytical and Applied Pyrolysis (Submitted)**.
- T. T. S. MATOSA, J. SCHULTZB, MUHAMMAD. YOUNAS. K, A. S. MANGRICH, B, B. R. ARAÚJOA, S. NAVICKIENEA, L. P. C. ROMÃOA. Removal of the pesticides thiacloprid and thiamethoxam from water using activated and magnetized biochars obtained from black wattle (*Acacia mearnsii* De Wild.) as adsorbents. **Separation and Purification Technology (Submitted)**.

